Aqueous Electrolytes Model Parameters and Process Simulation

Thomsen, Kaj

Link to article, DOI:
10.11581/dtu:00000074

Publication date:
1997

Document Version
Publisher's PDF, also known as Version of record

Aqueous electrolytes: model parameters and process simulation

Kaj Thomsen

Ph.D. Thesis

1997

Department of Chemical Engineering

Technical University of Denmark

DK-2800 Lyngby, Denmark

Preface

This thesis is submitted as partial fulfilment of the requirements for the Ph.D. degree at the Technical University of Denmark.

The work was carried out at the Department of Chemical Engineering, Technical University of Denmark, from September 1994 to August 1997 under the supervision of Professor Peter Rasmussen and Professor Rafiqul Gani. I thank both of my supervisors for all the hours they took out of their busy schedules to discuss matters concerning my project.

I am grateful to Dr. Mike Pinsky for inviting me to work at the FMC Chemical Research and Development Center in Princeton, New Jersey, USA. I want to thank for the productive discussions regarding industrial crystallizers, phase diagrams, and process simulation with Dr. Mike Pinsky, William Copenhafer, and Dave Smith.

It has been a pleasure to work at the Department of Chemical Engineering. I especially thank my fellow student Jørgen Peter Jensen for the many discussions about electrolyte thermodynamics.

Lyngby, August, 1997

Kaj Thomsen

Summary

This thesis deals with aqueous electrolyte mixtures. The Extended UNIQUAC model is being used to describe the excess Gibbs energy of such solutions. Extended UNIQUAC parameters for the twelve ions Na^+, K^+, NH_4^+, H^+, Cl^-, NO_3^-, SO_4^{2-}, HSO_4^-, OH^-, CO_3^{2-}, HCO_3^-, and $S_2O_8^{2-}$ are estimated. A computer program including a steady state process simulator for the design, simulation, and optimization of fractional crystallization processes is presented.

Chapter 1 is an introduction to aqueous electrolytes. The need for a thermodynamic model for electrolytes is described.

In chapter 2, thermodynamic concepts pertinent to the rest of the thesis are derived or defined. A description of the excess enthalpy and heat capacity of electrolyte solutions including the enthalpy contribution from chemical relaxation is presented.

Chapter 3 deals with the databank containing the experimental data used for the correlation of parameters for the thermodynamic model. This chapter includes an outline of some of the methods used for measuring the data.

In chapter 4, the thermodynamic model applied in this work is described. The need for a reference ion, relative to which the properties of other ions can be defined, is discussed.

The estimation of parameters for the Extended UNIQUAC model is described in chapter 5. Representative charts displaying model calculations of excess properties together with experimental data are presented. Generally, a good representation of the excess properties is obtained. The osmotic coefficient for sulphuric acid solutions is not represented very well. The reasons for this are discussed. The effect of defining the properties of ions relative to a reference ion is discussed.

In chapter 6, different types of phase diagrams for binary, ternary, and quaternary systems of ions are introduced. The calculation of such diagrams is described.

In chapter 7, results of the parameter estimation are presented in terms of phase diagrams for some representative systems. The ability of the model to predict the phase boundaries in quaternary systems is illustrated. Model extrapolations with respect to temperature and concentration are performed and shown to give good results.

Chapter 8 deals with the design, simulation and optimization of fractional crystallization processes. Equations for the type of multi-phase flash calculations required for aqueous electrolyte process simulations are presented. Operational parameters describing the incomplete solid-liquid separation in industrial crystallizers are introduced. Particular problems concerning the variables defining the composition of a stream of aqueous electrolytes is explained.

The design, simulation, and optimization of fractional crystallization processes is highlighted through case studies. In one case study, a patented process is simulated and optimized. The most significant result of the optimization is that the amount of water evaporated in the process can be reduced significantly. By simulation of the process, multiple steady states were detected and analyzed. A method to avoid the unwanted steady states is given.

Chapter 9 is the conclusion, summarizing the results of the project.

Resume på dansk

Denne afhandling omhandler vandige elektrolytopløsninger. Den udvidede UNIQUAC model anvendes til beskrivelse af excess Gibbs energien for sådanne opløsninger. Parametre for den udvidede UNIQUAC model bestemmes for de tolv ioner Na^+, K^+, NH_4^+, H^+, Cl^-, NO_3^-, SO_4^{2-}, HSO_4^-, OH^-, CO_3^{2-}, HCO_3^-, og $S_2O_8^{2-}$. Et computer program med en processimulator til anvendelse ved design, simulering, og optimering af fraktionering-ved-krystallisation processer præsenteres.

Kapitel 1 er en introduktion om vandige elektrolytter. Behovet for en termodynamisk model for elektrolytter beskrives.

I kapitel 2 defineres eller udledes termodynamiske begreber der er relevante for resten af denne afhandling. En beskrivelse af excess enthalpi og varmefylde for elektrolytopløsninger omfattende enthalpibidraget fra kemiske ligevægtsprocesser i opløsningen præsenteres.

Kapitel 3 handler om databanken med eksperimentelle data, der er blevet anvendt ved bestemmelsen af parametrene i den termodynamiske model. Dette kapitel indeholder også en kort beskrivelse af nogle af de målemetoder man anvender til bestemmelse af disse data.

I Kapitel 4 beskrives den termodynamiske model, der er blevet anvendt i dette arbejde. Behovet for en reference ion, i forhold til hvilken andre ioners egenskaber kan bestemmes, diskuteres.

Bestemmelsen af parametre i den udvidede UNIQUAC model beskrives i kapitel 5. Dette kapitel indeholder grafer med repræsentative eksempler på model beregninger af elektrolytters excess egenskaber. De experimentelle data, der ligger til grund for parameterbestemmelsen er afbildet på de samme grafer. Generelt er der opnået en god modelgengivelse af excess egenskaberne. Den osmotiske koefficient for svovlsyreopløsninger er dog ikke særlig godt gengivet. Mulige årsager til dette diskuteres. Virkningen af at definere ionernes egenskaber relativt til en reference ion diskuteres.

I kapitel 6 introduceres forskellige slags fasediagrammer for binære, ternære og kvaternære elektrolytsystemer. Det beskrives, hvordan sådanne fasediagrammer beregnes.

I kapitel 7 vises resultatet af parameterbestemmelsen i form af fasediagrammer for nogle repræsentative systemer. Modellens evne til at forudsige fasegrænser i kvaternære systemer illustreres gennem eksempler. Det illustreres tillige, at ekstrapolationer til højere temperaturer og koncentrationer foretaget med modellen, giver gode resultater.

Kapitel 8 omhandler design, simulering og optimering af fraktionering-ved-krystallisation processer. Ligningerne for den type af multifase ligevægtsberegninger, der kræves for at kunne simulere processer med vandige elektrolytter, præsenteres. Funktionelle parametre, der beskriver den ufuldstændige separation af væske og fast stof i industrielle krystallisatorer introduceres. Særlige problemer vedrørende de variable, der definerer sammensætningen af en elektrolytblanding, belyses.

Design, simulering og optimering af fraktionering-ved-krystallisation processer belyses gennem eksempler. I et af disse eksempler bliver en patenteret proces simuleret og optimeret. Det vigtigste resultat af optimeringen er, at den mængde vand, der skal fordampes i processen, kan mindskes betydeligt. Ved simulering af processen blev det vist, at den kan befinde sig i en af flere stationære tilstande. Disse stationære tilstande blev analyseret, og der angives en metode til at undgå uønskede stationære tilstande.

Kapitel 9 indeholder konklusioner og opsummerer projektets resultater.

Contents

1. Introduction

A thermodynamic model able to describe aqueous electrolyte systems is needed in order to develop software for the design, simulation, and optimization of processes with such systems.

The world-wide annual production rate of fertilizer chemicals such as potassium chloride, potassium sulphate, ammonium phosphates, and ammonium nitrate each exceed one million ton. The same figure for sodium chloride is 100 million ton. Some of the above mentioned salts are produced by fractional crystallization, a process in which several salts are separated as pure phases from a multi-component mixture.

Sometimes the precipitation and crystallization of electrolytes is an unwanted side effect to be avoided. This is for example the case with scaling, the formation of salt layers in boilers, heat exchangers, oil pipes or reverse osmosis units.

Waste water and flue gas treatment also often involves processes with electrolyte mixtures. Precipitation of phosphates, heavy metals and so on from wastewater requires knowledge of the solid-liquid equilibria for these ions. The removal of sulphur dioxide from flue gas with the production of gypsum involves several processes with electrolyte mixtures. The precipitation of salts also is a problem in straw firing and bio gas units.

While most other chemical processes can be simulated and optimized on computers today, the same is not true for processes involving electrolytes. Even today graphical methods are being applied for the design and simulation of such processes.

In a recent review by Loehe and Donohue, 1997, it was concluded that substantial prog??ress has been made in the modelling of strong electrolyte thermodynamics over the last 10 years, but “aside from the extensive empirical and semitheoretical results obtained from the Pitzer equations and the Helgeson formulations, there are as yet no comprehensive theories for the Gibbs or Helmholtz free energies of aqueous strong electrolyte systems that can provide accurate analytical expressions for real electrolyte properties such as density, enthalpies of mixing, and entropies of mixing using the same parameter set over a wide range of compositions and temperatures”!

Among the major advances in electrolyte thermodynamics in recent years Loehe and Donohue counts the Extended UNIQUAC model by Sander *et al.*, 1986.

In this thesis, it is shown that a simplified version of the model of Sander *et al.* is capable of describing the phase behaviour as well as the thermal properties of electrolyte mixtures in a wide temperature and concentration range. Furthermore this model is implemented in a computer program and used for simulating, optimizing and analyzing processes in electrolyte systems.

2. Thermodynamics of electrolyte solutions

2.1 Limiting laws

The calculation of mixture properties of an ideal solution only requires knowledge of the composition of the mixture and the pure component properties. The ideal non-electrolyte solution follows Raoults law

$$y_i P = x_i P_i^{sat} \quad \textbf{(2-1)}$$

y_i and x_i are the mole fractions of component *i* in the gas phase and the liquid phase. P is the total vapour pressure and P_i^{sat} is the vapour pressure of pure component *i*. Raoults law is a limiting law. In real solutions the solvent follows Raoults law more closely as the solution becomes more dilute in solutes.

The ideal dilute solution is a solution, where the solvent follows Raoults law and the solutes follow Henrys law

$$y_i P = x_i H_i \quad \textbf{(2-2)}$$

H_i is the Henrys law constant for solute *i*. The behaviour of real solutions approaches the behaviour described by equation 2-1 and 2-2 in sufficiently dilute solutions.

In electrolyte solutions, the ions interact strongly with each other and with the solvent through their electric charges, so deviations from ideality are important even at low concentrations. Also the ions are not volatile at atmospheric pressure and ambient temperature, so a different approach is needed in order to formulate a limiting law for the thermodynamic behaviour of electrolyte solutions.

Based on the assumption of each ion being surrounded by an ionic atmosphere consisting of ions of the opposite charge, the Debye-Hückel limiting law for electrolyte solutions was formulated by Peter Debye and Erich Hückel in 1923. The Debye-Hückel limiting law describes the non-ideal behaviour caused by electrostatic forces in extremely dilute electrolyte solutions. The limiting law expressed for a salt with the stoichiometric coefficients ν_i and the sum of stoichiometric coefficients ν is

$$\ln \gamma_{\pm} = -\frac{1}{\nu}\sum_i \nu_i z_i^2 A I^{½} + \ln x_w \qquad \textbf{(2-3)}$$

where $\gamma_{\pm}$ is the mean molal activity coefficient of ions in the solution, z_i is the charge of ion *i*,

$$A = \frac{F^3}{4\pi N_A}\left[\frac{d}{2(\varepsilon_0 \varepsilon_r RT)^3}\right]^{½} \qquad \textbf{(2-4)}$$

F (C mol^{-1}) is Faradays constant, N_A (mol^{-1}) Avogadros number, ε_0 the vacuum permittivity (C^2 J^{-1} m^{-1}), R the gas constant (J mol^{-1} K^{-1}), T is the temperature (K), d is the density (kg m^{-3}) and ε_r the relative permittivity (dielectric constant, dimensionless) of the solution. d and ε_r are both functions of temperature,

$$I = \frac{1}{2}\sum_i m_i z_i^2 \qquad \textbf{(2-5)}$$

is the ionic strength. m_i is the molality of ion *i*, x_w is the mol fraction of water.

The Debye-Hückel limiting law provides an accurate representation of the limiting behaviour of the activity coefficients in dilute ionic solutions. It is however not valid at ionic strengths higher than 0.01 mol (kg H_2O)$^{-1}$.

The Debye-Hückel limiting law 2-3 is derived from Debye-Hückel theory by neglecting terms that only play a role at concentrations higher than 0.01 mol (kg H_2O)$^{-1}$. An extended form of the Debye-Hückel limiting law includes some of these terms. It can be

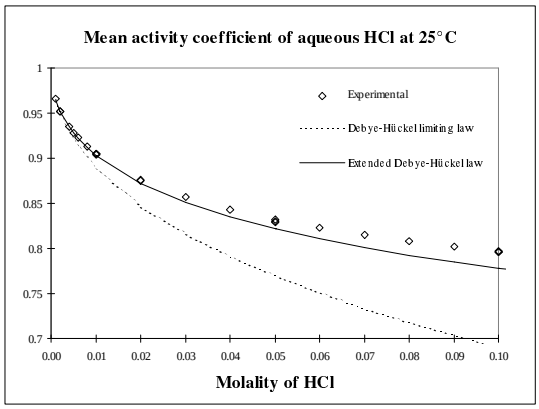

Figure 2-1: Mean molal activity coefficient of dilute aqueous HCl calculated with the Debye-Hückel limiting law and the extended Debye-Hückel law compared with experimental values.

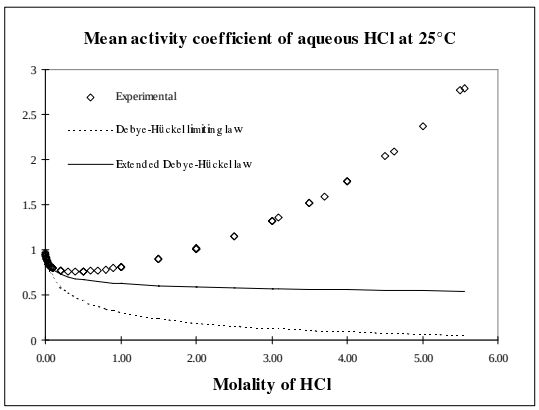

Figure 2-2: Mean molal activity coefficient of aqueous HCl calculated with the Debye-Hückel limiting law and the extended Debye-Hückel law compared with experimental values.

expressed as:

$$\ln \gamma_{\pm} = -\frac{1}{\nu}\sum_i \nu_i z_i^2 \frac{AI^{½}}{1+bI^{½}} + \ln x_w \qquad \textbf{(2-6)}$$

b is dependent on the size of the involved ions, but is usually considered constant. The extended Debye-Hückel law is applicable at ionic strengths up to 0.1 mol (kg H_2O)$^{-1}$.

In figures 2-1 and 2-2 the mean activity coefficient of HCl in water calculated with the Debye-Hückel limiting law and the extended Debye-Hückel law is compared to experimental values. The applied parameter values were b = 1.5 (kg mol^{-1})^{½}, T = 298.15 K, ε_r = 78.30, and d = 997.07 kg m^{-3}.

The Debye-Hückel limiting law and the extended Debye-Hückel law accurately describe the activity coefficients of very dilute ionic solutions. These equations are therefore often used for extrapolating the properties of electrolyte solutions to infinite dilution. As it appears from figure 2-2 however, the Debye-Hückel law is not suitable for describing the properties of real electrolyte solutions.

2.2 Gibbs energy function for real electrolyte solutions

Real electrolyte solutions can be described thermodynamically in terms of their deviation from ideality *i.e.* excess properties. Consider n_s mol of a salt with the stoichiometric coefficients ν_i. Assume that the salt is completely dissociated into ions in an aqueous solution containing n_w moles of water. The Gibbs free energy of the solution can then be expressed as

$$G = \sum_i n_i \mu_i = n_w \mu_w + n_s \sum \nu_i \mu_i \qquad \textbf{(2-7)}$$

where μ_i is the chemical potential of component i.

From classical, non-electrolyte thermodynamics we have at constant temperature

$$d\mu_i \equiv RTd(\ln \hat{f}_i) \quad \Rightarrow \quad \mu_i = \mu_i^{\bullet} + RT \ln \frac{\hat{f}_i}{f_i^{\bullet}} \qquad \textbf{(2-8)}$$

where R is the gas constant, T is the absolute temperature, $\hat{f}_i$ is the fugacity of component i in the solution at P and T, $\mu_i^{\bullet}$ is the chemical potential of component i in its standard state and $f_i^{\bullet}$ is the fugacity of component i in its standard state

Several different concentration scales are being used in electrolyte thermodynamics, that is molality (mol (kg H_2O)$^{-1}$) and mole fraction. The molarity (mol dm^{-3}) concentration scale is temperature dependent and therefore not practical in a thermodynamic model.

The activity coefficients differ according to the different concentration scales. Activity coefficients based on the mole fraction scale are called rational activity coefficients; activity coefficients based on the molality scale are the practical or molal activity coefficients.

Two different standard state conventions are in use for electrolyte solutions. According to the symmetrical convention, the activity coefficient of a component is unity in the (hypothetical) pure component at all temperatures. According to the unsymmetrical convention the activity coefficient of a component is unity at infinite dilution at all temperatures. Molal activity coefficients are always used with the unsymmetrical convention. The activity of any component is unity in the standard state of the component.

With the symmetrical convention, mole fraction scale, the fugacity of component *i* can be expressed as $\hat{f}_i = x_i f_i f_i^{\bullet}$, where f_i is the rational, symmetrical activity coefficient for component *i*. The chemical potential of component *i* then can be formulated by use of equation 2-8

$$\mu_i = \mu_i^0 + RT \ln(x_i f_i) \qquad \textbf{(2-9)}$$

where μ_i^0 is the chemical potential of pure component *i*. Usually the symmetrical convention, mole fraction scale is always chosen for the solvent.

With the unsymmetrical convention, mole fraction scale, the fugacity of component *i* can be expressed as $\hat{f}_i = x_i f_i^{\nabla} H_{i,x}$, where $H_{i,x}$ is the rational Henrys law constant and f_i^{∇} is the rational, unsymmetrical activity coefficient for component *i*. In the standard state of component *i*, the activity $x_i f_i^{\nabla}$ is unity and the fugacity therefore equal to $H_{i,x}$. The ratio $\frac{\hat{f}_i}{f_i^{\bullet}} = \frac{\hat{f}_i}{H_{i,x}} = x_i f_i^{\nabla}$, and according to equation 2-8, the chemical potential of component *i* can be expressed as

$$\mu_i = \mu_i^{\infty} + RT \ln(x_i f_i^{\nabla}) \quad \textbf{(2-10)}$$

where μ_i^{∞} is the chemical potential of component *i* in the standard state based on the unsymmetrical convention and the mole fraction scale.

On the molality scale, the activity of component *i* is $m_i\gamma_i$, where γ_i is the molal activity coefficient. The fugacity of component *i* in the solution, $\hat{f}_i = m_i \gamma_i H_{i,m}$, where $H_{i,m}$ is the molal Henrys law constant for component *i*. In the standard state, defined as the hypothetical ideal one molal solution, $m_i = m_{i,0} = 1$ mol (kg H_2O)$^{-1}$, and $\gamma_i = 1$. The standard state fugacity $f_i^{\bullet} = m_{i,0} H_{i,m}$. According to equation 2-8, the chemical potential of component *i* then can be expressed as

$$\mu_i = \mu_i^{\infty,m} + RT \ln\left(\frac{m_i}{m_{i,0}}\gamma_i\right) \quad \textbf{(2-11)}$$

where $\mu_i^{\infty,m}$ is the chemical potential of component *i* in the standard state based on the unsymmetrical convention and the molality scale. Usually $m_{i,0} = 1$ mol (kg H_2O)$^{-1}$ is omitted from the expression.

The chemical potential of an ion is independent of the definition of the standard state and the concentration unit. It can therefore be expressed in any of the three different ways

$$\begin{aligned} \mu_i &= \mu_i^0 + RT \ln(x_i f_i) \\ &= \mu_i^{\infty} + RT \ln(x_i f_i^{\nabla}) \\ &= \mu_i^{\infty,m} + RT \ln(m_i \gamma_i) \end{aligned} \quad \textbf{(2-12)}$$

By rearranging the first two terms on the right in equation 2-12 one obtains

$$\frac{\mu_i^0 - \mu_i^{\infty}}{RT} = \ln \frac{f_i^{\nabla}}{f_i} \quad \textbf{(2-13)}$$

At infinite dilution $f_i^{\nabla} = 1$, and the expression is reduced to

$$\frac{\mu_i^0 - \mu_i^{\infty}}{RT} = -\ln f_i^{\infty} \quad \textbf{(2-14)}$$

where f_i^{∞} is the symmetrical, rational activity coefficient of ion *i* at infinite dilution. By combining equations 2-13 and 2-14 a correlation between the rational, symmetrical activity coefficient and the rational unsymmetrical activity coefficient is obtained.

$$f_i^{\nabla} = \frac{f_i}{f_i^{\infty}} \tag{2-15}$$

By combining the first and the last right side terms of equation 2-12 one obtains

$$\frac{\mu_i^0 - \mu_i^{\infty,m}}{RT} = \ln\left(\frac{\nu_i n_s \gamma_i (n_w + n_s \sum \nu_i)}{n_w M_w \nu_i n_s f_i}\right) = \ln\left(\frac{\gamma_i}{x_w f_i \; M_w}\right) \tag{2-16}$$

M_w is the molar mass of water (kg mol^{-1}), the reference molality 1 mol (kg H_2O)$^{-1}$ makes the expression in the parenthesis dimensionless. At infinite dilution, x_w and γ_i both are close to unity, and f_i approaches f_i^{∞}. The expression then reduces to

$$\frac{\mu_i^0 - \mu_i^{\infty,m}}{RT} = -\ln(M_w f_i^{\infty}) \tag{2-17}$$

By inserting this expression in equation 2-16 and combining with equation 2-15 the following expression relating the molal activity coefficient to the rational symmetrical and the rational unsymmetrical activity coefficients is obtained.

$$\gamma_i = \frac{f_i}{f_i^{\infty}} x_w = f_i^{\nabla} x_w \tag{2-18}$$

From equations 2-14 and 2-17 it follows that

$$\frac{\mu_i^{\infty} - \mu_i^{\infty,m}}{RT} = -\ln M_w \approx 4.0165 \tag{2-19}$$

μ_i^{∞} and $\mu_i^{\infty,m}$ are both the chemical potential of ion *i* based on the unsymmetrical convention, but refer to two different concentration scales. The ratio between the mole fraction and the molality of ion *i*

$$\frac{x_i}{m_i} = \frac{\frac{n_s \nu_i}{n_w + n_s \sum \nu_i}}{\frac{n_s \nu_i}{n_w M_w}} = \frac{n_w M_w}{n_w + n_s \sum \nu_i} = x_w M_w \tag{2-20}$$

is equal to M_w at infinite dilution, whereas f_i^{∇} and γ_i both are unity. Extrapolation of measured chemical potentials to infinite dilution therefore yields the difference $RT\ln M_w$, as expressed in equation 2-19, depending on whether mole fractions or molalities are used as concentration unit.

2.3 *Activity and osmotic coefficients*

If the rational, symmetrical activity coefficients are being used for water and ions, the Gibbs free energy function for the real solution becomes (equations 2-7, 2-9 and 2-12)

$$G = n_w(\mu_w^0 + RT\ln(x_w f_w)) + n_s \sum \nu_i(\mu_i^0 + RT\ln(x_i f_i)) \quad \textbf{(2-21)}$$

In the ideal solution, all activity coefficients are unity, so the Gibbs free energy of the ideal solution becomes

$$G^{ideal} = n_w(\mu_w^0 + RT\ln x_w) + n_s \sum \nu_i(\mu_i + RT\ln x_i) \quad \textbf{(2-22)}$$

The expression for the excess Gibbs free energy becomes

$$\frac{nG^E}{RT} = \frac{G - G^{ideal}}{RT} = n_w \ln f_w + n_s \sum \nu_i \ln f_i \quad \textbf{(2-23)}$$

By partial molal differentiation of this expression, and by applying the Gibbs-Duhem relation

$$n_w d(\ln f_w) + n_s \sum \nu_i d(\ln f_i) = 0 \quad \textbf{(2-24)}$$

the activity coefficients are obtained

$$\left(\frac{\partial\left(\frac{nG^E}{RT}\right)}{\partial n_w}\right)_{T,P,n_i} = \ln f_w \quad \textit{and} \quad \left(\frac{\partial\left(\frac{nG^E}{RT}\right)}{\partial n_i}\right)_{T,P,n_j} = \ln f_i \quad \textbf{(2-25)}$$

By using equation 2-18, the activity coefficients for the ions can be converted to un-symmetrical or to molal activity coefficients. In section 2.7, it is shown how $\ln\gamma_i$ can be derived directly from an excess Gibbs function.

2.3.1 Mean molal activity coefficient

The mean molal activity coefficient, $\gamma_\pm$ of an electrolyte solution is the geometrical mean of the activity coefficients of the ions in the solution. Thus for a solution containing n mol ions, n_i mol of ion i

$$\ln \gamma_\pm = \frac{1}{n}\sum_{ions} n_i \ln \gamma_i = \ln x_w + \frac{1}{n}\sum_{ions} n_i \ln f_i^{\nabla} \quad \textbf{(2-26)}$$

Mean molal activity coefficients can be measured directly by potentiometric methods and are commonly tabulated.

2.3.2 Osmotic coefficient

In dilute aqueous solutions, the water activity and the water activity coefficient are very close to unity. In order to be able to report water activities without a large number of significant digits, the osmotic coefficient is commonly used. The osmotic coefficient is represented by the symbol Φ, and is defined

$$\Phi = -\frac{n_w}{n_s \sum \nu_i} \ln(x_w f_w) \qquad \textbf{(2-27)}$$

This is the practical or molal osmotic coefficient. The rational osmotic coefficient is based on the mole fraction scale

$$\Phi_x = \frac{\ln(x_w f_w)}{\ln x_w} \qquad \textbf{(2-28)}$$

it is rarely used however.

The molal and the rational osmotic coefficients both have the limiting value of unity at infinite dilution.

2.3.3 Vapour pressure

If water is the only volatile component of an aqueous electrolyte solution, the vapour pressure P of the solution can be expressed as

$$P = x_w f_w P_w^{sat} \qquad \textbf{(2-29)}$$

P_w^{sat} is the vapour pressure of pure water at the same temperature. This equation is derived from the isofugacity criterion, and is valid at pressures below 1 bar. Under these circumstances, pressure can be equated with fugacity and the Poynting factor is close to unity. The normal boiling point of saturated aqueous electrolyte mixtures is often above 110°C, which is the highest temperature of interest in this work.

2.4 *Equilibrium reactions*

The equilibrium between an aqueous phase and the solid salt $K_\kappa A_\alpha \cdot nH_2O$ consisting of κ cations K, α anions A, and n water molecules is described by the equation:

$$K_\kappa A_\alpha nH_2O\,(s) \leftrightarrow \kappa\,K\,(aq) + \alpha\,A\,(aq) + n\,H_2O \qquad \textbf{(2-30)}$$

At equilibrium, the chemical potential of the solid salt is equal to the sum of the chemical potentials of the salt's constituent parts. The condition for equilibrium therefore is:

$$\mu_{K_\kappa A_\alpha nH_2O\,(s)} = \kappa\,\mu_K + \alpha\,\mu_A + n\,\mu_w \qquad \textbf{(2-31)}$$

The equilibrium condition (2-31) can be expressed in terms of the standard chemical potentials and the activities of ions and water

$$\kappa\,\mu_K^{\infty,m} + \alpha\,\mu_A^{\infty,m} + n\mu_w^0 - \mu_{K_\kappa A_\alpha nH_2O\,(s)} = -\,RT\ln(K_{K_\kappa A_\alpha nH_2O}) \qquad \textbf{(2-32)}$$

where

$$K_{K_\kappa A_\alpha nH_2O} = a_K^\kappa\, a_A^\alpha\, a_w^n \qquad \textbf{(2-33)}$$

is the solubility product of the salt, $a_i = m_i\gamma_i$ for the ions and $a_w = x_w f_w$. The activity of solid salt is set equal to 1 because the solid salt is in its standard state.

The numerical value of the solubility product can be calculated from equation 2-32 based on the standard chemical potentials. To calculate the solubility product of a salt at a temperature different from the standard temperature, the standard chemical potentials need to be evaluated at this other temperature. The Gibbs-Helmholtz equation provides the relation

$$\frac{d\ln K}{dT} = \frac{\Delta H^0}{RT^2} \qquad \textbf{(2-34)}$$

where K is the solubility product of the salt given by equation 2-32 and ΔH^0 is the increment in standard state enthalpy by the reaction 2-30. By integrating this equation from the standard state temperature $T_0 = 298.15$K to the temperature T, one obtains

$$\ln K_T - \ln K_{T_0} = \int_{T_0}^{T} \frac{\Delta H^0}{RT^2}\,dT \qquad \textbf{(2-35)}$$

The temperature dependence of ΔH^0 is given by

$$\frac{d\Delta H^0}{dT} = \Delta C_p^0 \qquad \textbf{(2-36)}$$

where ΔC^0_p is the increment in standard state heat capacity by the reaction 2-30.

The standard state heat capacity of pure crystalline salts is often nearly constant in the temperature range from 0 to 110°C. For ions however, the standard state heat capacity rises steeply between 0 and 25°C, less steeply up to about 50°C and then decreases slightly. This is illustrated in figure 2-3, which is based on data for NaCl correlated by E.C.W. Clarke and D.N. Glew, 1985. The standard state heat capacity for NaCl at infinite dilution is the sum of the standard state heat capacities for Na^+ and Cl^-. Obviously ΔC^0_p can not be considered temperature independent. A three parameter correlation for $C^\infty_{p,i}$, the standard state heat capacity for ion *i*, of the form

$$C^\infty_{p,i} = a_i + b_i T + \frac{c_i}{T - T_{\Theta,i}} \qquad \textbf{(2-37)}$$

is suggested by Helgeson *et al.*, 1981. The term $T\text{-}T_{\Theta,i}$ provides for the steep change in $C^\infty_{p,i}$ below 25°C. In this work, $T_{\Theta,i}$ is given the constant value 200 K for all components, and the a_i, b_i, and c_i parameters are fitted to experimental heat capacity data rather than calculated as suggested by Helgeson *et al.*

The expression 2-37 for the standard state heat capacity can be used for water, ions and crystalline salts. For crystalline salts the *b* and the *c* parameters are set to zero, assuming that the heat capacity of all crystalline salts behave similar to that of NaCl (figure 2-3). ΔC^0_p can then be expressed in terms of Δa, Δb, and Δc, the increments in the *a*, *b*, and *c* parameters (equa-

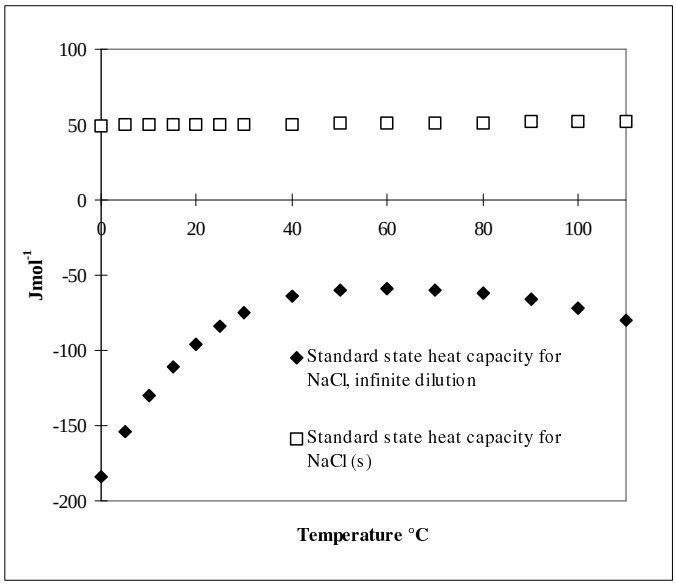

Figure 2-3: Standard state heat capacity of NaCl at infinite dilution and in solid state as a function of temperature

tion 2-37) by the reaction 2-30. Integration of equation 2-36 then gives

$$\Delta H_T^0 = \Delta H_{T_0}^0 + \Delta a(T - T_0) + 0.5\Delta b(T^2 - T_0^2) + \Delta c \ln \frac{T - T_\Theta}{T_0 - T_\Theta} \quad \textbf{(2-38)}$$

where $\Delta H^0{}_T$ is the increment in standard state enthalpies at the temperature T. By inserting this expression in equation 2-35 and integrating, one obtains

$$\begin{aligned} R\ln K_T = R\ln K_{T_0} - \Delta H_{T_0}^0\left(\frac{1}{T} - \frac{1}{T_0}\right) + \Delta a\left(\ln\frac{T}{T_0} + \frac{T_0}{T} - 1\right) \\ + 0.5\Delta b\left(\frac{(T - T_0)^2}{T}\right) + \frac{\Delta c}{T_\Theta}\left(\frac{T - T_\Theta}{T}\ln\frac{T - T_\Theta}{T_0 - T_\Theta} - \ln\frac{T}{T_0}\right) \end{aligned} \quad \textbf{(2-39)}$$

With this value of the equilibrium constant, the composition of the liquid phase in equilibrium with a solid phase can be calculated from equation 2-33 if the activity coefficients are known. If *s* solid salts are in equilibrium with the same liquid, all *s* salts must fulfil equation 2-33

$$K_k = \prod_i a_i^{\nu_{k,i}}, \quad k = 1..s \quad \textbf{(2-40)}$$

while for all other salts potentially formed by the system

$$K_k > \prod_i a_i^{\nu_{k,i}}, \quad k > s \quad \textbf{(2-41)}$$

The degree of saturation or the solubility index, SI, of a salt is defined as the activity product of a salt divided by its solubility product. For the salt in equation 2-30

$$SI = \frac{a_{\mathrm{K}}^{\kappa}\, a_{\mathrm{A}}^{\alpha}\, a_w^n}{K_{\mathrm{K}_\kappa\mathrm{A}_\alpha n H_2O}} \quad \textbf{(2-42)}$$

The solubility index of a salt is unity at saturation (equation 2-33). In a supersaturated solution it is greater than one and in unsaturated solutions it is less than one.

Dissociation equilibria can be treated in the same manner as described for solid liquid equilibria above. The hydrogen sulphate ion dissociates according to the equilibrium reaction

$$HSO_4^- \Leftrightarrow H^+ + SO_4^{2-} \quad \textbf{(2-43)}$$

If the HSO_4^- ion is given the stoichiometric coefficient -1, the equilibrium constant for this equilibrium reaction can be expressed in the exact same manner as the solubility product was in equation 2-33

$$K_{HSO_4^-} = a_{H^+}^1 \, a_{SO_4^{2-}}^1 \, a_{HSO_4^-}^{-1} \tag{2-44}$$

The degree of dissociation of HSO_4^- is defined

$$\alpha = \frac{n_{SO_4^{2-}}}{n_{SO_4^{2-}} + n_{HSO_4^-}} \tag{2-45}$$

2.5 *Thermal properties*

By differentiation of equation 2-9, applied to water, with respect to temperature at constant pressure and composition one obtains

$$\left[\frac{\partial \ln f_w}{\partial T}\right]_{P,x} = \left[\frac{\partial\left(\frac{\mu_w}{RT}\right)}{\partial T}\right]_{P,x} - \left[\frac{\partial\left(\frac{\mu_w^0}{RT}\right)}{\partial T}\right]_{P} = -\frac{H_{w,x}}{RT^2} + \frac{H_w^0}{RT^2} = -\frac{L_{w,x}}{RT^2} \tag{2-46}$$

where $H_{w,x}$ is the partial molal enthalpy of water at the specified composition, $H_w{}^0$ is the molal enthalpy of water in the standard state, and $L_{w,x}$ is the so-called relative molal enthalpy of water at the specified composition. A similar result is obtained for the ions by differentiation with respect to temperature of equation 2-12 using the second term on the right

$$\left[\frac{\partial \ln f_i^{\nabla}}{\partial T}\right]_{P,x} = \left[\frac{\partial\left(\frac{\mu_i}{RT}\right)}{\partial T}\right]_{P,x} - \left[\frac{\partial\left(\frac{\mu_i^{\infty}}{RT}\right)}{\partial T}\right]_{P} = -\frac{H_{i,x}}{RT^2} + \frac{H_i^{\infty}}{RT^2} = -\frac{L_{i,x}}{RT^2} \tag{2-47}$$

H_i^{∞} is the partial molal enthalpy of ion *i* in the standard state. The same result would have been obtained by differentiation of the logarithm of the molal activity coefficients. Equation 2-19 shows that the difference between the two standard state chemical potentials divided by *RT* is independent of temperature. The partial molal enthalpy at infinite dilution therefore is the same in these two standard states.

The relative enthalpy at constant composition of an electrolyte solution is given by

$$L_x = \sum_{w+i} n_i L_{i,x} = n_s L_{\varphi,x} \quad \textbf{(2-48)}$$

the term '$w+i$' means that the summation is over water and ions. $L_{\varphi,x}$ is the apparent relative molal enthalpy of the salt at the specified composition. For systems where chemical relaxation due to hydrolysis/association/dissociation reactions take place, the enthalpy of the electrolyte solution

$$H_x = \sum_{w+i} n_i H_{i,x} = n_s L_{\varphi,x} + \sum_i n_i H_i^{\infty} + n_w H_w^0 \quad \textbf{(2-49)}$$

is more useful. Equation 2-49 is the general equation from which the partial molal enthalpies of water and salt can be evaluated by numerical differentiation

$$H_w = \left[\frac{\partial H_x}{\partial n_w}\right]_{T,n=Eq} = L_w + H_w^0 \quad \textbf{(2-50)}$$

the subscript $n = Eq$ means that mol of salt is constant but the composition is the equilibrium composition. L_w is the relative molal enthalpy of water. The partial molal enthalpy H_s of salt and the relative molal enthalpy of salt L_s are given by

$$H_s = \left[\frac{\partial H_x}{\partial n_s}\right]_{T,n=Eq} = L_s + \sum_i \nu_i H_i^{\infty} \quad \textbf{(2-51)}$$

where the stoichiometric coefficient ν_i indicates that the summation only includes the ions of the original salt, not the ions formed by chemical relaxation. The relative enthalpy L of the solution and the apparent relative molal enthalpy L_φ of the salt are then given by

$$L = n_w L_w + n_s L_s = n_s L_\varphi \quad \textbf{(2-52)}$$

The temperature derivative of L is the relative heat capacity J

$$J = \left[\frac{\partial L}{\partial T}\right]_{n=Eq} = n_s\left(C_{p,\varphi} - \sum_i \nu_i C_{p,i}^{\infty}\right) \quad \textbf{(2-53)}$$

$C^{\infty}_{p,i}$ is the standard state heat capacity of ion i. $C_{p,\varphi}$ is the apparent molal heat capacity of the salt. $C_{p,\varphi}$ can be obtained from the apparent relative molal enthalpy of the salt as

$$C_{p,\varphi} = \left[\frac{\partial L_\varphi}{\partial T}\right]_{n=Eq} + \sum_i \nu_i C_{p,i}^{\infty} \quad \textbf{(2-54)}$$

It is observed that the relative molal enthalpy defined in equation 2-52 and the relative heat capacity defined in equation 2-53 are equal to zero in the standard state of the ions only if no hydrolysis/association/dissociation reactions occur. The activity coefficients are unity in the standard state, but equilibrium constants maintain their value.

The heat capacity C_p of an electrolyte solution is the sum of the standard state heat capacities of the components and the relative heat capacity, *i.e.*

$$C_p = \sum_{w+i} n_i C^0_{p,i} + J = n_w C^0_{p,w} + n_s C_{p,\varphi} \Rightarrow C_{p,\varphi} = \frac{C_p - n_w C^0_{p,w}}{n_s} \qquad \textbf{(2-55)}$$

which explains the term "apparent" and establishes an important relation between the apparent molal heat capacity of a salt and the heat capacity of a salt solution.

2.5.1 Heat of dilution

The enthalpy change per mole of salt associated with the dilution of a salt solution from molality m_1 to molality m_2 at constant temperature is the integral heat of dilution, $\Delta H(m_1 \rightarrow m_2)$. This is a measurable quantity and it is related to the apparent relative molal enthalpy L_φ of the salt:

$$\Delta H(m_1 \rightarrow m_2) = L_\varphi(m_2) - L_\varphi(m_1) \qquad \textbf{(2-56)}$$

where $L_\varphi(m)$ is the apparent relative molal enthalpy at the molality m. The integral heat of dilution from molality m to infinite dilution becomes

$$\Delta H(m \rightarrow 0) = L_\varphi(0) - L_\varphi(m) \qquad \textbf{(2-57)}$$

Sometimes experimental heat of dilution data are extrapolated to infinite dilution by means of the extended Debye-Hückel law and presented in the literature as apparent relative molal enthalpy (L_φ) data.

The differential heat of dilution is the partial molal relative enthalpy of solvent L_w as defined by equation 2-50

2.5.2 Heat of solution

The integral heat of solution at infinite dilution, $\Delta H^{s,\infty}$ is the enthalpy change for the dissolution of 1 mole of crystalline salt in an infinite excess of pure water at constant temperature defined by

$$\Delta H^{s,\infty} = L_{\varphi}(0) + \sum_i \nu_i H_i^{\infty} - H_c^0 \qquad \textbf{(2-58)}$$

where H^0_c is the standard state enthalpy of the pure crystalline salt. The integral heat of solution, ΔH^s is the enthalpy change for dissolving 1 mol of crystalline salt to form a solution of molality m

$$\Delta H^{s} = \Delta H^{s,\infty} + L_{\varphi}(m) - L_{\varphi}(0) = \sum_i \nu_i H_i^{\infty} + L_{\varphi}(m) - H_c^0 \qquad \textbf{(2-59)}$$

The differential heat of solution ΔH^{ds} is the enthalpy change per mole salt dissolved in a solution already containing dissolved salt

$$\Delta H^{ds} = \Delta H^{s,\infty} + \frac{\Delta L_{\varphi}}{\Delta n_s} \rightarrow \Delta H^{s,\infty} + L_s \;\; for\; \Delta n_s \rightarrow 0 \qquad \textbf{(2-60)}$$

2.6 Volumetric properties

The partial molal volume of water can be derived by differentiation of equation 2-9, applied to water, with respect to pressure at constant temperature and composition

$$\left[\frac{\partial \ln f_w}{\partial P}\right]_{T,x} = \left[\frac{\partial\left(\frac{\mu_w}{RT}\right)}{\partial P}\right]_{T,x} - \left[\frac{\partial\left(\frac{\mu_w^0}{RT}\right)}{\partial P}\right]_{T} = \frac{V_w}{RT} - \frac{V_w^0}{RT} \qquad \textbf{(2-61)}$$

where V_w is the partial molal volume of water at the specified composition, $V_w{}^0$ is the molal volume of water in the standard state. A similar result is obtained for the ions by differentiation with respect to pressure of equation 2-12 using the second term on the right

$$\left[\frac{\partial \ln f_i^{\nabla}}{\partial P}\right]_{T,x} = \left[\frac{\partial\left(\frac{\mu_i}{RT}\right)}{\partial P}\right]_{T,x} - \left[\frac{\partial\left(\frac{\mu_i^{\infty}}{RT}\right)}{\partial P}\right]_{T} = \frac{V_i}{RT} - \frac{V_i^{\infty}}{RT} \qquad \textbf{(2-62)}$$

V_i^{∞} is the partial molal volume of ion *i* in the standard state. The same result would have been obtained by differentiation of the logarithm of the molal activity coefficients.

The apparent molal volume V_φ of a salt is defined by an expression similar to the definition of the apparent molal heat capacity in equation 2-55:

$$V_\varphi = \frac{V - n_w V_w^0}{n_s} \qquad \textbf{(2-63)}$$

V is the volume of the solution, V_w^0 is the standard state molal volume of water.

2.7 *Deriving molal activity coefficients directly from a G^E function*

If the rational activity coefficients are being used for water and the molal activity coefficients are being used for the ions, the Gibbs free energy function for the real solution becomes (equations 2-7, 2-9 and 2-12)

$$G = n_w(\mu_w^0 + RT\ln(x_w f_w)) + n_s \sum \nu_i(\mu_i^{\infty,m} + RT\ln(m_i\gamma_i)) \qquad \textbf{(2-64)}$$

In the ideal solution, the activity coefficients are all unity and the Gibbs free energy function becomes

$$G^{ideal} = n_w(\mu_w^0 + RT\ln x_w) + n_s \sum \nu_i(\mu_i^{\infty,m} + RT\ln m_i) \qquad \textbf{(2-65)}$$

The excess Gibbs energy function then becomes

$$\frac{nG^E}{RT} = \frac{G - G^{ideal}}{RT} = n_w \ln f_w + n_s \sum \nu_i \ln \gamma_i \qquad \textbf{(2-66)}$$

By partial differentiation of this expression with respect to mol water one obtains

$$\left(\frac{\partial\left(\frac{nG^E}{RT}\right)}{\partial n_w}\right)_{T,P,n_i} = \ln f_w + n_w\left(\frac{\partial \ln f_w}{\partial n_w}\right)_{T,P,n_i} + n_s \sum \nu_i\left(\frac{\partial \ln \gamma_i}{\partial n_w}\right)_{T,P,n_i} \qquad \textbf{(2-67)}$$

By use of the Gibbs-Duhem equation (2-24) this can be reduced to

$$\left(\frac{\partial\left(\frac{nG^E}{RT}\right)}{\partial n_w}\right)_{T,P,n_i} = \ln f_w + \frac{\left(n_s \sum \nu_i\right)^2}{(n_w + n_s \sum \nu_i) n_w} = \ln f_w + \frac{\left(1 - x_w\right)^2}{x_w} \qquad \textbf{(2-68)}$$

By partial differentiation of equation 2-66 with respect to mol ion, one obtains

$$\left(\frac{\partial\left(\frac{nG^E}{RT}\right)}{\partial n_i}\right)_{T,P,n_i,\, i\neq j} = \ln\gamma_i - \frac{n_s \sum \nu_i}{n_w + n_s \sum \nu_i} = \ln\gamma_i + x_w - 1 \qquad \textbf{(2-69)}$$

$\ln f_w$ and $\ln\gamma_i$ thus are not partial molar properties with respect to the excess Gibbs energy function 2-66. This is a result of the particular concentration dependence of the molal activity coefficient (equation 2-18).

In the Pitzer methodology (Pitzer, 1991) the standard states for water and ions are the same as above. The Gibbs free energy of the ideal solution however, is defined by

$$G^{ideal} = n_w(\mu_w^0 - RTM_w \sum m_i) + n_s \sum \nu_i(\mu_i^{\infty,m} + RT \ln m_i) \qquad \textbf{(2-70)}$$

The expression 2-64 for the Gibbs free energy of the real solution is combined with the definition of the osmotic coefficient, equation 2-27 to yield

$$G = n_w(\mu_w^0 - RT\Phi M_w \sum m_i) + n_s \sum \nu_i(\mu_i^{\infty,m} + RT \ln m_i\gamma_i) \qquad \textbf{(2-71)}$$

The excess Gibbs free energy function then becomes

$$\frac{nG^E}{RT} = \frac{G - G^{ideal}}{RT} = n_s \sum \nu_i\left(1 - \Phi + \ln\gamma_i\right) = n_w \ln x_w f_w + n_s \sum \nu_i\left(1 + \ln\gamma_i\right) \qquad \textbf{(2-72)}$$

The definition of the ideal solution (2-70) was aimed at obtaining explicit terms for (1-Φ) and $\ln\gamma_i$. By partial differentiation of the excess Gibbs free energy function in equation 2-72 with respect to mol water, one obtains

$$\left(\frac{\partial\left(\frac{nG^E}{RT}\right)}{\partial n_w}\right)_{T,P,n_i} = \ln(x_w f_w) + n_w\left(\frac{\partial \ln x_w f_w}{\partial n_w}\right)_{T,P.n_i} + n_s \sum \nu_i\left(\frac{\partial \ln \gamma_i}{\partial n_w}\right)_{T,P,n_i} \qquad \textbf{(2-73)}$$

$$= \ln(x_w f_w) + \frac{n_s \sum \nu_i}{n_w} = \frac{n_s \sum \nu_i}{n_w}(1 - \Phi) = \frac{1 - x_w}{x_w}(1 - \Phi)$$

By partial differentiation of equation 2-72 with respect to mol of ion *i* one obtains

$$\left(\frac{\partial\left(\frac{nG^E}{RT}\right)}{\partial n_i}\right)_{T,P,n_j,j\neq i} = n_w\left(\frac{\partial \ln x_w f_w}{\partial n_i}\right)_{T,P,n_j,j\neq i} + \ln(\gamma_i) + n_s \sum \nu_i \left(\frac{\partial \ln \gamma_i}{\partial n_i}\right)_{T,P,n_j,j\neq i} \qquad \textbf{(2-74)}$$

$$= \ln \gamma_i$$

Due to the two different definitions of the ideal solution, the excess Gibbs free energy function used in the Pitzer methodology is different from the function in equation 2-66. The difference between the two excess Gibbs energy functions is

$$\frac{G^E - G^E_{Pitzer}}{RT} = -n_w \ln x_w - n_s \sum \nu_i \qquad \textbf{(2-75)}$$

this difference does not indicate that one excess Gibbs free energy function is better than the other but only reflects the two different definitions of the ideal solution.

3. Databank

Experimental data are necessary for the estimation of parameters for a thermodynamic model and at the same time serve to validate the model. Henrik Nicolaisen, 1994, described a databank containing experimental activity/osmotic coefficient and SLE data for aqueous electrolytes. This databank has been expanded to also contain data on the thermal properties of aqueous electrolyte solutions. A considerable amount of SLE and activity/osmotic coefficient data has also been added. The databank now contains the following sorts of data (with reference to defining equation)

- Water activity (2-29)
- Osmotic coefficient in binary and ternary solutions (2-27)
- Mean molal activity coefficient (2-26)
- Degree of dissociation (2-45)
- Apparent relative molal enthalpy (2-52)
- Heat of dilution (2-56)
- Differential heat of dilution (2-50)
- Integral heat of solution (2-59)
- Apparent molal heat capacity (2-54)
- Heat capacity (2-55)
- Solid liquid equilibrium in binary, ternary, and quaternary solutions (2-40 and 2-41)
- Densities of binary and ternary solutions
- Thermodynamic properties of pure components
- Original articles for about half of the experimental data

Some major sources of experimental data are NBS special publication 485, 537 and 718 (NBS 1977, NBS 1979, and NBS 1986). These publications contain bibliographies of sources of data on electrolytes. Recent experimental data have been found in international journals.

Besides experimental data, the databank also contains data that are correlated. This is for example the case with aqueous sodium chloride. For this system, data correlated by Clarke and Glew, 1985, have been included in the databank, and have replaced experi-

mental data for the excess properties of the aqueous sodium chloride system in estimating parameters for the thermodynamic model. Clarke and Glew's correlated data are based on 2428 experimental measurements from 94 different sources.

3.1 Osmotic coefficients

Osmotic coefficients can be calculated from vapour pressures, freezing point depressions, boiling point elevations, activity coefficients, or they can be measured relative to an *isopiestic standard*. "isopiestic" means "of equal pressure". An isopiestic standard is a solute for which the solvent activity is well defined as a function of concentration and temperature. Solutions of NaCl, KCl, H_2SO_4, or $CaCl_2$ are the most commonly used isopiestic standards.

In the isopiestic method, samples of different test solutions in open containers, together with one or more samples of solutions of the isopiestic standard(s), are placed in a sealed chamber. Through a common vapour phase, the solutions are allowed to exchange solvent until thermodynamic equilibrium is reached. The equilibration period is usually several days. When equilibrium is reached, the samples are weighed and the osmotic coefficients for the samples can be calculated. Using more than one isopiestic standard in one such experiment serves as an assurance that equilibrium is reached.

The reported values of osmotic coefficients from different isopiestic studies of the same salt usually differ by less than 3%. For the isopiestic standards, the same figure is 0.5%. The main sources of errors are insufficient equilibration time, impurities of the salt, and errors in the weighing procedure. Osmotic coefficients measured by other methods usually differ slightly more.

The isopiestic method can only be used at molalities higher than 0.1. The driving force for the transport of solvent through the common vapour phase is the partial molal derivative of the chemical potential of the solvents in the standard solution and in the sample solution. In very dilute solutions, the chemical potential of the solvent does not change significantly by dilution or concentration. Therefore the driving force for equilibration is small in dilute solution, and the accuracy of the results decreases with decreasing concentration. (Rard and Platford, 1991).

The definition of the osmotic coefficients includes an assumed dissociation (equation 2-27). It means that the sum of stoichiometric coefficients $\sum\nu_i$ is given a fixed value, independent of the actual degree of dissociation of the electrolyte. Osmotic coefficients for hydrogen sulphate salts and hydrogen carbonate salts thus can be found reported in the literature as either osmotic coefficients of 2-1 electrolytes or of 1-1 electrolytes. The assumed dissociation therefore needs to be included in the databank along with the experimental data.

3.2 Degree of dissociation

Experimental values of the degree of dissociation are so far only recorded for the hydrogen sulphate ion in the databank. Methods of measurements of the degree of dissociation of the hydrogen sulphate ion include Raman spectroscopy (Dawson *et al.*, 1986), volumetric measurements (Lindstrom and Wirth, 1969), conductivity measurements, besides the obvious methods of deriving the degree of dissociation from activity coefficient, heat capacity and heat of dilution data. The latter type of data have not been included in the databank, as the activity coefficient, heat capacity, and heat of dilution data better can be used directly for the estimation of parameters in the electrolyte model.

In Raman spectroscopy, measurements of the relative intensities of a Raman line are made. The intensity of a line is assumed proportional to the concentration of the ion or molecule that gave rise to the line. Thus, the degree of dissociation at different total concentrations of the electrolyte can be derived.

By the volumetric method, the apparent molal volume of the pertinent electrolyte is first determined from relative density measurements. The apparent molal volume of the electrolyte needs to be known as a function of ionic strength, so several measurements need to be made. It is assumed that the apparent molal volumes of ions are additive and only functions of ionic strength. According to Massons rule (Masson, 1929), the apparent molal volumes of salts are in fact linear functions of the square root of the molarity. According to Robinson and Stokes, 1965, this rule holds up to surprisingly high concentrations.

The apparent molal volume of completely dissociated sodium hydrogen sulphate can be calculated at a certain ionic strength, as the apparent molal volume of sodium sulphate plus the apparent molal volume of hydrochloric acid minus the apparent molal volume of sodium chloride.

The apparent molal volume of the completely undissociated (1-1) electrolyte can be found by first measuring the apparent molal volume of very dilute solutions of sodium hydrogen sulphate and use values of dissociation constants known from conductivity measurements, in order to find the apparent molal volume of sodium hydrogen sulphate at infinite dilution. If sodium hydrogen sulphate follows Massons rule, the apparent molal volume of the undissociated electrolyte will be a linear function of the square root of molarity. The slope of this linear function and the degree of dissociation can then be derived from the differences between the apparent molal volume of the real electrolyte, the completely dissociated electrolyte and the completely undissociated electrolyte.

In dilute solutions, results obtained by Raman spectroscopy and those obtained by volumetric measurements are consistent, while some deviations between results obtained by the two different methods are observed at higher concentrations.

The databank currently contains 11 data sets with 114 experimental measurements of degree of dissociation. The data concerns sulphuric acid, and the sodium and ammonium salts of hydrogen sulphate.

3.3 Heats of dilution and solution

Heat of dilution (solution) measurements can be performed by mixing known masses of solution and solvent (solute) initially kept in separate compartments in a calorimeter. When mixing the two samples a temperature change is observed. The typical amount of initial solution is 1 kg, the amount of solvent added in one experiment can be up to 1 kg, the temperature change during the mixing process is typically 0.5 to 5 degree. By measuring the heat capacity of the solution, the enthalpy of mixing can be calculated. A newer method involves the use of a heat-flow microcalorimeter. In this type of calorimeter, continuos streams of electrolyte solution and solvent are mixed in one chamber. A stream of solvent with a flow rate equal to the sum of the above two streams is passing through another chamber. Thermopiles surrounding the two chambers are connected

in opposition. The resulting signal from the thermopiles is proportional to the enthalpy of dilution (Busey *et al.*, 1984).

If heat of dilution experiments are carried out by adding so small amounts of solvent that the molality of the salt can be considered constant, the partial molal enthalpy of solvent can be derived from the measured heat effect.

In heat of solution experiments, the differential and the integral heats of solution are measured. These properties are defined in equations 2-59 and 2-60. By extrapolating the measured data to infinite dilution, the integral heat of solution at infinite dilution can be found.

Heat of dilution experiments yield differences in the apparent relative molal enthalpy L_φ of the salt,

$$\Delta H(m_1 \rightarrow m_2) = L_\varphi(m_2) - L_\varphi(m_1) \qquad \textbf{(2-56)}$$

Heat of solution experiments yield values of the partial molal enthalpy of the salt plus the integral heat of solution at infinite dilution.

$$\Delta H^{ds} = \Delta H^{s,\infty} + \frac{\Delta L_\varphi}{\Delta n_s} \rightarrow \Delta H^{s,\infty} + L_s \quad for\ \Delta n_s \rightarrow 0 \qquad \textbf{(2-60)}$$

In both cases, the extended Debye-Hückel limiting law is usually being applied for extrapolating the data to infinite dilution in order to calculate the apparent molal relative enthalpy of the salt and the integral heat of solution at infinite dilution.

The partial molal enthalpy of a salt that does not undergo dissociation or hydrolysis is at sufficient dilution given by the extended Debye-Hückel law. The derivation follows from equations 2-47 and 2-6

$$\left[\frac{\partial(\ln\gamma_\pm)}{\partial T}\right]_x = -\frac{1}{\nu}\sum_i \nu_i z_i^2 \frac{dA}{dT}\frac{I^{½}}{1+bI^{½}} = -\frac{1}{\nu}\frac{L_s^{D-H}}{RT^2}$$
$$\Rightarrow \quad L_s^{D-H} = RT^2 \frac{dA}{dT}\sum_i \nu_i z_i^2 \frac{I^{½}}{1+bI^{½}} \qquad \textbf{(3-1)}$$

The temperature derivative of the Debye-Hückel parameter A is available from correlations of A as a function of temperature. One such correlation is being presented in equation 4-8. $RT^2 dA/dT \sum \nu_i z_i^2$ is the *Debye-Hückel limiting slope* for relative enthalpy. The partial molal relative enthalpy of salt can be calculated from equation 3-1 as a function

of the ionic strength at concentrations, where the extended Debye-Hückel limiting law is valid.

The Debye-Hückel contribution to the activity coefficient of water, can be obtained from the Gibbs-Duhem relation

$$n_w d\left(\ln f_w\right) + n_s \sum \nu_i d\left(\ln f_i\right) = 0 \qquad \textbf{(2-24)}$$

as

$$\ln f_w = M_w \frac{2A}{b^3}\left[1 + bI^{½} - \frac{1}{1+bI^{½}} - 2\ln\left(1+bI^{½}\right)\right] \qquad \textbf{(3-2)}$$

from which the partial molal enthalpy of water in very dilute solutions can be obtained as

$$\begin{aligned}\left[\frac{\partial\left(\ln f_w\right)}{\partial T}\right]_x &= \frac{dA}{dT}\frac{2M_w}{b^3}\left[1 + bI^{½} - \frac{1}{1+bI^{½}} - 2\ln\left(1+bI^{½}\right)\right] = -\frac{L_w^{D-H}}{RT^2} \\ \Rightarrow \quad L_w^{D-H} &= -RT^2\frac{dA}{dT}\frac{2M_w}{b^3}\left[1 + bI^{½} - \frac{1}{1+bI^{½}} - 2\ln\left(1+bI^{½}\right)\right]\end{aligned} \qquad \textbf{(3-3)}$$

The relative enthalpy of the solution is the sum of the partial molal enthalpies (equation 2-48)

$$L^{D-H} = RT^2\frac{dA}{dT}\left(n_s\sum_i \nu_i z_i^2 \frac{I^{½}}{1+bI^{½}} - \frac{2n_w M_w}{b^3}\left(1 + bI^{½} - \frac{1}{1+bI^{½}} + 2\ln(1+bI^{½})\right)\right) \qquad \textbf{(3-4)}$$

The apparent relative molal enthalpy is the relative molal enthalpy per mol salt (equation 2-48)

$$\begin{aligned}L_\varphi^{D-H} &= RT^2\frac{dA}{dT}\sum_i \nu_i z_i^2\left(\frac{I^{½}}{1+bI^{½}} - \frac{1}{Ib^3}\left(1 + bI^{½} - \frac{1}{1+bI^{½}} + 2\ln(1+bI^{½})\right)\right) \\ &= \frac{3}{\left(bI^{½}\right)^3}\left(\frac{3}{2} + \ln(1+bI^{½}) - 2\left(1+bI^{½}\right) + \frac{1}{2}\left(1+bI^{½}\right)^2\right)\frac{2}{3}RT^2\frac{dA}{dT}\sum_i \nu_i z_i^2 I^{½} \\ &= -\frac{RT^2}{A}\frac{dA}{dT}\left(\nu\ln\gamma_{\pm} + \frac{n_w}{n_s}\ln f_w\right)\end{aligned} \qquad \textbf{(3-5)}$$

It is one of the first two expressions in equation 3-5 that is used for extrapolating the apparent relative molal enthalpy. The rearrangement in the second line is included in order to show how a linear dependency between apparent relative molal enthalpy data

and the square root of the ionic strength can be established. The simple relation between enthalpy and activity coefficients is illustrated in the third line.

Usually, the *b* parameter is calculated for the specific electrolyte in order to improve the extrapolation. In order to extend the validity of expressions 3-1 and 3-5 to the ionic strengths at which heat of dilution and heat of solution experiments take place, the empirical term $BI+CI^{3/2}$ is added to equation 3-1 and 3-5. *B* and *C* are parameters to be determined from the experimentally measured enthalpies.

The databank currently contains 444 heat of dilution data sets with 1776 experimental data points, 55 differential heat of dilution data sets with 99 experimental data points, mainly for hydrochloric acid and sulphuric acid. There are 75 apparent relative molal enthalpy data sets with 1742 experimental data points, and 66 integral heat of solution data sets with 313 experimental data points.

3.4 Heat capacity

The determination of the apparent molal heat capacity of salts usually includes the determination of the apparent molal volume of the salt. Perron *et al.*, 1974, describe their method in detail. With a flow microcalorimeter the relative difference in volumetric specific heat σ (J K^{-1} cm^{-3}) with respect to that of pure solvent, σ^0 is measured. The total heat capacity, C_p for a solution of volume V is $V\sigma$. The partial molal heat capacity of pure water is $C_{p,w}{}^0=V_w{}^0\sigma^0$, where $V_w{}^0$ is the standard state molal volume of water. By inserting these expressions in the definition of the apparent molal heat capacity equation 2-55 one obtains

$$C_{p,\varphi} = \frac{V\sigma - n_w V_w^0 \sigma^0}{n_s} \qquad \textbf{(3-6)}$$

From the definition of the apparent molal volume, equation 2-63, one obtains

$$\frac{n_w V_w^0}{n_s} = \frac{V}{n_s} - V_\varphi = \frac{1}{c} - V_\varphi \qquad \textbf{(3-7)}$$

where *c* is the concentration in mol cm^{-3}. By inserting this expression into equation 3-6, one obtains

$$C_{p,\varphi} = V_\varphi \sigma^0 + \frac{\sigma - \sigma^0}{c} \qquad \textbf{(3-8)}$$

Knowing σ and σ^0 the apparent molal heat capacity of a salt can be calculated from equation 3-8, if the apparent molal volume is known. The apparent molal volume can be determined to great accuracy with a flow densimeter.

Apparent molal heat capacity data can be extrapolated to infinite dilution by means of the extended Debye-Hückel law. The expression follows by differentiation of equation 3-5 with respect to temperature

$$C_{p,\varphi}^{D-H} - \sum_i \nu_i C_{p,i}^{\infty} = \frac{dL_\varphi^{D-H}}{dT}$$
$$= \left(2RT\frac{dA}{dT} + RT^2\frac{d^2A}{dT^2}\right)\sum_i \nu_i z_i^2 \left(\frac{I^{½}}{1+bI^{½}} - \frac{1}{Ib^3}\left(1+bI^{½} - \frac{1}{1+bI^{½}} + 2\ln(1+bI^{½})\right)\right)$$
$$= \frac{3}{\left(bI^{½}\right)^3}\left(\frac{3}{2} + \ln(1+bI^{½}) - 2\left(1+bI^{½}\right) + \frac{1}{2}\left(1+bI^{½}\right)^2\right)\left(2RT\frac{dA}{dT} + RT^2\frac{d^2A}{dT^2}\right)\frac{2}{3}\sum_i \nu_i z_i^2 I^{½} \qquad \textbf{(3-9)}$$

$(2RT(dA/dT)+RT^2(d^2A/dT^2))2/3\sum \nu_i z_i^2$ is the Debye-Hückel limiting slope for heat capacity. Equation 3-9 is usually extended with the empirical term $BI+CI^{3/2}$ in order to extend its applicability to the concentration range of the experiments. The values of B and C are different from those used in the expression for apparent relative molal enthalpy.

At infinite dilution, the value of the apparent molal heat capacity of a salt equals the sum of the standard state heat capacities of the salts constituent parts (equation 3-9). Experimental data for apparent molal heat capacity therefore serves both to evaluate the standard state heat capacity of ions and the relative heat capacity of electrolyte solutions.

The databank currently contains 286 data sets with 2926 experimental measurements of apparent molal heat capacities of salts. Most of these experimental data are accompanied by the corresponding experimental values of the apparent molal volumes. The volumetric data however have not been included in the databank yet. There are 533 data sets with 1394 measurements of weight specific heat, which are converted to apparent molal heat capacities before being used for parameter estimation.

3.5 *Retrieval of data*

The databank currently contains 2944 data sets for activity coefficients, and thermal properties. The 2944 data sets contain 20899 experimental data points. There are 3460 data sets with solubility data, containing 23095 experimental data points for binary, ternary, and quaternary systems. The data come from 1120 different sources. The data sets are given in the databank with one of 19 different concentration units, one of 6 different energy units, one of three different temperature units.

A computer program, RTRV was made for the retrieval of data from the databank. The program retrieves the data specified by the user and converts all concentration units to molalities, divides all energy units by the appropriate gas constant based on the Kelvin temperature scale, and all temperature units to Kelvin. The data, along with an identification number that tells from which source the data came, are stored in a file.

In RTRV, the user first specifies the ions of interest. Next, it can be specified which one or more types of data should be retrieved from the databank, and in what temperature range. The user can also specify a certain concentration range for the data.

Before using the experimental data for parameter estimation, the data must be visually inspected for consistency. The osmotic coefficients for a salt can for example be retrieved at a certain temperature. After retrieval, the data can be imported into a spreadsheet and be displayed graphically so that data from different sources can be compared visually. If some data diverge significantly from others, the source of the data can be checked for typing errors. If the data are systematically different from data from other sources, they can be marked with a zero in the databank. RTRV gives the option of retrieving all data, or only the data not marked with a zero.

SLE-data are more complicated to check visually than the activity coefficient and thermal property data. In systems with many double salts, the identification of the solid phases may be different from source to source. The newest data are not always the most reliable. RTRV gives a number of options for retrieving SLE-data from the databank:

- Retrieve only binary data. Often binary data are found in data sets dealing with ternary or quaternary systems. Binary solubilities can easily be compared visually as a function of temperature, as one expects to find a continued solubility curve in the

whole temperature range. The number of hydrate water in the solid phase can be different on different sections of the solubility curve. From the binary data, it is often possible to determine the correct number of hydrate water for the solid phase in a certain temperature interval. If a binary data point from a data set containing quaternary data gives an unexpected number of hydrate water, the quaternary data set can be investigated further, in order to find out what the correct number of hydrate water is. Many of the experimental SLE-data are of Russian origin, which complicates such investigations.

- Retrieve only data for a certain two-salt saturation point. Two-salt saturation points are points in the ternary phase diagram, where two solid salts are in equilibrium with the same liquid. It is expected that the two-salt saturation points for a certain salt pair form a continuous line as a function of temperature. If deviations from this behaviour occur, the sources of data must be investigated.

- Retrieve only three-salt saturation points. Three salt saturation points are invariant points in ternary systems. That is, three-salt saturation points, according to Gibbs phase rule, can only exist at one temperature, pressure, and composition for each compatible three salt set. Three salt saturation points occur as intersections of the two-salt saturation lines when these are plotted as a function of temperature in a ternary phase diagram. If the two-salt saturation lines have already been checked, the validity of the three-salt saturation points thus can be confirmed or rejected based on the existence and the temperature dependence of the two salt saturation lines.

- Retrieve ternary data at a certain temperature. The saturation lines in a ternary phase diagram at fixed temperature are expected to form continuous lines interrupted by two- or three-salt saturation points. By graphical inspection of experimental data it is thus possible to determine visually if the data from different sources agree. Again, the sources of data can be investigated in order to determine which data are most reliable.

A general discussion of the phase diagrams discussed above is given in chapter 6.

The computer program RTRV also has the function of retrieving thermodynamic properties and parameters to be used as input for a parameter estimation. Another computer program UPDBANK was constructed for automatically updating the thermodynamic properties and parameters in the databank after a parameter estimation is finished.

4. Thermodynamic model

4.1 Extended UNIQUAC model

The thermodynamic model used in this work is the Extended UNIQUAC model described earlier by Nicolaisen *et al.*, 1993. The model is a local composition model derived from the original UNIQUAC model (Abrams and Prausnitz, 1975; Maurer and Prausnitz, 1978) by adding a Debye-Hückel term (Sander, 1984; Sander *et al.*, 1986 a and b). The Extended UNIQUAC model thus consists of three terms: a combinatorial or entropic term, a residual or enthalpic term and an electrostatic term

$$G^E = G^E_{Combinatorial} + G^E_{Residual} + G^E_{Debye\text{-}Hückel} \quad \textbf{(4-1)}$$

The combinatorial and the residual terms are identical to the terms used in the traditional UNIQUAC equation. The combinatorial, entropic term is

$$\frac{G^E_{Combinatorial}}{RT} = \sum_i x_i \ln\left(\frac{\phi_i}{x_i}\right) - \frac{z}{2}\sum_i q_i x_i \ln\left(\frac{\phi_i}{\theta_i}\right) \quad \textbf{(4-2)}$$

$z = 10$ is the co-ordination number. x_i is the mole fraction, ϕ_i is the volume fraction, and θ_i is the surface area fraction of component i

$$\phi_i = \frac{x_i r_i}{\sum_l x_l r_l}; \qquad \theta_i = \frac{x_i q_i}{\sum_l x_l q_l} \quad \textbf{(4-3)}$$

r_i and q_i are volume and surface area parameters for component i. The residual, enthalpic term is

$$\frac{G^E_{Residual}}{RT} = -\sum_i x_i q_i \ln\left(\sum_k \theta_k \psi_{kl}\right) \quad \textbf{(4-4)}$$

the parameter ψ_{kl} is given by

$$\psi_{kl} = \exp\left(-\frac{u_{kl} - u_{ll}}{T}\right) \quad \textbf{(4-5)}$$

u_{kl} and u_{ll} are interaction energy parameters. The interaction energy parameters are considered temperature dependent in this model

$$u_{kl} = u^0_{kl} + u^t_{kl}(T - 298.15) \quad \textbf{(4-6)}$$

which is also being used for the case $k=l$. The combinatorial and the residual terms of the UNIQUAC excess Gibbs energy function are based on the rational, symmetrical activity coefficient convention. The Debye-Hückel, electrostatic term however is expressed in terms of the rational, symmetrical convention for water, and the rational, unsymmetrical convention for ions. Fowler and Guggenheim, 1949, suggested the following expression for the Debye-Hückel contribution to the excess Gibbs energy:

$$\frac{G^{E}_{Debye\text{-}Hückel}}{RT} = -x_w M_w \frac{4A}{b^3}\left[\ln\left(1+bI^{½}\right) - bI^{½} + \frac{b^2 I}{2}\right] \qquad \textbf{(4-7)}$$

x_w is the mole fraction of water, M_w kg mol^{-1} is the molar mass of water. A is the Debye-Hückel parameter defined in equation 2-4. Based on table values of the density d of pure water, and the relative permittivity of water, ε_r, the Debye-Hückel parameter A can be approximated in the temperature range 273.15 K < T < 383.15 K by

$$A = \left[1.131 + 1.335\cdot 10^{-3}\cdot(T-273.15) + 1.164\cdot 10^{-5}\cdot(T-273.15)^2\right] kg^{½}\,mol^{-½} \qquad \textbf{(4-8)}$$

b is considered constant, equal to 1.50 (kg mol^{-1})^{½}. I is the ionic strength defined in equation 2-5.

By partial molal differentiation of the combinatorial and the residual UNIQUAC terms, the combinatorial and the residual parts of the rational, symmetrical activity coefficients are obtained (equation 2-25)

$$\ln f_i^{C} = \ln\left(\frac{\phi_i}{x_i}\right) + 1 - \frac{\phi_i}{x_i} - \frac{z}{2}q_i\left[\ln\left(\frac{\phi_i}{\theta_i}\right) + 1 - \frac{\phi_i}{\theta_i}\right] \qquad \textbf{(4-9)}$$

$$\ln f_i^{R} = q_i\left[1 - \ln\left(\sum_k \theta_k \psi_{ki}\right) - \sum_k \frac{\theta_k \psi_{ik}}{\sum_l \theta_l \psi_{lk}}\right]$$

The infinite dilution terms are obtained by setting x_w=1 in equation 4-9

$$\ln f_i^{\infty,C} = \ln\frac{r_i}{r_w} + 1 - \frac{r_i}{r_w} - \frac{z}{2}q_i\left[\ln\frac{r_i q_w}{r_w q_i} + 1 - \frac{r_i q_w}{r_w q_i}\right] \qquad \textbf{(4-10)}$$

$$\ln f_i^{\infty,R} = q_i\left[1 - \ln\psi_{wi} - \psi_{iw}\right]$$

By partial molal differentiation of the Debye-Hückel excess Gibbs energy term 4-7, one obtains for water

$$\ln f_w^{D-H} = M_w \frac{2A}{b^3}\left[1+bI^{½} - \frac{1}{1+bI^{½}} - 2\ln\left(1+bI^{½}\right)\right] \quad \textbf{(4-11)}$$

and for the ions

$$\ln f_i^{\nabla,D-H} = -z_i^2 \frac{AI^{½}}{1+bI^{½}} \quad \textbf{(4-12)}$$

The activity coefficient for water is calculated by adding the three terms

$$\ln f_w = \ln f_w^C + \ln f_w^R + \ln f_w^{D-H} \quad \textbf{(4-13)}$$

and the activity coefficient for ion *i* is obtained as the rational, unsymmetrical activity coefficient

$$\ln f_i^{\nabla} = \ln f_i^C - \ln f_i^{\infty,C} + \ln f_i^R - \ln f_i^{\infty,R} + \ln f_i^{\nabla,D-H} \quad \textbf{(4-14)}$$

which can be converted to a molal activity coefficient by use of equation 2-18.

The thermal properties are derived from the model as described in chapter 2.

4.1.1 The Debye-Hückel term

The geometrical mean of the rational, unsymmetrical Debye-Hückel contribution to the activity coefficients for the ions in a solution containing *n* mol ions, n_i mol of ion *i* can be calculated from equation 4-12 as

$$\ln f_{\pm}^{\nabla,D-H} = -\frac{1}{n}\sum_i n_i z_i^2 \frac{AI^{½}}{1+bI^{½}} \quad \textbf{(4-15)}$$

which is consistent with the expression for the *mean molal activity coefficient* according to the extended Debye-Hückel law, equation 2-6. In the very dilute region, where the extended Debye-Hückel law approaches validity, it is customary to equal the molal and the rational, unsymmetrical activity coefficients (Harned and Owen, 1964), because the mole fraction of water is very close to unity in such solutions (equation 2-18).

The Debye Hückel law is based on the assumption of infinite dilution. The expression (4-8) for the Debye-Hückel *A* parameter is only valid in solutions so dilute that the density of the solution equals the density of pure water. The derivation of the Debye-

Hückel expression includes a conversion from molarity to molality. The relationship between the molarity c_i and the molality m_i of component i is

$$c_i = m_i \rho (1 - weight\ \ fraction\ ions) \quad \textbf{(4-16)}$$

where ρ is the density kg dm^{-3} of the solution. In very dilute solutions this relationship reduces to

$$c_i = m_i \rho_w \quad \textbf{(4-17)}$$

where ρ_w is the density kg dm^{-3} of pure water. It is the relation 4-17 that leads to the appearance of the density of pure water in the Debye-Hückel A parameter in equation 2-4. The solubility of NaCl at 25°C is 26.43% by weight, the density of the saturated solution is 1200 kg m^{-3}. The conversion factor in equation 4-16 thus becomes 0.883 kg dm^{-3} while the density of pure water at the same temperature is 997.07 kg m^{-3} yielding a factor of 0.997 kg dm^{-3} in equation 4-17. The Debye-Hückel A parameter calculated with the factor from equation 4-16 for a saturated NaCl solution is 1.106 (kg mol^{-1})^{½}, while the same parameter calculated with the density of pure water is 1.176 (kg mol^{-1})^{½}. The value of the Debye-Hückel contribution to the activity coefficients thus only is changed a few percent by the use of the approximation in 4-17.

Another assumption used in the derivation of the extended Debye-Hückel law is the validity of the Coulombs law expression for the electrostatic attraction and repulsion forces. In this expression, the relative permittivity of water is being used to describe the medium through which the electrostatic forces act. In a saturated solution of KNO_3 at 100°C (71% by weight), the number of ions is approximately equal to the number of water molecules. In such a solution, there simply is not enough water to form the "ionic atmospheres" assumed in the Debye-Hückel theory, and the Coulomb forces can not be acting through a pure aqueous medium.

Electrostatic forces are present at all concentrations in electrolyte solutions and must be accounted for. No significantly better expression for the electrostatic contribution to the activity coefficients is known. Therefore the extended Debye-Hückel law is applied in the whole concentration range.

From equation 4-12 it is seen that the Debye-Hückel contribution to the rational, unsymmetrical activity coefficient approaches $\exp(-z_i^2 A/b)$ at high ionic strengths. At 25°C

this value corresponds to 0.46 for a univalent ion and 0.04 for a bivalent ion. A rewriting of equation 4-14 yields

$$f_i^{\nabla} = \frac{f_i^{C} f_i^{R} f_i^{\nabla,D-H}}{f_i^{C,\infty} f_i^{R,\infty}} \qquad \textbf{(4-18)}$$

At high concentrations, where the extended Debye-Hückel law is not valid, the Debye-Hückel contribution to the unsymmetrical activity coefficient therefore is a factor of approximately $\exp(-z_i^2 A/b)$. This must be considered a quite significant contribution.

Good results have been obtained with the Extended UNIQUAC model in its present form, but an improved expression for the electrostatic contribution to the excess Gibbs energy function might benefit the model. As it is now, the combinatorial and the residual terms of the excess Gibbs energy functions must make up for the shortcomings of the Debye-Hückel term.

4.2 Model parameters

From the above description of the Extended UNIQUAC model, it can be seen that the parameters in the model are the volume and surface area parameters r_i and q_i for species i, the binary interaction energy parameter u_{ij} for the interaction between species i and j, and the like species interaction energy parameter u_{ii}.

The values of the r_i and q_i volume and surface area parameters for non-electrolyte species are usually calculated on the basis of the geometry of the species (Abrams and Prausnitz, 1975). For electrolyte species, the dimension of an ion in a crystal lattice probably only has little to do with its effective dimension in an aqueous solution, due to hydration. The r_i and q_i parameters have therefore in this work been treated as adjustable parameters, that were fitted to experimental data.

The binary interaction energy parameter u_{ij} is defined in equation 4-6. It consists of a base value and a temperature gradient, which both were fitted to experimental data. In this work the water-water and the like cation interaction energy parameters have been fixed at zero, while the like anion interaction energy parameters were fitted to experimental data.

The binary interactions are calculated from differences in interaction energy parameters, and by allowing the anions to have different u_{ii} parameters greater flexibility is added to the model.

4.3 Model application

It is not possible to measure the activity coefficient of an ion independently of other ions because electroneutrality is required. Therefore, by convention, the properties of ions are measured *relative* to the properties of the hydrogen ion. The Gibbs free energy of formation, the enthalpy of formation and the heat capacity of the hydrogen ion in its standard state, the hypothetical ideal one molal solution, are by convention all fixed at zero at all temperatures.

The differences in standard chemical potential in the different standard states for component *i* are given in equation 2-17 and 2-19

$$\mu_i^{\infty,m} = \mu_i^0 + RT\ln\left(M_w f_i^{\infty}\right) = \mu_i^{\infty} + RT\ln M_w \qquad \textbf{(4-19)}$$

It is obviously not possible to use a standard chemical potential of zero for the hydrogen ion in all three of these standard states simultaneously. In order to be able to define the infinite dilution activity coefficient of other ions relative to the value for the hydrogen ion, the convention

$$\ln f_{H^+}^{\infty}(T) \equiv 0 \quad \Rightarrow \quad \mu_{H^+}^0 = \mu_{H^+}^{\infty}, \quad \left(q_{H^+} = 10^{-15}, \quad r_{H^+} = 0.13779\right) \qquad \textbf{(4-20)}$$

at all temperatures, was adopted.

The value of the *r* parameter in equation 4-20 is calculated from equation 4-10 on the basis of the *r* parameter for water given by Abrams and Prausnitz, 1975.

It can be seen from equation 4-10 that the *q* parameter for the hydrogen ion actually should be zero in order to give an infinite dilution term of zero. To avoid numerical exceptions however, the value of ten to the minus 15th was used. The interaction energy parameters for the interaction of the hydrogen ion with other ions and with water were assigned fixed values, which result in no interaction between the hydrogen ion and other components. With this *q* parameter and these interaction energy parameters, the hydrogen ion contributes nothing to the residual part of the excess Gibbs energy function

(equation 4-4). The activity coefficient of the hydrogen ion is then governed entirely by the combinatorial and the Debye-Hückel terms.

Another choice of convention for the hydrogen ion could be

$$\ln M_w f^{\infty}_{H^+} \equiv 0 \quad \Rightarrow \quad \mu^{\infty,m}_{H^+} = \mu^{0}_{H^+}, \quad \left(q_{H^+} = 10^{-15}, \quad r_{H^+} = 0.58685 \cdot 10^{-2}\right) \qquad \textbf{(4-21)}$$

which would result in the hydrogen ion having the chemical potential zero in the standard state of pure component.

With the convention in equation 4-20 and with the absence of interaction energy parameters the hydrogen ion becomes a reference ion for single ion activities and for thermal properties.

In order to describe the activity coefficients and the thermal properties of aqueous HCl for example, only parameters for the chloride ion need to be fitted. The necessary parameters are the r and q parameters for the chloride ion and the temperature dependent interaction energy parameter, $u_{Cl\text{-}w}$ for the interaction between water and chloride ion. Independent of the initial guess, for each fixed value of the $u_{Cl\text{-}Cl}$ parameter, the final parameters will always have the same value. The resulting agreement between experimental and calculated data is well within the accepted deviations as defined in section 5-1, and the result can not be improved by changing the parameters for the hydrogen ion.

It is however not possible to determine an unambiguous value of the infinite dilution activity coefficient for the chloride ion on the basis of data for aqueous hydrochloric acid alone. For each fixed value of the $u_{Cl\text{-}Cl}$ parameter, another value of the infinite dilution activity coefficient is obtained.

In order to describe the thermodynamic properties of aqueous NaCl then, it is not enough to fit the r and q parameters for the Na^+ ion and the interaction energy parameters for the interaction between Na^+ and water and between Na^+ and Cl^-. Also the $u_{Cl\text{-}Cl}$ parameter needs to be fitted in order to describe the system. A parameter estimation based on experimental data for hydrochloric acid as well as for sodium chloride needs to be performed. Although a good agreement between experimental and calculated data is achieved by this parameter estimation, unambiguous values of the infinite dilution activity coefficients can not be determined from this system either.

5. Estimation of parameters

5.1 Computer program

A computer program, ESTIM, for the estimation of parameters in the Extended UNIQUAC model was developed. The program includes an implementation of the Marquardt method for non-linear least squares minimization from the Harwell subroutine library (Fletcher, 1971). The Nelder-Mead simplex search method as described by Fredenslund *et al.*, 1977, was implemented in the program as a supplement to the gradient based Marquardt method. Alternating between these two minimization methods was found to yield good results.

The Marquardt method was modified to include a maximum step length for each type of parameter. The *r* and *q* parameters for example can only be changed by 0.5 in each iteration. If the step predicted by the Marquardt routine changes these parameters with a value larger than 0.5, a reduction factor is used to reduce the step length, without changing the search direction. By this modification, large steps that often lead to extreme values of the parameters are avoided.

ESTIM calculates osmotic coefficient, mean molal activity coefficient, degree of dissociation, apparent relative molal enthalpy, heat of dilution, differential heat of dilution, integral heat of solution, apparent molal heat capacity, heat capacity, and solid liquid equilibrium of an electrolyte solution, based on the Extended UNIQUAC model. The calculated results are compared with the corresponding experimental data and added to the objective function as squared residuals

$$F = \sum_{\gamma LC\text{-}data} \left[w_i \left(y^{calc} - y^{\exp} \right) \right]^2 + \sum_{SLE\text{-}data} \left[w_i \ln(SI) \right]^2 \qquad \textbf{(5-1)}$$

γLC-data are all experimental data different from solid-liquid equilibrium data. *SLE-data* are solid-liquid equilibrium data. w_i is the weighting factor for data of type *i*. *SI* is the solubility index of a salt, equal to the activity product of the salt divided by its solubility product as defined in equation 2-42.

By using the solubility index, rather than calculating the actual equilibrium composition by an iterative procedure, a considerable amount of time can be saved. The optimal parameter set resulting from a parameter estimation is slightly different, depending on whether the objective function is based on solubility index or on actual equilibrium concentrations.

As described in section 2-4, 'Equilibrium reactions', if *s* salts are in equilibrium with the same liquid at a certain concentration, their solubility indices must all be unity at that composition of the liquid. At the same time, the solubility indices of all other salts must be less than unity.

When the object function is formed, the natural logarithms of the solubility indices of the *s* salts are calculated. If *s* is larger than one, the sum of the numerical values of the natural logarithms of the solubility indices is calculated. It is then checked, if other salts have solubility indices larger than unity in the same solution. If that is the case, the calculated residual is multiplied by a factor of $1+\sum\ln(SI_{other\ salts})$, where 'other salts' are the salts, that should not precipitate in the solution.

All parameters presented in this thesis are based on an objective function using the solubility index as a measurement of the deviation from equilibrium for solid-liquid equilibrium data. The parameters fitted for the FMC Corporation for simulation of pro??cesses in their soda ash and their sodium/ammonium peroxodisulphate plants were based on an objective function using the actual equilibrium concentrations in order to optimize the agreement with experimental solid-liquid equilibrium data.

The weighting factors in the objective function, equation 5-1, were specified so that an experimental data point is satisfactorily represented, when the weighted residual is less than unity. For osmotic coefficients and mean ionic activity coefficients, a weighting factor of 20 has been used. This corresponds to a weighted residual of one if the calculated and the experimental data differ by 0.05. For heat of dilution data w_i=0.01 mol J^{-1}, allowing a difference of 100 J mol^{-1} between calculated and experimental data. For heat capacity data converted to apparent molal heat capacities, w_i=0.12 K mol J^{-1} corresponding to a difference of 8 J mol K^{-1}. For degree of dissociation data, w_i=20, corresponding to a difference of 0.05. Finally w_i=10 for SLE-data.

The parameter estimation program, ESTIM, includes a number of options to be specified by the user in an input file:

- Identification of the parameters to be estimated
- The number of iterations to be performed in each of the minimization algorithms
- A "starting molality" and "step molality", tells the program to only include data with a concentration less than the starting molality in the estimation procedure. When the estimation is finished, the program increases the maximum molality by the step molality and starts a new parameter estimation with the parameters already obtained from the more dilute solution as a starting guess. This continues until all data are included
- A number of data points to dismiss, tells the program to perform a parameter estimation and then dismiss the experimental data point that is responsible for the largest contribution to the objective function. The parameter estimation then continues with the already obtained parameters as a starting guess. This option tells the program how many times to repeat this pattern. The number of data points to dismiss can typically be set to 10 out of 1500 data points.
- Option to not perform an optimization, but just calculate the squared residuals and show the results in a file. This option makes it easier to identify a type of data or a certain data set with particular large deviations.

When a parameter estimation is finished, ESTIM creates a file with the estimated parameters. This file is formatted so that it can be used directly as a new input file containing a starting guess for the parameters. Thus manual typing of the estimated parameters is eliminated.

With the options described above, ESTIM can be programmed to keep running for days and weeks, depending on the number of experimental data points and the speed of the computer.

5.2 *The aqueous (Na^+, K^+, H^+) (Cl^-, NO_3^-, SO_4^{2-}, OH^-, CO_3^{2-}, HCO_3^-) system*

Except for the carbonate/hydrogen carbonate system, the electrolytes considered in this system are all regarded as strong electrolytes, completely dissociated at the involved

concentrations. The formation of association products such as $NaSO_4^-$, $NaCO_3^-$, HNO_3 (aq), and H_2CO_3 (aq) is not considered.

According to Haase *et al.*, 1965, about 95% of the nitric acid molecules in a 2 molal solution are dissociated at 25°C. Therefore only solutions more dilute than 2 molal in HNO_3 are considered in this work.

No information on the degree of dissociation of hydrochloric acid in aqueous solutions was found in the literature. The existence of HCl in the vapour phase in equilibrium with aqueous hydrochloric acid however is well documented (Bach, 1976) and indicates its aqueous presence. The purpose of this work has mainly been to describe solid-liquid equilibrium processes which seldom include strongly acidic solutions. HCl has therefore been considered fully ionized in all solutions more dilute than 6 molal, although it might be possible to consider it fully ionized at higher concentrations.

The hydroxide ion was included because of its presence in the carbonate/hydrogen carbonate system and as a dissociation product of water, not in order to describe the precipitation of solid NaOH or solid KOH. The upper limit for OH^- concentration was set to 6 molal.

No interaction energy parameter for nitrate ion - carbonate ion was estimated because of lack of data for this system. The sulphate ion was only considered in neutral to basic solutions, so the formation of hydrogen sulphate ion was ignored. The carbonate-hydrogen carbonate system was only considered in the region, where the formation of carbonic acid or carbon dioxide could be ignored. The only cation that was considered for the carbonate-hydrogen carbonate system was the sodium ion.

5.2.1 Experimental data

The types of experimental data that were used for the estimation of model parameters for this system are osmotic coefficients, mean activity coefficients, heat of dilution data, heat capacity data and solid-liquid equilibrium data. In principle, all parameters could be estimated from experimental activity coefficients and thermal properties alone. For most systems however, these types of data do not cover the whole temperature and concentration range, making the use of solid-liquid equilibrium data necessary.

In two cases correlated data were used instead of experimental data. For the binary system water-sodium chloride, only data from Clarke and Glew, 1985, were used. Experimental data for this system are plentiful, the correlated data were used in order to limit the number of data for this system to a reasonable amount. For the binary system water-nitric acid, mainly data correlated by Clegg and Brimblecombe, 1990, were used. The exception is the thermal properties at temperatures below 25°C. The correlated values of the apparent molal heat capacity for aqueous HNO_3 at temperatures below 25°C are (as pointed out by Clegg and Brimblecombe, 1990) significantly higher than the values determined experimentally by Hovey and Hepler, 1989. Apparent molal heat capacities for aqueous HNO_3 at temperatures below 25°C from the latter work were therefore used. None of Clegg and Brimblecombes correlated data on thermal properties was used at temperatures below 25°C.

A total of 8691 binary and ternary experimental + correlated data from 403 different sources were used for this system. The data covered the temperature range from 0 to 110°C.

5.2.2 Thermodynamic properties

Values of the standard thermodynamic properties: Gibbs free energy of formation, enthalpy of formation, and heat capacities for ions and salts are necessary in order to calculate equilibrium constants and thermal properties. Most of the thermodynamic properties needed for this system could be found in the NIST tables (NIST, 1990). For several double salts, one or more thermodynamic properties could not be found in these tables and therefore had to be fitted to experimental data.

The heat capacity correlation for ions, equation 2-37 requires three parameters for each ion. These parameters all had to be fitted to experimental data, as the correlation (equation 2-37)

$$C^{\infty}_{p,i} = a_i + b_i T + \frac{c_i}{T - T_{\Theta,i}} \qquad \textbf{(2-37)}$$

with $T_{\Theta,i}$ = 200 K for all components, is only being used in this work. For consistency in the heat capacity calculations, the same correlation is used for water. The three parameters for the heat capacity of water were estimated from the 5 parameter DIPPR cor-

relation for the heat capacity of pure water (DIPPR, 1983) in the temperature range 0-110°C. The heat capacity of water is nearly constant in this temperature range. The largest deviation between the water heat capacity calculated with the DIPPR correlation and the corresponding value calculated with the correlation 2-37 is 0.08 J mol^{-1} K^{-1}.

5.2.3 Estimation of model parameters

Initial estimates of the model parameters were found by fitting the parameters of the anions to experimental data for the corresponding acid. Next parameters for the cations were fitted relative to the parameters for the anions. Finally, all parameters were fitted simultaneously.

The first step in the parameter estimation was to obtain parameters for aqueous hydrochloric acid and nitric acid solutions. In each of these binary systems 4 parameters had to be determined, namely the volume and the surface area parameter for the anion, the water-anion and the anion-anion interaction energy parameters. The surface area parameter for the anion was fixed while the three other parameters for each binary system were estimated from experimental data for that system.

Subsequently cation parameters were estimated from experimental data for binary aqueous solutions of NaCl, KCl, $NaNO_3$, and KNO_3. With the anion parameters known, five parameters had to be determined for each of the subsystems Na^+-Cl^--NO_3^--H_2O and K^+-Cl^--NO_3^--H_2O. These five parameters are the volume and the surface area parameters for the cation, the water-cation and the two cation-anion interaction energy parameters. As for the anions, the surface area parameters for the cations were fixed while the four other parameters in each of the above subsystems were estimated from experimental data.

The Na^+-K^+ and Cl^--NO_3^- interaction energy parameters were estimated on the basis of ternary SLE data containing these ion pairs. Finally, all the parameters in the Na^+-K^+-Cl^--NO_3^--H_2O system were estimated simultaneously based on experimental data.

Subsequently the hydroxide, the sulphate and the carbonate/hydrogen carbonate ions were added to the system. This was done by estimating parameters for each ion based

on the pertinent experimental data, without changing the parameters of the core system, H^+-Na^+-K^+-Cl^--NO_3^--H_2O.

5.2.4 Estimation of thermodynamic properties

Thermodynamic properties that were not found in the NIST tables had to be fitted to experimental data. In a single case, namely crystalline sodium sesquihydrate (trona), Na_2CO_3•$NaHCO_3$•$2H_2O$, the value given for the Gibbs free energy of formation at 298.15K in the NIST tables was not used, as it seemed to contradict experimental data. Due to insufficient experimental data involving the double salt Darapskite, $NaNO_3$•Na_2SO_4•H_2O, the heat capacity of this salt could not be estimated but was fixed at 300 J mol^{-1} K^{-1}. The thermodynamic properties estimated are thus

- The three parameters in the heat capacity correlation, equation 2-37, for all ions. Due to insufficient experimental heat capacity data for the carbonate and the hydrogen carbonate ions no such parameters were estimated for these ions. The values given in the NIST tables for the standard state heat capacity at 25°C were used for these ions in the whole temperature range.
- The Gibbs free energy of formation of crystalline glaserite, $NaK_3(SO_4)_2$, darapskite, $NaNO_3$•Na_2SO_4•H_2O, burkeite, Na_2CO_3•$2Na_2SO_4$, trona, Na_2CO_3• $NaHCO_3$•$2H_2O$, and wegscheiderite, Na_2CO_3•$3NaHCO_3$.
- The enthalpy of formation of crystalline darapskite and burkeite.
- The heat capacity of crystalline glauber salt, Na_2SO_4•$10H_2O$, glaserite, burkeite, trona, and wegscheiderite.

These thermodynamic properties were estimated simultaneously with the model parameters for the pertinent ions.

Fifty-three model parameters and 32 thermodynamic properties and parameters were estimated from the 8691 experimental + correlated data points for this system of nine ions and water.

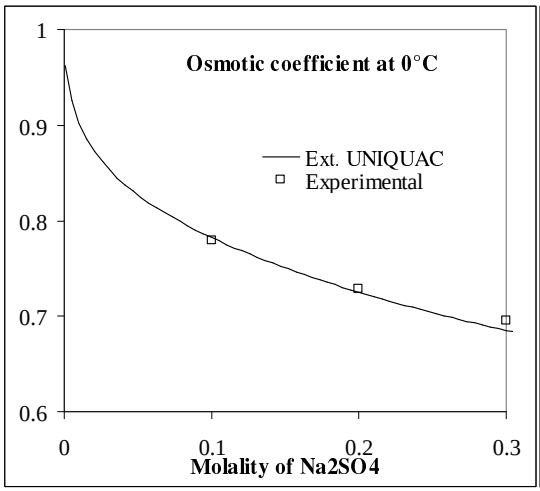

Figure 5-1: The osmotic coefficient of aqueous sodium sulphate solutions at 0°C

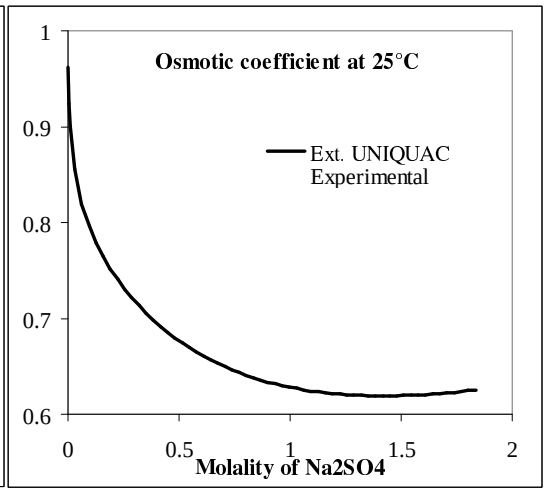

Figure 5-2: The osmotic coefficient of aqueous sodium sulphate solutions at 25°C

5.2.5 Results

Figures 5-1 to 5-3 show the osmotic coefficient of aqueous sodium sulphate solutions at 0, 25, and 80°C, calculated with the Extended UNIQUAC model at concentrations up to the saturation point at the three temperatures. Experimental data used in the parameter estimation are plotted together with the model calculations. The experimental data at 0°C are from an isopiestic study by Platford, 1973, those at 25°C are from 17 different sources, and those at 80°C are from an isopiestic study by Moore *et al.*, 1972).

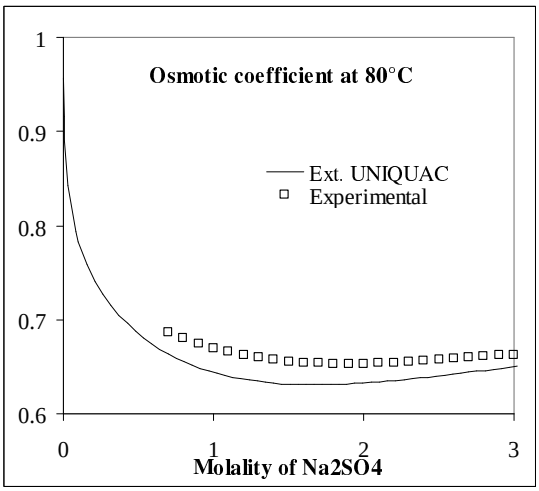

Figure 5-3: The osmotic coefficient of aqueous sodium sulphate solutions at 80°C

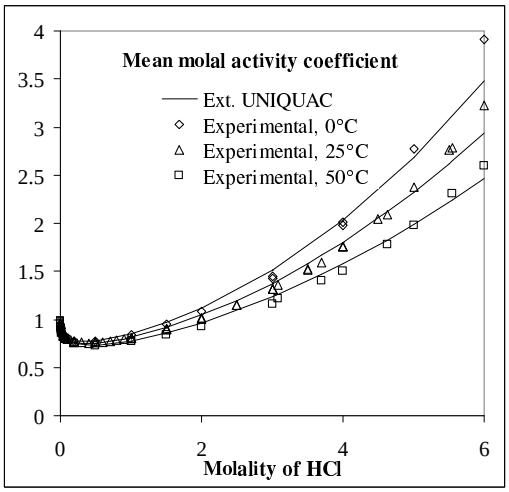

Figure 5-4: The mean molal activity coefficient of aqueous HCl at three different temperatures.

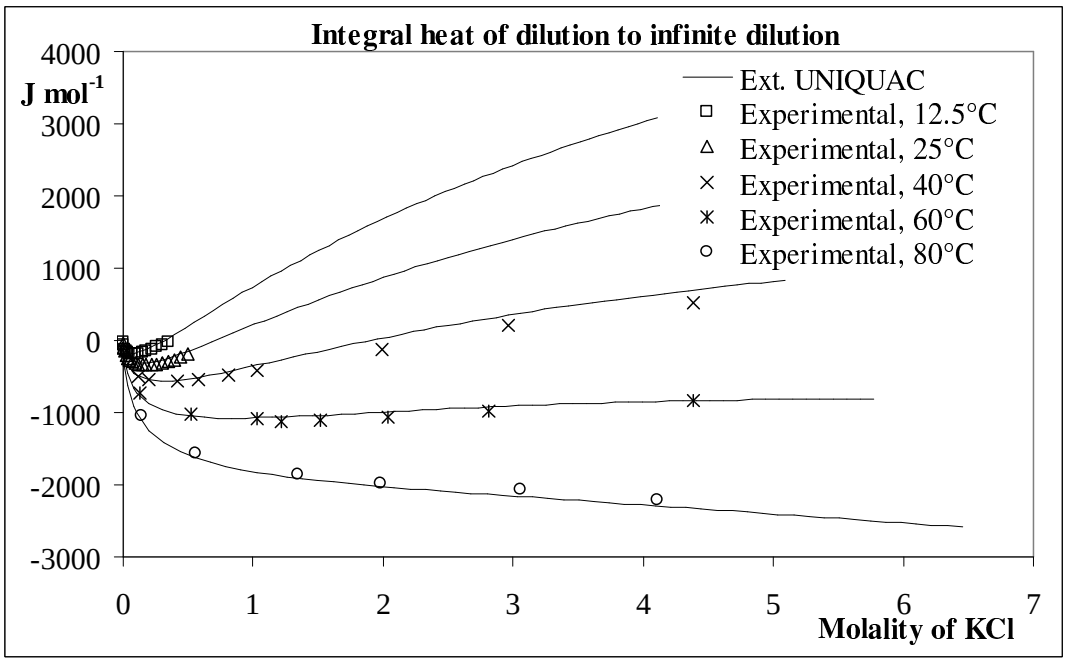

Figure 5-5: The integral heat of dilution of KCl to infinite dilution at five different temperatures.

The root mean square deviation between the 185 experimental data and the calculated values of the osmotic coefficients shown in figure 5-1 to 5-3 is 0.02.

Figure 5-4 shows the mean molal activity coefficient of hydrochloric acid at three different temperatures. Also in this case, the differences between calculated and experimental values are very small. The experimental values in this case come from 6 different sources.

In figure 5-5 calculated and experimental values of the integral heat of dilution to infinite dilution for KCl at five different temperatures are shown. The experimental integral heat of dilution data at 12.5 and 25°C are from Lange and Monheim, 1930, those at 40, 60, and 80°C are from Snipes *et al.*, 1975. An almost exact match is achieved at all these temperatures.

Figure 5-6 shows the apparent molal enthalpy of NaOH at four different temperatures. The experimental data plotted in figure 5-6 are from five different sources. Also in this case, only minor deviations are observed. The intercept of the apparent molal heat capacity curves of figure 5-6 with the ordinate axis, is the standard state heat capacity of

NaOH at infinite dilution at the respective temperatures. A strong dependency on temperature is observed.

Without taking the temperature dependence of the standard state heat capacity of the ions into consideration (equation 2-37), it would not be possible to correlate apparent molal heat capacity.

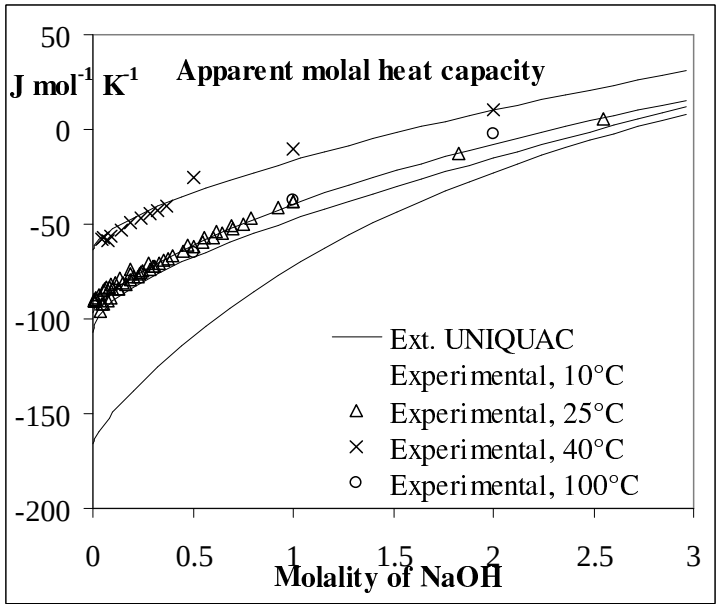

Figure 5-6: The apparent molal heat capacity of NaOH at four different temperatures

5.3 Potassium carbonate/hydrogen carbonate

In the first parameter estimation, described in section 5.1, the interaction energy parameters for the carbonate and the hydrogen carbonate ion with the sodium, chloride, sulphate, and hydroxide ions were estimated. This parameter set was intended for use by the FMC Corporation to simulate their solution mining processes, and was therefore partially based on experimental data proprietary to that company.

Another parameter estimation was therefore performed for this system, only including experimental data from the open literature. In this parameter estimation, also the potassium ion was included.

Potassium carbonate and potassium hydrogen carbonate have the peculiar characteristics that they are far more soluble at 25°C than the corresponding sodium salts. The opposite is the case with the chlorides, sulphates and nitrates of these cations. In addition, sodium and potassium carbonate might form hydrated solid solutions at temperatures below 35°C (Hill and Miller, 1927). According to Hill and Miller, the solid solution can be decribed as $(Na_2, K_2)CO_3 \cdot 6H_2O$, with varying amounts of sodium and potassium. Osaka, 1911, and Kremann and Zitek, 1909, claimed to have determined the same precipitate to be the salt $Na_2CO_3 \cdot K_2CO_3 \cdot 12H_2O$. Harvie *et al.*, 1984, modelled the system

at 25°C and found that the solid phase actually could be described as $Na_2CO_3 \cdot K_2CO_3 \cdot 12H_2O$. It was decided in this work also to let this "salt" describe the limited part of the phase diagram, where the solid solution appears. Actually the chemical formula used for the salt in this work is $NaKCO_3 \cdot 6H_2O$.

The *tetragene* salt, $K_2CO_3 \cdot NaHCO_3 \cdot 2H_2O$, was discovered by Hill and Smith, 1929. A tetragene salt is a salt built up of two different cations and two different anions (Meyerhoffer, 1903). Hill and Smith, 1929, and Hill, 1930a, give experimental solubility data for this salt at 25 and 35°C. Another tetragene salt, $2K_2CO_3 \cdot KHCO_3 \cdot NaHCO_3 \cdot 1½H_2O$ is described by Sedel'nikov and Trofimovich, 1959. Their data, at 75°C only, however are not sufficient for estimating the thermodynamic properties of this salt. Model predictions for a multi component solution containing the four ions the salt consists of, might therefore yield inaccurate results.

A total of 1660 experimental data points including osmotic coefficient, heat of dilution, heat capacity, and binary/ternary solid liquid equilibrium data from 91 different sources were used in the parameter estimation. The experimental data covered the temperature range from 0 to 110°C. Eighteen model parameters were estimated for this system

- The r and q parameters for the carbonate and the hydrogen carbonate ions.
- The interaction energy parameters for the interaction of the carbonate and hydrogen carbonate ions with water and the sodium, potassium, chloride, and sulphate ions.
- The interaction energy parameter for the interaction of the carbonate ion with the hydrogen carbonate and hydroxide ions.
- The u_{ii} parameters for the carbonate and the hydrogen carbonate ions.

Twenty five thermodynamic properties and parameters were estimated

- The standard state Gibbs free energy of formation of burkeite, trona wegscheiderite, $KHCO_3$, $NaKCO_3 \cdot 6H_2O$, $K_2CO_3 \cdot Na_2CO_3$, $K_2CO_3 \cdot NaHCO_3 \cdot 2H_2O$, and $K_2CO_3 \cdot 2KHCO_3 \cdot 1½H_2O$. The value for the tetragene salt $K_2CO_3 \cdot NaHCO_3 \cdot 2H_2O$ was estimated from the pertinent quaternary solubility data. The standard state Gibbs free energy of formation for $KHCO_3$ is actually given in the NIST tables, but it was found necessary to modify it in order to get a reasonable agreement between calculated and experimental data.

- The standard state enthalpy of formation of $NaKCO_3 \cdot 6H_2O$, $K_2CO_3 \cdot 2KHCO_3 \cdot 1½H_2O$, $K_2CO_3 \cdot NaHCO_3 \cdot 2H_2O$, and burkeite,.
- The standard state heat capacity of $K_2CO_3 \cdot 1½H_2O$, $KHCO_3$, burkeite, trona, weg-scheiderite, $K_2CO_3 \cdot Na_2CO_3$, and $K_2CO_3 \cdot 2KHCO_3 \cdot 1½H_2O$.
- The three parameters in the correlation for the standard state heat capacity of the carbonate and the hydrogen carbonate ions.

The model parameters and the thermodynamic properties for this system were estimated without changing any of the model parameters for the (Na^+, K^+, H^+) (Cl^-, NO_3^-, SO_4^{2-}, OH^-) system.

5.3.1 Results

Figures 5-7 and 5-8 show the integral heat of dilution to infinite dilution curves for sodium carbonate and sodium hydrogen carbonate. On the curves, experimental data from heat of dilution experiments are plotted. The heat of dilution from one molality to another is defined in equation 2-56. It is the difference in apparent relative molal enthalpy at the two molalities. The integral heat of dilution to infinite dilution on the other hand is the apparent relative molal enthalpy at infinite dilution minus the same property at a finite molality (equation 2-57). Thus, heat of dilution data can be plotted on a curve representing the integral heat of dilution to infinite dilution.

The experimental data in figure 5-8 are from Leung and Millero, 1975. The heat of di-

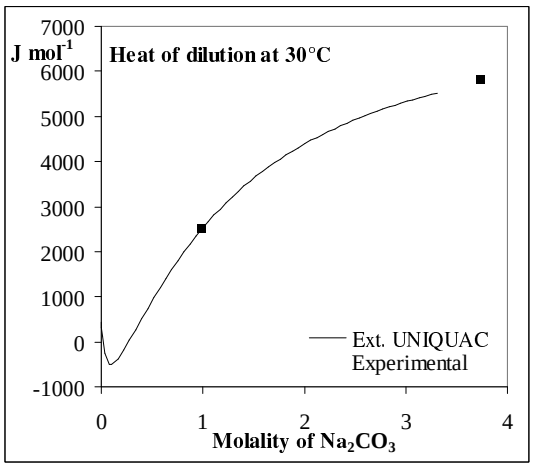

Figure 5-7: Heat of dilution data for sodium carbonate at 30°C

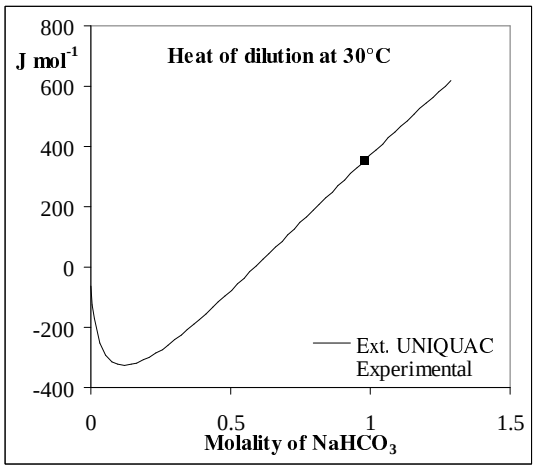

Figure 5-8: Heat of dilution data for sodium hydrogen carbonate at 30°C

lution experiment was performed by diluting a stock solution with the molality 0.97942. The heat of dilution to infinite dilution of the stock solution is marked in figure 5-8 with a black square. As heat of dilution data are relative, this point was actually chosen at the point where the line: 'molality=0.97942' intersects the calculated integral heat of dilution to infinite dilution curve. The open squares in figure 5-8 represent the diluted solutions. The abscissa of each point is the molality of the diluted solution and the ordinate is calculated by subtracting the experimental heat of dilution from the integral heat of dilution to infinite dilution of the stock solution.

In figure 5-7 heat of dilution data from two different sources are plotted. One of the sources is Leung and Millero, 1975. Their stock solution was a 0.98860 molal Na_2CO_3 solution (marked with a black square in figure 5-7). Six dilutions of this stock solution were performed. The points representing the diluted curves were calculated as described above. All the experimental points from this source coincide with the calculated curve (figure 5-7). The other series of heat of dilution data marked on figure 5-7 are from Swallow and Alty, 1931. Here the stock solution had a concentration of 3.7 molal (marked with a black square). The diluted solutions are marked in figure 5-7 with open squares. The three heat of dilution experiments to molalities of about 1.55 are in good agreement with the calculated curve, while those to greater dilution fall below the curve.

It was found that the solid solution found in the sodium/potassium carbonate system could be well represented by the salt $NaKCO_3 \cdot 6H_2O$. An improved agreement could not be obtained by excluding data for this salt. The estimated value of the standard state Gibbs energy of formation for this salt is -2495.69 kJ mol^{-1}. Harvey *et al.*, 1984, who modelled the system at 25°C found the value -2495.18 kJ mol^{-1}. The value of the standard state Gibbs energy of formation for $KHCO_3$ was estimated to be -868.70 kJ mol^{-1}, Harvey *et al.* estimated it to be 867.74 kJ mol^{-1}. The value given in the NIST tables is -863.5 kJ mol^{-1}.

5.4 Sulphuric acid, the ammonium and the peroxodisulphate ions

Peroxodisulphate salts can be produced by electrolytic oxidation of a solution of the corresponding sulphate salt in sulphuric acid. The electrolytic oxidation takes place according to the scheme

$$2HSO_4^- \Rightarrow S_2O_8^{2-} + 2H^+ + 2e^- \quad \textbf{(5-2)}$$

Hydrogen is formed at the cathode (P. Kofstad, 1987). In order to be able to simulate this process, parameters for the hydrogen sulphate ion, the ammonium ion and the peroxodisulpate ions are needed in addition to the already available parameters.

Model parameters and thermodynamic properties for this system were estimated without changing any of the original parameters from the (Na^+, K^+, H^+) (Cl^-, NO_3^-, SO_4^{2-}, OH^-) system.

5.4.1 The ammonium ion

First, the ammonium ion was added. 1558 experimental data points from 83 different sources were available in the databank for this system. Eight model parameters were estimated for this system

- The *r* and *q* parameters for the ammonium ion
- The interaction energy parameters for the interaction of the ammonium ion with water, sodium, potassium, chloride, sulphate, and nitrate ion

According to Gorshtein, and Silant'eva, 1954, mixtures of potassium and ammonium chloride form solid solutions in the temperature range from 25 to 75°C. Two-salt saturation points however, are given as the composition of a liquid in equilibrium with equal amounts of potassium and sodium chloride. Five different double salts, for which no thermodynamic property data are found in the NIST tables, are encountered in the system. Twelve thermodynamic properties were estimated for this system

- The standard state heat capacity for the ammonium ion. There were not enough heat capacity data to fit the three parameters for the standard state heat capacity correlation. One value of the standard state heat capacity was therefore used in the whole temperature range.
- The standard state Gibbs free energy of formation of $(NH_4)_2SO_4 \cdot 3NH_4NO_3$, $(NH_4)_2SO_4 \cdot 2NH_4NO_3$, $Na_2SO_4 \cdot (NH_4)_2SO_4 \cdot 4H_2O$, $2NaNO_3 \cdot NH_4NO_3$, and $3KNO_3 \cdot NH_4NO_3$.
- The standard state enthalpy of formation and heat capacity of $(NH_4)_2SO_4 \cdot 3NH_4NO_3$, $(NH_4)_2SO_4 \cdot 2NH_4NO_3$, $Na_2SO_4 \cdot (NH_4)_2SO_4 \cdot 4H_2O$. The salts $2NaNO_3 \cdot NH_4NO_3$ and

$3KNO_3 \cdot NH_4NO_3$ only appear in experimental data points at 25°C. Therefore the enthalpy of formation and the heat capacity of these two salts could not be estimated.

5.4.1.1 Results

As examples of the correlation results for the ammonium ion, figure 5-9 shows the apparent molal enthalpy of ammonium nitrate solutions at concentrations up to 25 molal. The experimental data plotted together with the calculated curve are from Vanderzee *et al.* ,1980. In dilute solutions of ammonium nitrate, some dissociation of the ammonium ion takes place. The data by Vanderzee *et al.* are corrected for dissociation i.e. the heat effect from the dissociation is subtracted from the experimental data. The dissociation of the ammonium ion is not considered in this work, the corrected data were therefore used rather than the "raw" data.

Figure 5-10 shows the mean ionic activity coefficient of ammonium chloride solutions calculated with the Extended UNIQUAC. The experimental data in this figure are from Hamer and Wu, 1972.

As it appears from the examples in figures 5-9 and 5-10, a good fit was obtained for the ammonium ion. The only exception might be the osmotic coefficients of ammonium sulphate, where some deviation between correlated and calculated data is seen. This

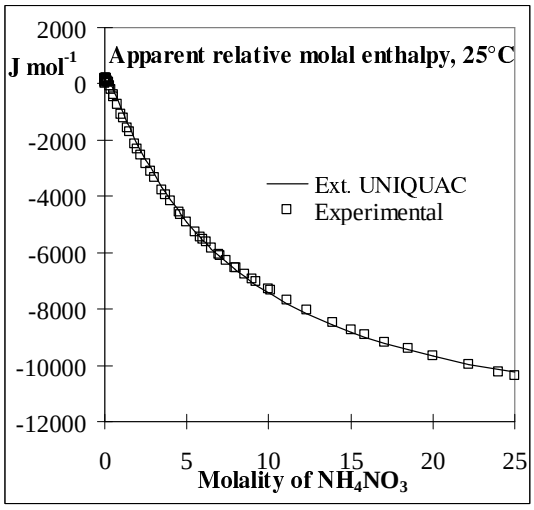

Figure 5-9: The apparent relative molal enthalpy of ammonium nitrate.

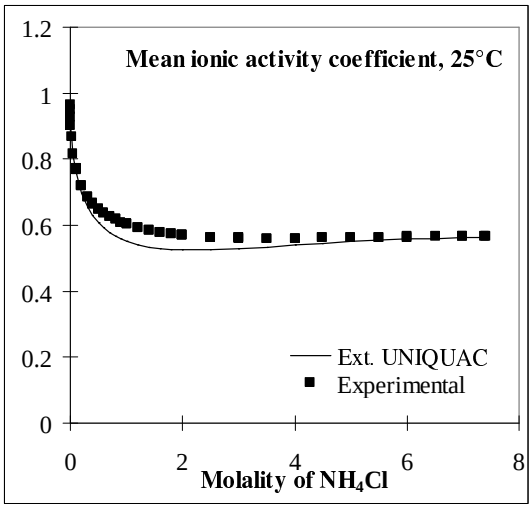

Figure 5-10: The mean molal activity coefficient of ammonium chloride.

however will not be illustrated here.

5.4.2 Sulphuric acid

Parameters for the hydrogen sulphate ion were fitted to experimental data for sulphuric acid. Eight model parameters were estimated for this system

- The r and q parameters for the hydrogen sulphate ion
- The interaction energy parameters for the interaction of the hydrogen sulphate ion with water and the sulphate, sodium, potassium, and ammonium ions.
- The u_{ii} parameter for the hydrogen sulphate ion.

Also three parameters for the standard state heat capacity of the hydrogen sulphate ion were estimated.

The experimental data available for this system included osmotic coefficient, activity coefficient, degree of dissociation of the hydrogen sulphate ion, differential heat of dilution, heat of dilution, heat capacity and solid-liquid equilibrium data for the sodium, potassium, and ammonium sulphates in sulphuric acid solutions.

The calculation of the solubility of glauber salt, $Na_2SO_4 \cdot 10H_2O$, involves the use of the water activity lifted to the power of ten, according to equation 2-33. The model must therefore predict the water activity and its temperature dependence very exactly in order to give the correct solubilities.

It was found impossible to fit the osmotic and activity coefficients of even dilute sulphuric acid and the solubility of glauber salt in sulphuric acid solutions simultaneously. Osmotic and activity coefficient data for aqueous sulphuric acid was then excluded from the parameter estimation in order to be able to calculate solid-liquid equilibria satisfactorily.

The number of data points employed in this parameter estimation was then reduced to 301 experimental data from 17 different sources. These data covered the temperature range from 0 to 100°C and the concentration range from infinite dilution to 12 molal H_2SO_4.

5.4.2.1 Results

Figure 5-11 shows the degree of dissociation of the hydrogen sulphate ion in sulphuric acid at 25°C for concentrations up to 12 molal. The experimental data by Lindstrom and Wirth, 1969, measured by a volumetric method, and those by Chen and Irish, 1971, measured with Raman spectroscopy are plotted together with the degree of dissociation calculated with the Extended UNIQUAC model.

In figure 5-12 the differential heat of dilution of sulphuric acid solutions calculated with the Extended UNIQUAC model is plotted together with the smoothed data of Giauque *et al.*, 1960.

Figure 5-13 shows the calculated degree of dissociation of the hydrogen sulphate ion in aqueous solutions of ammonium hydrogen sulphate plotted together with the experimental data of Dawson *et al.*, 1986, measured with Raman spectroscopy. In all three of these figures, the fit is very satisfactory.

Figure 5-14 shows the osmotic coefficients of sulphuric acid calculated with the model and compared to osmotic coefficients from a review by Rard *et al.*, 1976. Large deviations are seen throughout the displayed concentration range.

As pointed out by Rard *et al.*, 1976, and by Cabani and Gianni, 1972, there are particular problems in determining the thermodynamic properties of the hydrogen sulphate ion.

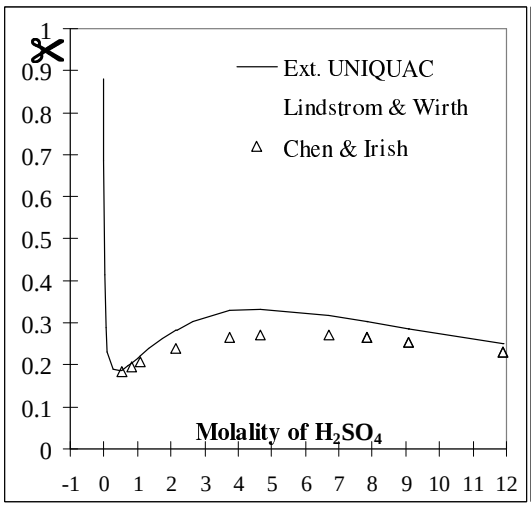

Figure 5-11: The degree of dissociation of hydrogen sulphate in sulphuric acid at 25°C.

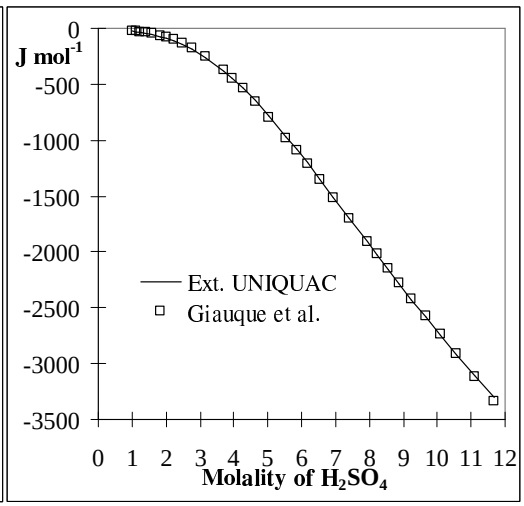

Figure 5-12: The differential heat of dilution of aqueous sulphuric acid at 25 °C.

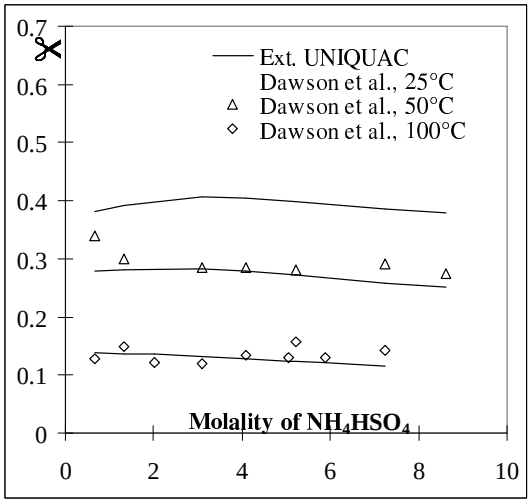

Figure 5-13: The degree of dissociation of the hydrogen sulphate ion in aqueous NH_4HSO_4 at three different temperatures.

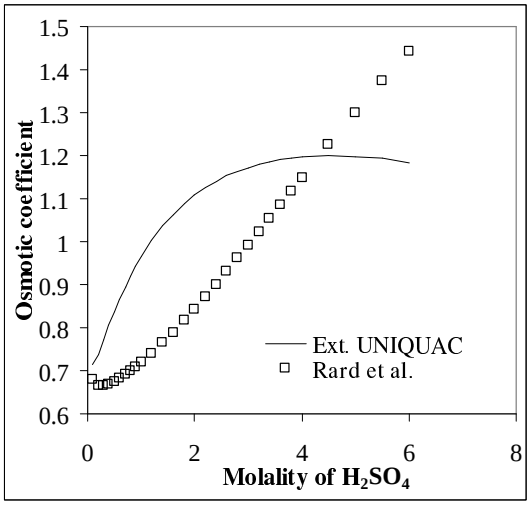

Figure 5-14 The osmotic coefficient of aqueous sulphuric acid solutions at 25°C. The experimental data were not included in the parameter estimation.

Due to the dissociation of the hydrogen sulphate ion, sulphuric acid data such as chemical potential, heat of dilution, and apparent molal heat capacity, can not be extrapolated to infinite dilution by means of the extended Debye-Hückel law by the common method, outlined in chapter 3. The degree of dissociation of the hydrogen sulphate ion as a function of temperature and concentration needs to be determined at the same time as the property being extrapolated in order to use the extended Debye-Hückel law.

The second dissociation constant for sulphuric acid therefore is only known to an accuracy of ±9%! It means that the accepted value (NIST, 1990) of the standard chemical potential of the hydrogen sulphate ion might be inaccurate. In the case of the hydrogen sulphate ion, it might therefore have been justified to include the standard state potential of the hydrogen sulphate ion in the parameter estimation. The

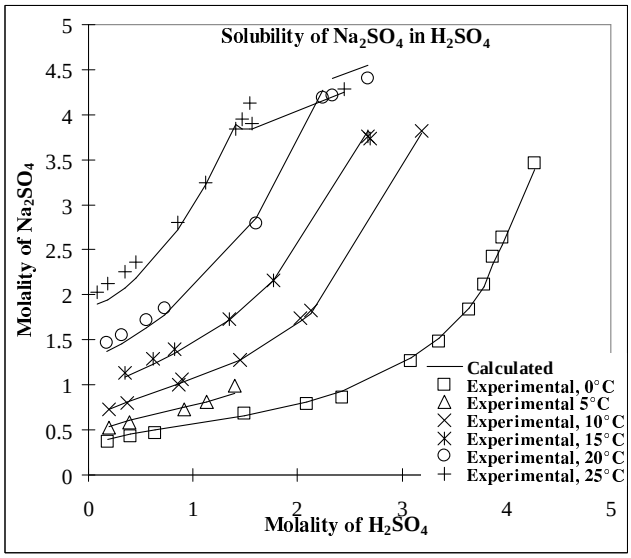

Figure 5-15: The solubility of sodium sulphate in aqueous sulphuric acid at six different temperatures.

same applies to the hydrogen carbonate ion.

Figure 5-15 shows the solubility of sodium sulphate in sulphuric acid solutions. The solid phase is glauber salt at temperatures below 20°C. The transition points where sodium sulphate and glauber salt are in equilibrium with the same liquid are indicated at the 20 and the 25°C curve. The experimental data marked in figure 5-15 are from a number of different sources. The agreement between calculated and experimental solubilities indicates that the water activity in such solutions is predicted correct by the model, as the activity product of glauber salt is $a_{Na^+}^2 a_{SO_4^{2-}} a_w^{10}$! A similar agreement between experimental and calculated solubilities was obtained for sodium, potassium, and ammonium sulphate in sulphuric acid solutions at temperatures between 0 and 100°C.

5.4.3 The peroxodisulphate ion

Parameters for the peroxodisulphate ion were fitted to experimental data for the sodium and ammonium peroxodisulphates in pure water and in sulphuric acid and sulphate solutions. Only 183 experimental data points from six different sources were available. About half of these experimental data were the proprietary property of the FMC Corporation. For this reason, the numerical values of the estimated parameters are not given in this thesis. The experimental data points covered the temperature range from 10 to 40°C.

Due to the limited number of experimental data, the following constraints for the peroxodisulphate ion were made. The r and q parameters were equated, the u_{ii} parameter was not given temperature dependence, and the standard state heat capacity was not estimated, but maintained at the value given by Olofsson *et al.*, 1978, as it was not found in the NIST tables.

Seven model parameters were estimated for this system

- The $r = q$ parameter for the peroxodisulphate ion,
- The interaction energy parameters for the interaction of the peroxodisulphate ion with water, and the sodium, ammonium, sulphate, and hydrogen sulphate ions,
- The u_{ii} parameter for the peroxodisulphate ion.

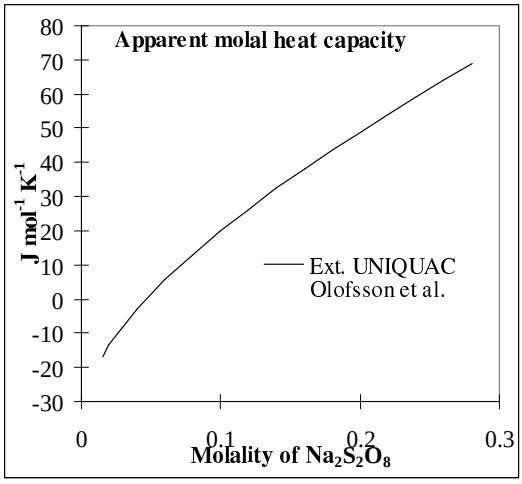

Figure 5-16: The apparent molal heat capacity of sodium peroxodisulphate at 25°C

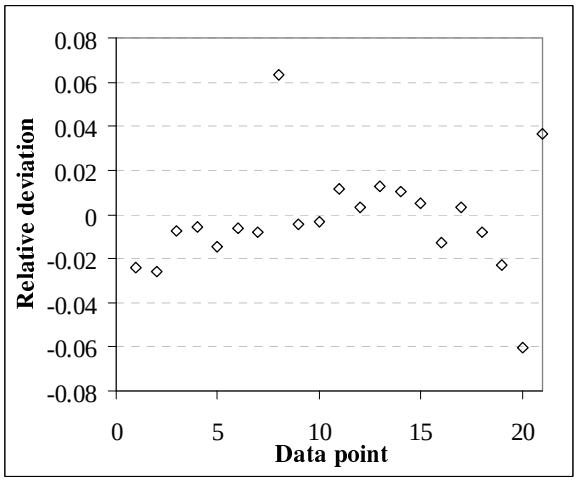

Figure 5-17: The solubility of ammonium peroxodisulphate in aqueous sulphuric acid. Relative deviation.

Five thermodynamic properties were estimated

- The standard state Gibbs energy of formation and heat capacity of $Na_2S_2O_8$ and $(NH_4)_2S_2O_8$
- The standard state enthalpy of formation of $Na_2S_2O_8$.

5.4.3.1 Results

Figure 5-16 shows the calculated apparent molal heat capacity of sodium peroxodisulphate. The experimental data plotted in the same figure are from Olofsson et al., 1978. Relative deviations between calculated and experimental solubilities of ammonium peroxodisulphate in aqueous sulphuric acid at 10, 20, and 30°C are shown in figure 5-17. The relative deviations for the 21 data points are calculated as (experimental weight percent - calculated weight percent)/experimental weight percent.

5.5 Infinite dilution terms

In section 4-3 it was described, that ln to the infinite dilution activity coefficient of the hydrogen ion was set to zero in this work. It was done in order to be able to define the infinite dilution activity coefficient of other ions relative to the value for the hydrogen ion.

Figure 5-18 shows the natural logarithm to the infinite dilution activity coefficients of the ions considered in this work as a function of temperature. It is seen that the cations have positive values, only slightly dependent on temperature, while all anions have negative values, with strong temperature dependence.

Figure 5-19 shows the corresponding values for the parameter set of Henrik Nicolaisen, 1994. Here the cations have negative values, the sulphate ion has positive values, and the chloride ion has negative values. The value for the sulphate ion is almost constant, while those of the three other ions have strong temperature dependency. The parameters from Henrik Nicolaisens work were not estimated relative to any reference ion. By using the hydrogen ion as a reference ion with respect to the infinite dilution activity coefficients, the infinite dilution activity coefficients of other ions obviously attain systematic values (figure 5-18).

An attempt to add the nitrate ion to the parameter set of Henrik Nicolaisen gave an unsatisfactory result (Thomsen, 1994). Henrik Nicolaisen equated the *r* and *q* parameters

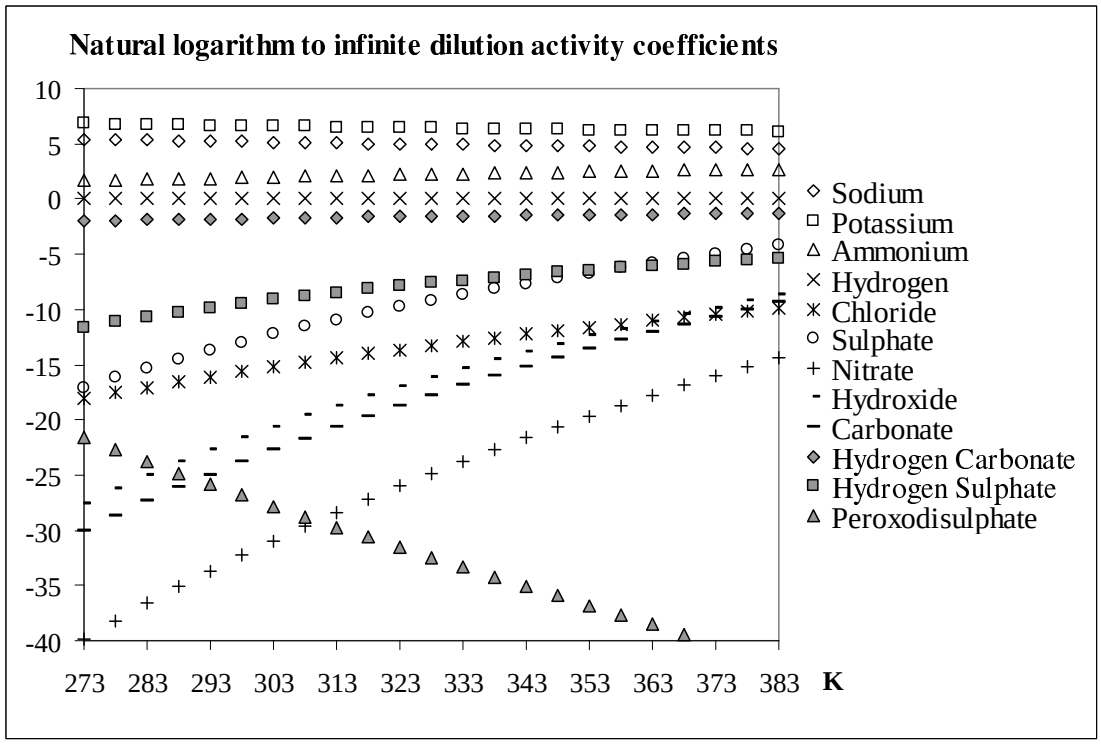

Figure 5-18: The natural logarithm to the infinite dilution activity coefficients of the ions considered in this work, as a function of temperature.

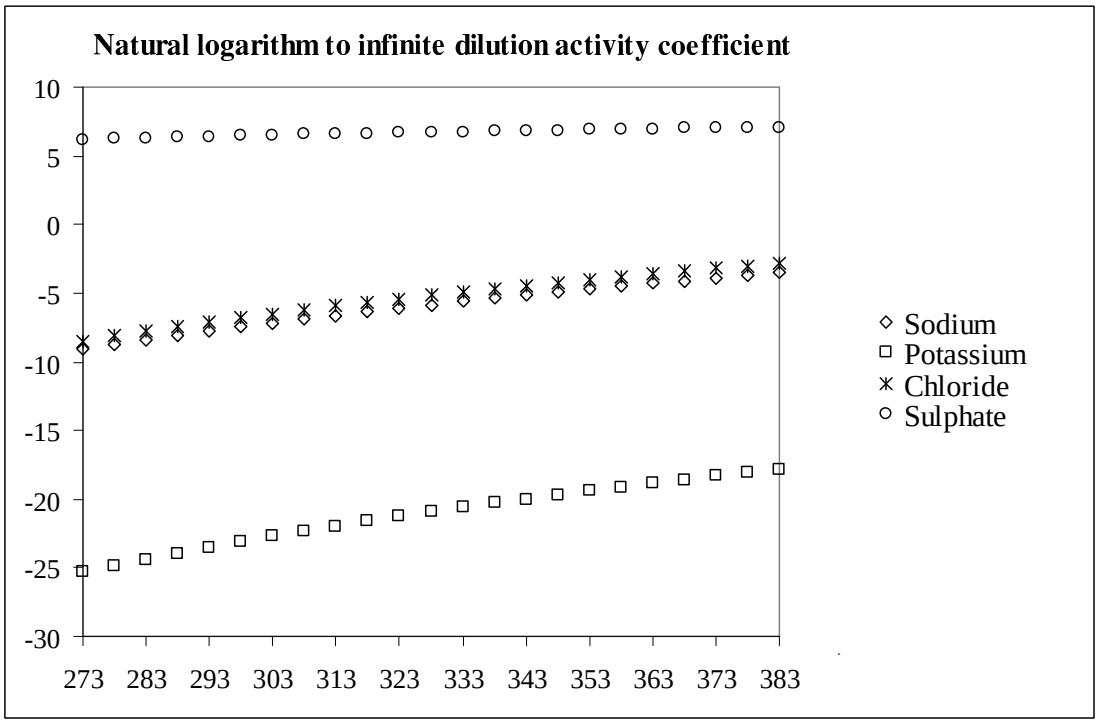

Figure 5-19: The natural logarithm to the infinite dilution activity coefficients, based on the parameters from the work of Henrik Nicolaisen, 1994.

for each ion, and he used fixed values of the u_{ii} parameters for all ions. In this work the values of the r and q parameters have not been related, and the u_{ii} parameters for the anions have been estimated too. The additional parameters, and the use of the hydrogen ion as a reference ion have made the model more flexible, so that it can encompass more ions.

5.6 Heat capacity correlation

The parameters for the heat capacity correlation, equation 2-37, $C^0_{p,i} = a_i + b_i T + \frac{c_i}{T - 200}$ were estimated together with the model parameters based on experimental data. Figure 5-20 shows the correlation result for NaCl. The standard state heat capacity data from Clarke and Glew, 1985, shown in figure 5-20, were *not used* directly for the estimation of the standard state heat capacity parameters. The standard state heat capacity parameters for the sodium and the chloride ions in aqueous solution were estimated from heat capacity data for all salts containing the sodium and the chlo-

ride ions. The standard state heat capacity for NaCl at infinite dilution, depicted in figure 5-20, is the sum of the standard state heat capacities of the sodium and the chloride ions in aqueous solution.

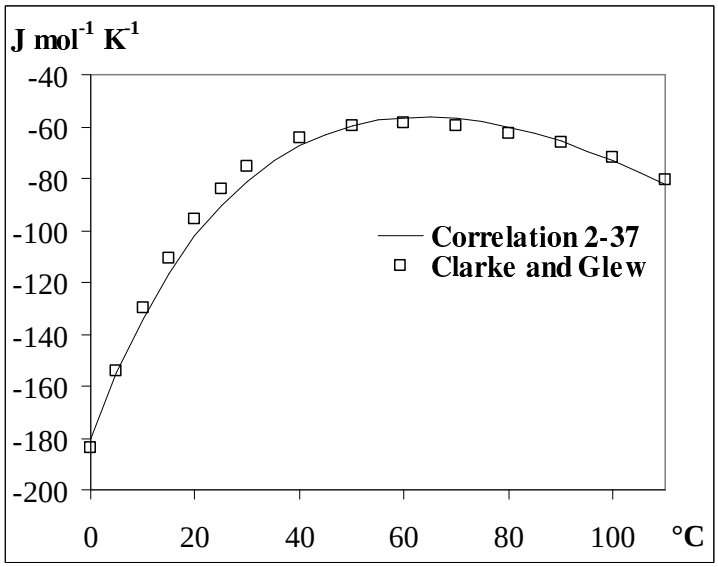

Figure 5-20: The standard state heat capacity of aqueous NaCl as a function of temperature, calculated with correlation 2-37, and compared with data by Clarke and Glew, 1985.

5.7 Parameters

The model parameters obtained by the minimization of the objective function (5-1) are shown in tables 1 to 3. In table 1, the volume and surface area parameters, r and q, for water and the ions are shown along with the a, b, and c parameters for the $C_{p,i}^{0}$ correlation (equation 2-37) yielding $C_{p,i}^{0}$ in J mol^{-1} K^{-1}. The r and q parameters for water were not estimated but are those values assigned to water by Abrams and Prausnitz, 1975. The parameters assigned to the hydrogen ion are explained in section 4-3. Tables 2 and 3 give the values of the estimated interaction energy parameters.

Table 1: UNIQUAC r and q parameters and a_i, b_i, and c_i parameters for $C^0_{p,i}$ (J mol^{-1} K). The values in shaded fields were not estimated.

	r_i	q_i	a_i	b_i	c_i
H_2O	0.9200	1.4000	58.370	0.03896	523.88
H^+	0.13779	10^{-15}	0	0	0
Na^+	1.4034	1.1990	600.62	-1.1006	-23232
K^+	2.2304	2.4306	415.09	-0.8142	-16316
NH_4^+	4.8154	4.6028	71.008	0	0
Cl^-	10.386	10.197	400.35	-1.1312	-18574
SO_4^{2-}	12.794	12.444	643.30	-1.7605	-37903
HSO_4^-	19.588	22.495	647.30	-1.5857	-17536
NO_3^-	5.4041	6.2074	2.2926	0.12110	-9753.2
OH^-	9.3973	8.8171	1418.2	-3.4446	-51473
CO_3^{2-}	11.090	11.320	850.61	-2.8040	-21308
HCO_3^-	3.7550	4.7120	585.75	-1.3612	-21374
$S_2O_8^{2-}$	*	*	-110.00	0	0

Table 2: $u_{ij}^0 = u_{ji}^0$ parameters for calculating UNIQUAC interaction energy parameters ($u_{ij} = u_{ij}^0 + u_{ij}^t(T\text{-}298.15)$). An asterisk replaces parameter values in fields, where the parameter is based on experimental data proprietary to the FMC Corporation. "None" indicates that no parameter has been estimated for this pair. The values in shaded fields were not estimated.

	H_2O	H^+	Na^+	K^+	NH_4^+	Cl^-	SO_4^{2-}	HSO_4^-	NO_3^-	OH^-	CO_3^{2-}	HCO_3^-	$S_2O_8^{2-}$
H_2O	0												
H^+	10^5	0											
Na^+	733.286	10^{10}	0										
K^+	535.023	10^{10}	-46.194	0									
NH_4^+	54.0297	10^{10}	375.977	184.288	0								
Cl^-	1523.39	10^{10}	1443.23	1465.18	1385.31	2214.81							
SO_4^{2-}	752.879	10^{10}	845.135	913.824	677.178	2036.06	1265.83						
HSO_4^-	602.252	10^{10}	469.488	445.673	418.886	None	1004.16	822.989					
NO_3^-	998.920	10^{10}	797.474	818.568	807.246	2175.02	1757.79	None	2753.71				
OH^-	600.495	10^{10}	1398.14	1805.75	2500.0	1895.52	1225.67	2500.0	1379.95	1562.88			
CO_3^{2-}	328.141	10^{10}	476.956	1370.57	None	2372.94	1158.91	2500.0	None	1339.04	1065.97		
HCO_3^-	118.702	10^{10}	980.982	1123.44	None	2014.18	956.609	2500.0	None	2500.0	565.786	253.461	
$S_2O_8^{2-}$	*	10^{10}	*	None	*	None	*	*	None	2500.0	None	None	*

Table 3: $u_{ij}^t = u_{ji}^t$ parameters for calculating UNIQUAC interaction energy parameters ($u_{ij} = u_{ij}^0 + u_{ij}^t(T\text{-}298.15)$). An asterisk replaces parameter values in fields, where the parameter is based on experimental data proprietary to the FMC Corporation. "None" indicates that no parameter has been estimated for this pair. The values in shaded fields were not estimated.

	H_2O	H^+	Na^+	K^+	NH_4^+	Cl^-	SO_4^{2-}	HSO_4^-	NO_3^-	OH^-	CO_3^{2-}	HCO_3^-	$S_2O_8^{2-}$
H_2O	0												
H^+	0	0											
Na^+	0.4872	0	0										
K^+	0.9936	0	0.1190	0									
NH_4^+	0.5855	0	-0.2920	1.0985	0								
Cl^-	14.631	0	15.635	15.329	14.848	14.436							
SO_4^{2-}	9.4905	0	11.681	12.278	10.356	12.407	8.3194						
HSO_4^-	5.5499	0	6.5329	5.2231	5.1053	None	8.7877	5.7939					
NO_3^-	9.3251	0	9.3047	10.302	9.9705	13.449	6.9013	None	2.2866				
OH^-	8.5455	0	20.278	27.283	None	13.628	8.5902	0	6.6369	5.6169			
CO_3^{2-}	-0.5059	0	2.8191	5.0517	None	8.9402	6.7255	0	None	3.8129	-4.4653		
HCO_3^-	0.9600	0	13.296	2.7217	None	11.636	8.6656	0	None	0	-1.2033	1.2824	
$S_2O_8^{2-}$	*	0	*	None	*	None	*	*	None	0	None	None	*

5.8 *Thermodynamic properties*

The thermodynamic properties estimated from the experimental data are shown in table 4.

Table 4: Thermodynamic properties estimated from experimental data. The values in shaded fields were not estimated but assigned as fixed values due to insufficient data. "None" indicates that the property could not be estimated due to insufficient data. Values in brackets were not estimated, but were found in the NIST tables. The two salts with 1½ hydrate water had their stoichiometric coefficients multiplied by two in order to maintain integer stoichiometric coefficients. The thermodynamic properties of these salts should therefore be divided by two in order to reflect the chemical formula (indicated by asterisk).

	ΔG_f^0 (kJ mol^{-1})	ΔH_f^0 (kJ mol^{-1})	C_p (Jmol^{-1} K^{-1})
Na_2SO_4•$10H_2O$	{-3646.85}	{-4327.26}	492.2
$NaK_3(SO_4)_2$	-2622.82	{-2854.62}	287.5
$NaNO_3$•Na_2SO_4•H_2O	-1876.74	-2152.96	300
Na_2CO_3•$2Na_2SO_4$	-3593.19	-3921.49	840.07
Na_2CO_3•$NaHCO_3$•$2H_2O$	-2380.11	{-2684.9}	256.80
Na_2CO_3•$3NaHCO_3$	-3602.78	{-3982.7}	182.03
K_2CO_3•$1½H_2O$	{-2865.00*}	{-3218.40*}	1199.0*
$KHCO_3$	-868.70	{-963.20}	85.51
$NaKCO_3$•$6H_2O$	-2495.69	-2920.78	300
K_2CO_3•Na_2CO_3	-2121.47	{-2299.1}	420.23
K_2CO_3•$NaHCO_3$•$2H_2O$	-2410.63	-2718.66	300
K_2CO_3•$2KHCO_3$•$1½H_2O$	-6341.55*	-7026.36*	193.74*
$(NH_4)_2SO_4$•$3NH_4NO_3$	-1454.53	-2278.72	987.19
$(NH_4)_2SO_4$•$2NH_4NO_3$	-1270.61	-1914.10	764.42
Na_2SO_4•$(NH_4)_2SO_4$•$4H_2O$	-3127.82	-3752.02	874.92
$2NaNO_3$•NH_4NO_3	-920.19	None	None
$3KNO_3$•NH_4NO_3	-1366.4	None	None
$Na_2S_2O_8$	-1638.13	-1893.64	665.38
$(NH_4)_2S_2O_8$	-1273.60	{-1648.1}	569.60

5.9 Comment

The procedure for estimating parameters for the core system of ions, described in section 5.2.3 is very difficult, and maybe impossible to reproduce. Another procedure that yields other numerical values of the parameters, but with the same agreement between experimental and calculated data is therefore suggested.

Instead of initially fixing the values of the surface area parameters for the anions and estimating the three remaining parameters, the u_{ii} parameter for the anions should initially be fixed at for example 2500 at all temperatures. The three parameters to estimate for an anion are then the volume and surface area parameters, and the water-anion interaction energy parameter. These parameters are estimated from experimental data for the acid corresponding to the anion.

When cations are added, the surface area parameters of the cations should also not be given fixed values initially. The volume and surface area parameters for the cations and the interaction energy parameters for all the cation-water and cation-anion interactions can be estimated simultaneously. When the objective function cannot be minimized further, all parameters for the system are estimated simultaneously, including the u_{ii} parameters for the anions.

This method was tested on the system, H^+-Na^+-K^+-NH_4^+-Cl^--NO_3^--H_2O with the u_{ii} parameters for the anions given an initial value of 2500. It was not tested whether or not the result of the parameter estimation depended on the initial value of the u_{ii} parameters for the anions.

6. Phase diagrams

This chapter is a rewriting of the first part of the article "Simulation and optimization of fractional crystallization processes" by Kaj Thomsen, Peter Rasmussen and Rafiqul Gani, submitted for publication to Chemical Engineering Science in the spring of 1997.

The computer program IVC-ELEC was developed for the calculation and display of phase diagrams and activity coefficients/thermal properties of electrolyte solutions based on an activity coefficient model. Presently the Extended UNIQUAC model is the only activity coefficient model implemented in the program. IVC-ELEC also contains a process simulator and optimizer for electrolyte processes. This feature was described in the second part of the above article. In this thesis, the feature is described in chapter 8.

IVC-ELEC is designed so that all output from the program can easily be imported into a spreadsheet for further treatment and display.

6.1 Introduction

The design, simulation, and optimization of fractional crystallization processes for electrolyte mixtures require a detailed knowledge of the phase equilibria for such systems. Fitch, 1970, described a graphical method for the design of fractional crystallization processes based on phase diagrams from solubility data. Cisternas and Rudd, 1993, suggested methods for identifying optimal process designs for fractional crystallization processes, also based on phase diagrams from solubility data.

The amount of solubility data available in the open literature is very limited and the quality of the data is questionable. The use of phase diagrams based on experimental solubility data alone will therefore be of limited scope in the design, simulation and optimization of electrolyte processes.

Berry and Ng, 1996, recognized the need for phase diagrams at various temperatures for design of fractional crystallization processes. The method suggested by Berry and Ng for calculating quaternary phase diagrams however requires that the activity coefficients at the two- and three-salt saturation points either are known *a priori* or are set equal to one. In this work, no such assumptions are made because the two- and three-salt

saturation points are calculated directly through the Extended UNIQUAC activity coefficient model.

An important function of phase diagrams is to be a visual tool for verifying the calculations and predictions of a thermodynamic model by comparing calculated phase diagrams with experimental ones. IVC-ELEC gives the user the option of retrieving experimental data from the IVC-SEP electrolyte databank (IVC-SEP, 1997) and display the experimental data along with the calculated phase diagram.

Phase diagrams may also be considered visual tools, which can be employed to design fractional crystallization processes. Information on which salt(s) can be encountered in a given electrolyte system as a function of temperature is important for the design of such processes. Also the process paths for fractional crystallization processes can be displayed in phase diagrams. Phase diagrams may thus be used to verify and analyze proc-

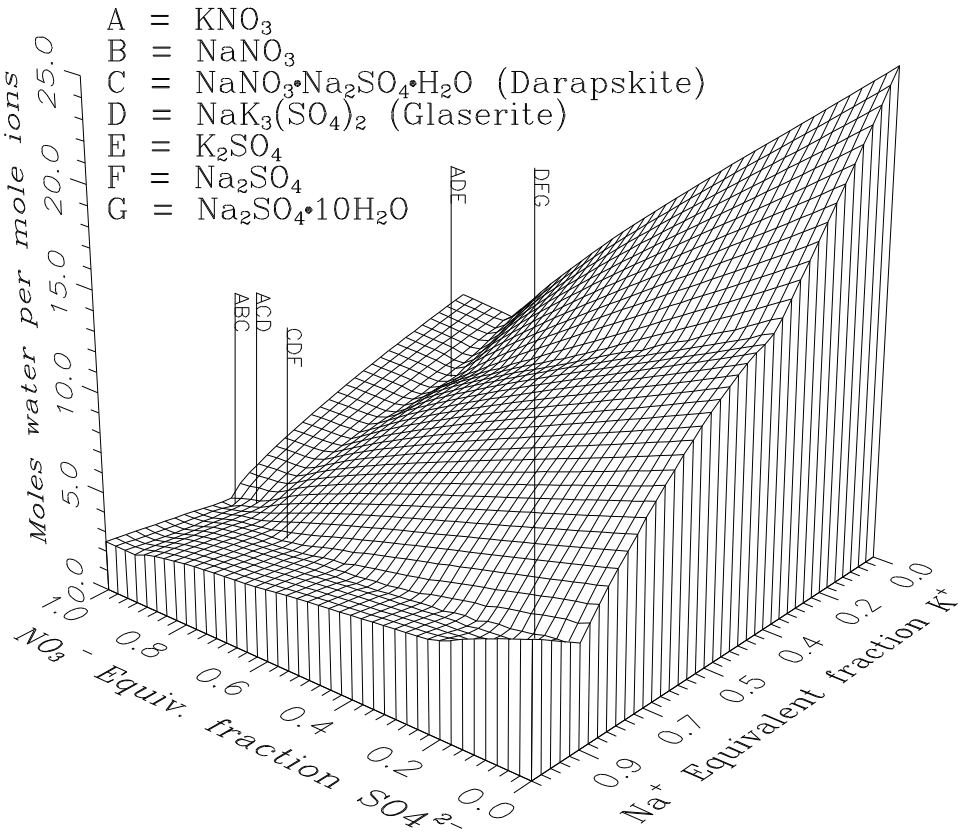

Figure 6-1:Three-dimensional quaternary phase diagram for the (Na^+, K^+, NO_3^-, SO_4^{2-}, H_2O) system at 30°C

ess simulation and optimization results. For systems with more than four ions however, the use of phase diagrams becomes impractical.

In this chapter, a method for the calculation of various types of phase diagrams for aqueous electrolyte systems is outlined.

6.2 *Calculation of phase diagrams*

In section 2.4, it was explained that the equilibrium between an aqueous phase and the solid salt $K_\kappa A_\alpha \cdot nH_2O\ (s)$ consisting of κ cations K, α anions A, and n water molecules can be described by the equation

$$K_\kappa A_\alpha nH_2O\,(s) \leftrightarrow \kappa\,K\,(aq) + \alpha\,A\,(aq) + n\,H_2O \qquad \textbf{(2-30)}$$

At equilibrium, the composition of the liquid phase can be calculated from equation (2-

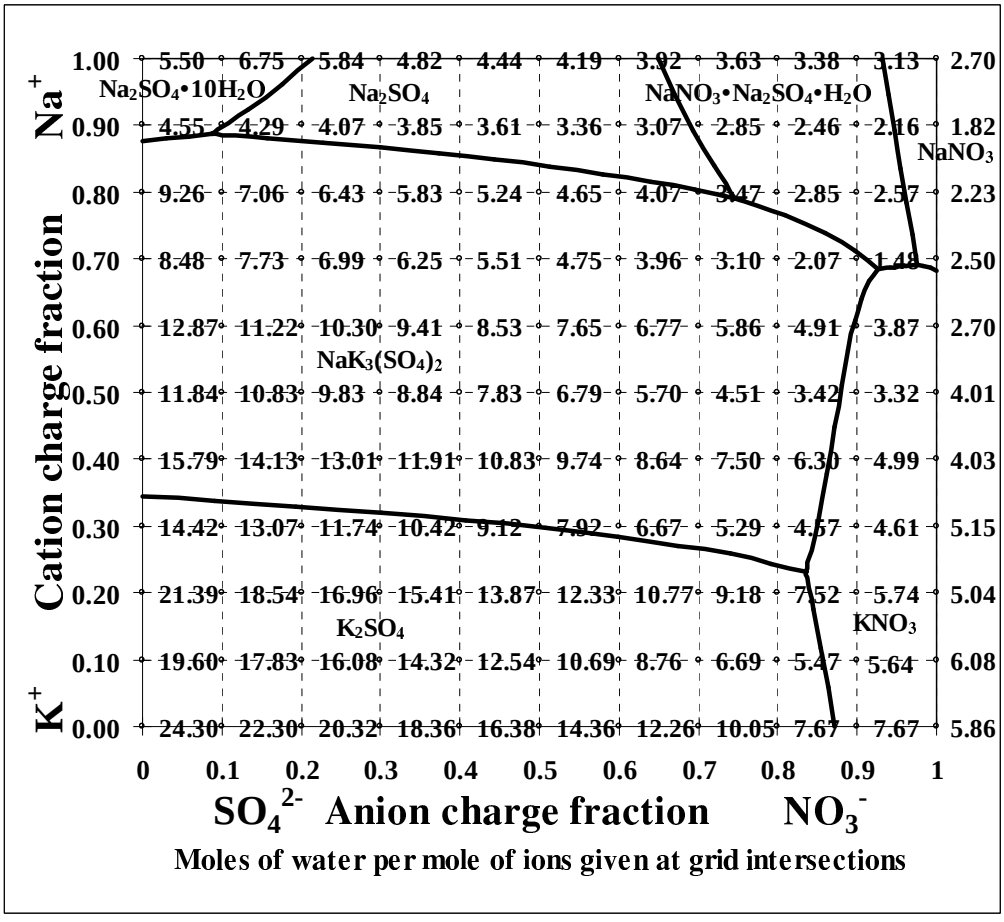

Figure 6-2: Jänecke projection of quaternary phase diagram for the (Na^+, K^+, NO_3^-, SO_4^{2-}, H_2O) system at 30°C

40). An *s*-salt saturation point has to fulfil the condition (2-40) for all *s* salts:

$$K_k = \prod_i a_i^{\nu_{k,i}}, \quad k = 1..s \tag{2-40}$$

while for all other salts potentially formed by the system:

$$K_k > \prod_i a_i^{\nu_{k,i}}, \quad k > s \tag{2-41}$$

In equations 2-40 and 2-41 $\nu_{k,i}$ is the stoichiometric coefficient of component *i* in salt *k*. Equation 2-40 is solved by a full Newton-Raphson method using analytical composition derivatives of the activity coefficients. The *s* iteration variables are the amounts of each of the *s* salts in the saturation point. The chemical equilibria in the solution, due to hydrolysis/dissociation/association reactions, all have to fulfil equation 2-40. Thus, the number of iteration variables is incremented for each equilibrium reaction present in the system. In section 6.3 the expressions for the jacobian matrix for a system of SLE and chemical equilibria equations are given.

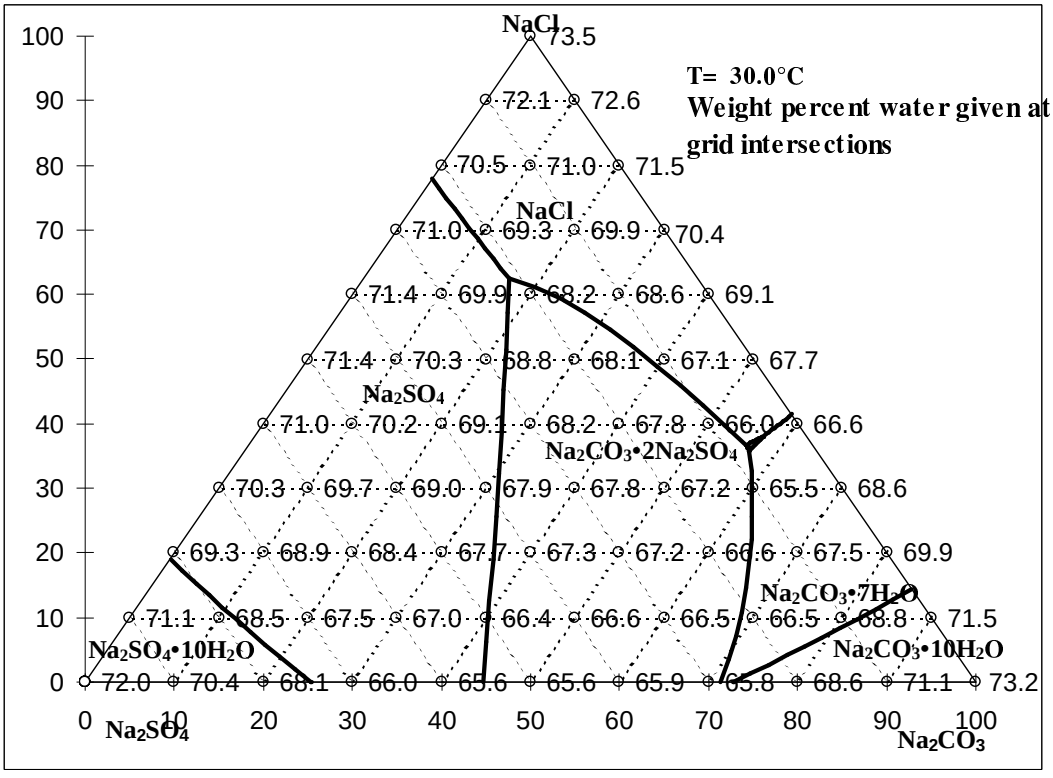

Figure 6-3: Triangular diagram for the quaternary system (Na^+, Cl^-, SO_4^{2-}, CO_3^{2-}, H_2O) at 30°C. The unit is weight percent.

6.2.1 Saturation points at fixed temperature

The curves in a phase diagram at a fixed temperature for solvent + n ions mark the compositions of the liquid phase in equilibrium with n-2 solid phases. Curve intersections mark the compositions of the liquid phase in equilibrium with n-1 solid phases. Some systems have one or more invariant points. i.e. one or more temperatures where a liquid phase can be in equilibrium with n solid phases. At the invariant point, a curve intersection thus marks the composition of a liquid phase in equilibrium with n solid phases.

The calculation of phase diagrams starts with locating all curve intersections in the diagram. For a quaternary system (n = 4), curve intersections are three-salt saturation points (figures 6-1, 6-2 and 6-3). All combinations of three salts possibly formed by the system are examined. If any combination of three salts satisfies the conditions (2-40) and (2-41) with s equal three, a three-salt saturation point is found.

After the curve intersections in the phase diagrams are found, two-salt saturation points

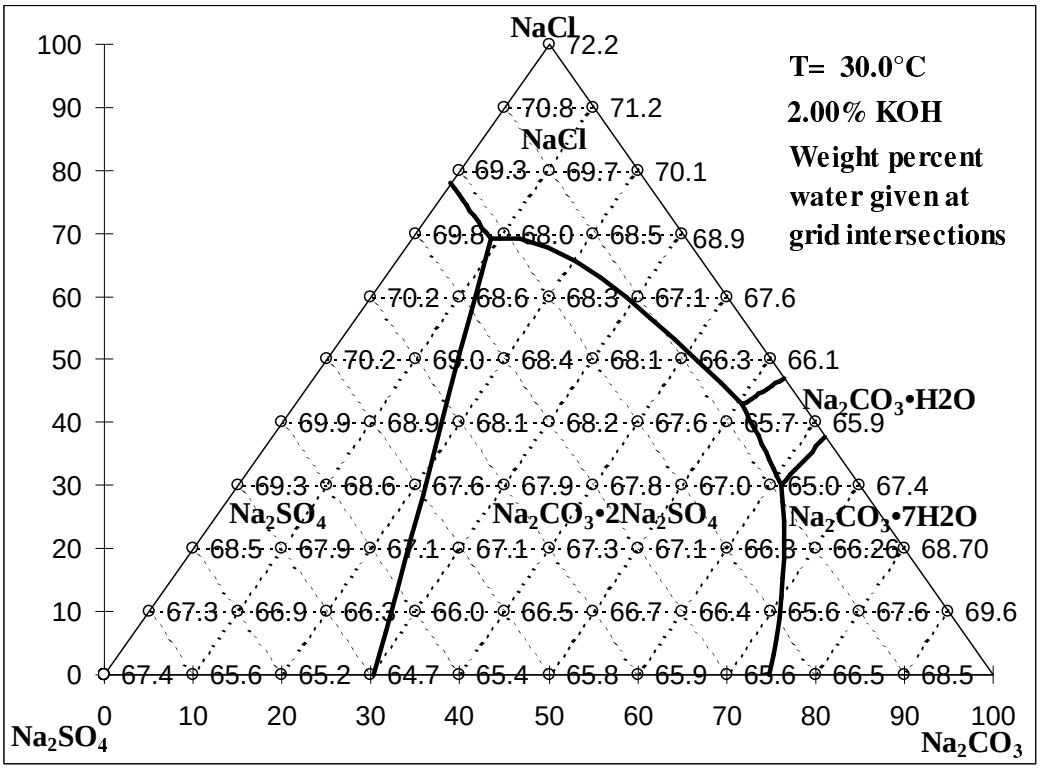

Figure 6-4: Same phase diagram as in figure 6-3, but with a constant concentration of two weight percent potassium hydroxide everywhere in the diagram.

on the edges of the diagrams are located. The edges of quaternary phase diagrams are ternary systems (figures 6-2 and 6-3). The two-salt saturation points are found, as combinations of two salts satisfying (2-40) and (2-41) with *s* equal two.

At this point, we know which salts form three-salt saturation points in the interior of the phase diagram and which salts form two-salt saturation points on the edges of the diagram. Next, this information is analyzed to determine which points are connected to each other by a curve. We know the composition of the liquid phase at both ends of each phase diagram curve. A suitable number of points on a straight line joining the ends of the curve provide initial guesses for calculating the exact location of the curve. Finally, single salt saturation concentrations are calculated in a number of points to determine the solubility surfaces.

Figure 6-1 shows the three dimensional quaternary phase diagram for the (Na^+, K^+, NO_3^-, SO_4^{2-}, H_2O) system at 30°C. This type of diagram is not very practical to work with due to its three dimensional nature. Figure 6-2 shows the same diagram as a Jänecke projection (Jänecke, 1906). At all grid intersections, the number of moles water

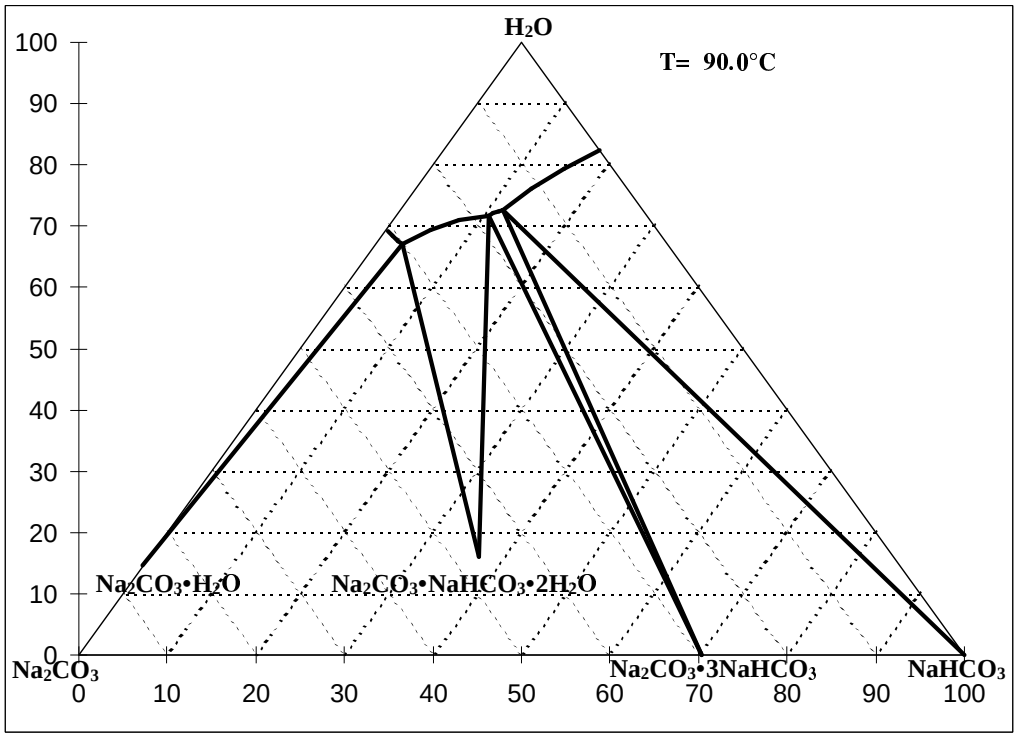

Figure 6-5: Ternary solubility diagram for the sodium carbonate-bicarbonate system at 90°C, the unit is weight percent

per mole of ions is indicated. In this way, figure 6-2 provides the same information as figure 6-1, and is much easier to work with.

For quaternary systems with either three anions and one common cation or three cations and one common anion the quaternary phase diagram becomes triangular. The calculation of curve intersections and curves in this sort of diagrams follows the same pattern as described above for the quadratic phase diagram. A triangular phase diagram for a quaternary system is shown in figure 6-3. Note that in figure 6-3 the water content is shown in weight per cent of the saturated solution while the relative amounts of salts are given in weight per cent on dry basis.

Figure 6-4 is a phase diagram at the same temperature and with the same components as the phase diagram in figure 6-3. In figure 6-4, however, there is a constant concentration of two weight percent potassium hydroxide everywhere in the phase diagram. Figure 6-4 is therefore a phase diagram with six components. As it appears from figure 6-4, the

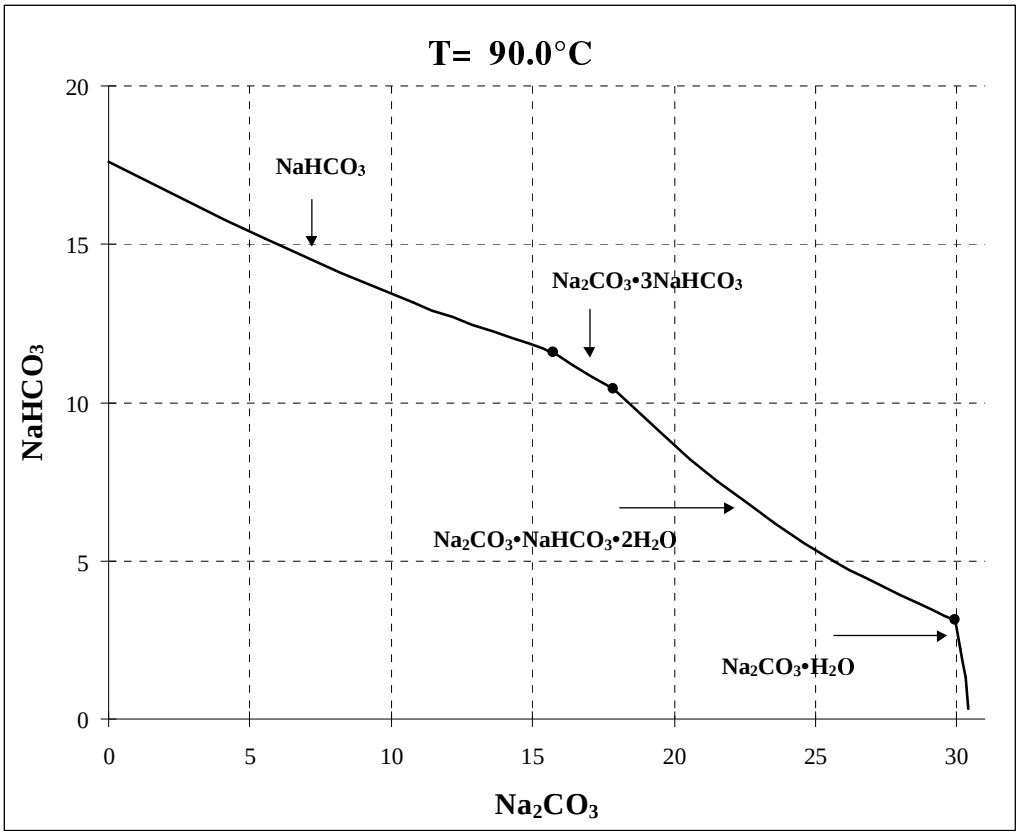

Figure 6-6: Same as figure 6-5 but in orthogonal coordinates. Two-salt saturation points are marked by dots.

addition of two weight percent potassium hydroxide has the effect that the two decahydrates disappear from the phase diagram, and the field representing the monohydrate of sodium carbonate, which is barely visible in figure 6-3, becomes larger. IVC-ELEC offers the option of calculating any of the available phase diagram types with a constant concentration of another salt.

The calculation procedure for ternary phase diagrams is the same as that for quaternary phase diagrams. The ternary phase diagram can optionally be calculated as a triangular or an orthogonal diagram (figures 6-5 and 6-6). In figure 6-5, help lines that point to the solid phase in equilibrium with the liquid phase for each segment of the solid-liquid equilibrium curve is included. By including these help lines, it is easier to see, which segments of the equilibrium curve correspond to specific solid phases. The help lines are optionally included by the IVC-ELEC program. The corresponding orthogonal phase diagram in figure 6-6 does not give this information, but might be more practical than the triangular diagram in terms of displaying the solubility limits.

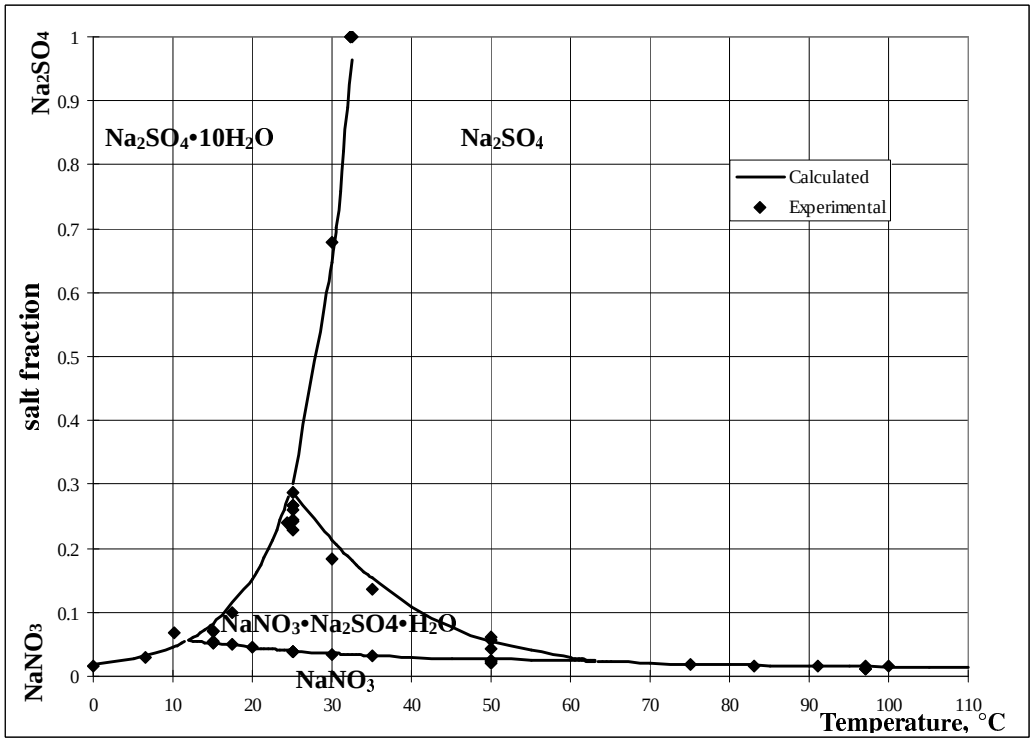

Figure 6-7: Temperature/Two-salt saturation point diagram for sodium nitrate/sulphate. Experimental data are marked with diamonds.

6.2.2 Saturation points at varying temperature

When saturation points are plotted in a phase diagram as a function of temperature, the curves in a solvent + n ions system mark the compositions of the liquid phase in equilibrium with n-1 solid phases. Curve intersections mark the compositions of the liquid phase in equilibrium with n solid phases.

The temperature/two-salt saturation point diagram shown in figure 6-7 is a good source of information when designing fractional crystallization processes. The pictured system is ternary and curves thus connect the two-salt saturation points at different temperatures. This diagram shows all the phases that can be encountered in the ternary system over a temperature range. In figure 6-7, the phase diagram predicted by the Extended UNIQUAC model is compared with experimental data (from the IVC-SEP electrolyte databank) for the ternary system sodium-nitrate/sulphate.

The temperature/two-salt saturation point phase diagram shows the relative concentrations of two salts rather than concentrations. The unit “salt fraction” in figure 6 is on

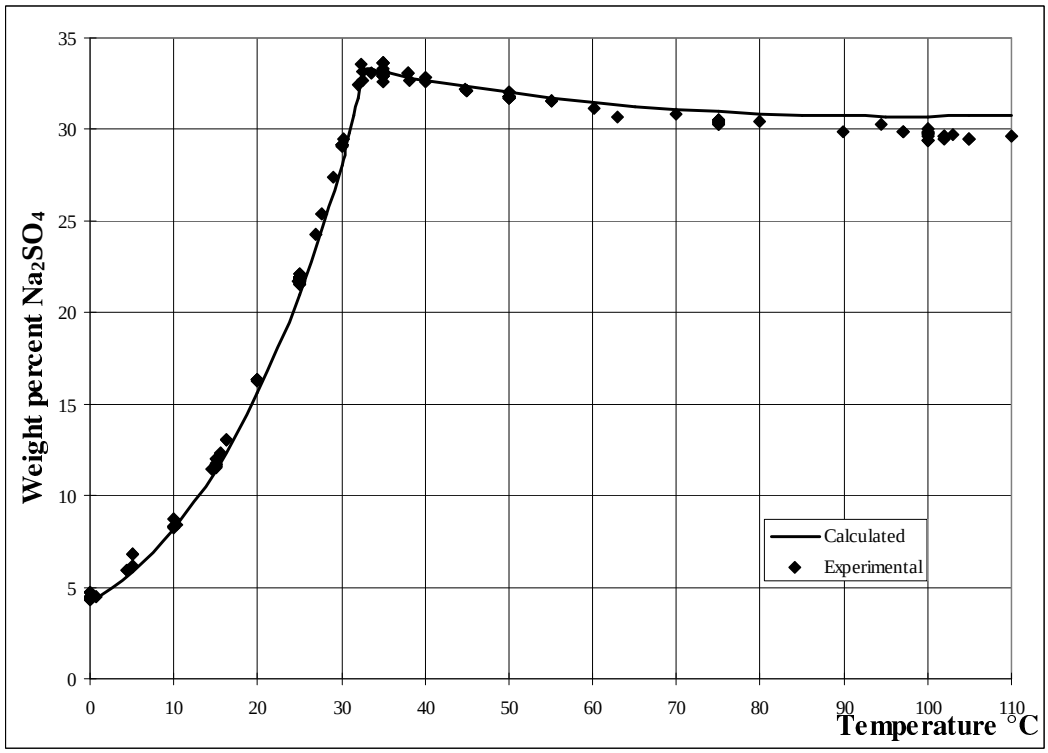

Figure 6-8: The solubility of Na_2SO_4 as a function of temperature. Experimental data marked with diamonds.

equivalent basis, i.e.

$$salt\ \ fraction\ Na_2SO_4 = \frac{2m_{Na_2SO_4}}{2m_{Na_2SO_4} + m_{NaNO_3}} \tag{6-1}$$

where m_k is the molality of salt *k*. In conjunction with binary solubility diagrams however, this type of diagram also serves as a verification of the thermodynamic model being used.

An example of a binary solubility diagram is shown in figure 6-8. Also in this case, experimental binary solubility data have been retrieved from the databank and displayed along with the calculated curve. The abrupt change in the direction of the solubility curve in figure 6-8 at 32°C is due to an *invariant point* at this temperature. In the aqueous sodium sulphate system, there are two independent components, which according to Gibbs phase rule allows a maximum of four different phases simultaneously. At 32°C, Na_2SO_4 (s), and Na_2SO_4•10H2O (s) are in equilibrium with a liquid phase and a vapour phase. Thus no degree of freedom is left in this system, and the point is called an invariant point.

6.3 Equilibrium calculations

For the salt in equation 2-30, the equilibrium condition can be written

$$\begin{aligned} K_{\mathrm{K}_\kappa\mathrm{A}_\alpha nH_2O} &= a_{\mathrm{K}}^{\kappa} a_{\mathrm{A}}^{\alpha} a_{H_2O}^{n} = \left(m_{\mathrm{K}} x_w f_{\mathrm{K}}^{\nabla}\right)^{\kappa} \left(m_{\mathrm{A}} x_w f_{\mathrm{A}}^{\nabla}\right)^{\alpha} \left(x_w f_w\right)^{n} \\ &= M_w^{-(\kappa+\alpha)} \left(x_{\mathrm{K}} f_{\mathrm{K}}^{\nabla}\right)^{\kappa} \left(x_{\mathrm{A}} f_{\mathrm{A}}^{\nabla}\right)^{\alpha} \left(x_w f_w\right)^{n} \end{aligned} \tag{6-2}$$

The conversion from molalities to mole fractions is based on equation 2-20. M_w is the molar mass of water (kg mol^{-1}). On logarithmic form the expression becomes:

$$\ln\left(K_{\mathrm{K}_\kappa\mathrm{A}_\alpha nH_2O}\right) = \sum_{w+i} \nu_i \ln\left(x_i f_i\right) - (\kappa+\alpha)\ln M_w \tag{6-3}$$

In equation 6-3 and in the rest of this section, for simplicity the same symbol, f_i, is used for both the symmetrical and the unsymmetrical rational activity coefficients.

The function

$$g = \sum_{w+i} \nu_i \ln\left(x_i f_i\right) - (\kappa+\alpha)\ln M_w - \ln\left(K_{\mathrm{K}_\kappa\mathrm{A}_\alpha nH_2O}\right) \tag{6-4}$$

is formed. g equals zero at equilibrium. It is desired to find an expression for the derivative of g with respect to the reaction coordinate (extent of reaction) of an equilibrium reaction. This equilibrium reaction can be a solid-liquid equilibrium like the reaction in equation 2-30 or a hydrolysis/association/dissociation equilibrium like the dissociation of the hydrogen sulphate ion, described in equation 2-43. The components of this equilibrium reaction are indexed with j. By applying the chain rule the following expression is obtained:

$$\frac{dg}{d\varepsilon} = \sum_{w+j} \left[\frac{\partial g}{\partial n_j} \right]_{n_k, k \neq j} \cdot \frac{dn_j}{d\varepsilon} = \sum_{w+j} \left[\frac{\partial g}{\partial n_j} \right]_{n_k, k \neq j} \nu_j \qquad \textbf{(6-5)}$$

Here ε is the reaction coordinate with respect to which the differentiation is taking place. ν_j is the stoichiometric coefficient of component j.

Partial differentiation of equation 6-4 with respect to moles of component j yields:

$$\frac{\partial g}{\partial n_j} = \sum_{w+i} \nu_i \left(\left[\frac{\partial (\ln f_i)}{\partial n_j} \right]_{n_k, k \neq j} + \frac{\left[\frac{\partial x_i}{\partial n_j} \right]_{n_k, k \neq j}}{x_i} \right) = \sum_{w+i} \nu_i \left(\left[\frac{\partial (\ln f_i)}{\partial n_j} \right]_{n_k, k \neq j} - \frac{1}{n} + \frac{\delta_{ij}}{n_i} \right) \qquad \textbf{(6-6)}$$

δ_{ij} is Kroneckers delta, n is the total number of moles. The values of $\left[\frac{\partial \ln f_i}{\partial n_j} \right]_{n_k, k \neq j}$ are obtained directly from the thermodynamic routines. Applying equation 6-5, one obtains the expression for the derivative of g with respect to the reaction coordinate:

$$\frac{dg}{d\varepsilon} = \sum_{w+i} \sum_{w+j} \nu_i \nu_j \left(\left[\frac{\partial (\ln f_i)}{\partial n_j} \right]_{n_k, k \neq j} - \frac{1}{n} + \frac{\delta_{ij}}{n_i} \right) \qquad \textbf{(6-7)}$$

For a system of equilibrium reactions, the expression becomes:

$$\frac{dg_k}{d\varepsilon_h} = \sum_{w+i} \sum_{w+j} \nu_{k,i} \nu_{h,j} \left(\left[\frac{\partial (\ln f_i)}{\partial n_j} \right]_{n_k, k \neq j} - \frac{1}{n} + \frac{\delta_{ij}}{n_i} \right) \qquad \textbf{(6-8)}$$

$\nu_{k,i}$ is the stoichiometric coefficient of component i in reaction k. ε_h is the reaction coordinate of reaction h. This is the expression being used in IVC-ELEC to set up the jacobian matrix before solving a system of solid-liquid-equilibrium and chemical equilib-

rium equations. One advantage by using reaction coordinates rather than the amounts of ions as iteration variables is that electroneutrality is automatically maintained.

7. Correlation results

In this chapter, the results of the parameter estimation for the Extended UNIQUAC model is presented in terms of phase diagrams for some representative systems.

7.1 Single salt solubility

Figure 7-1 shows the calculated solubility of some of the salts for which parameters have been estimated in this work. Experimental data from a large number of sources are plotted together with the calculated curves. In most cases, the difference between cal-

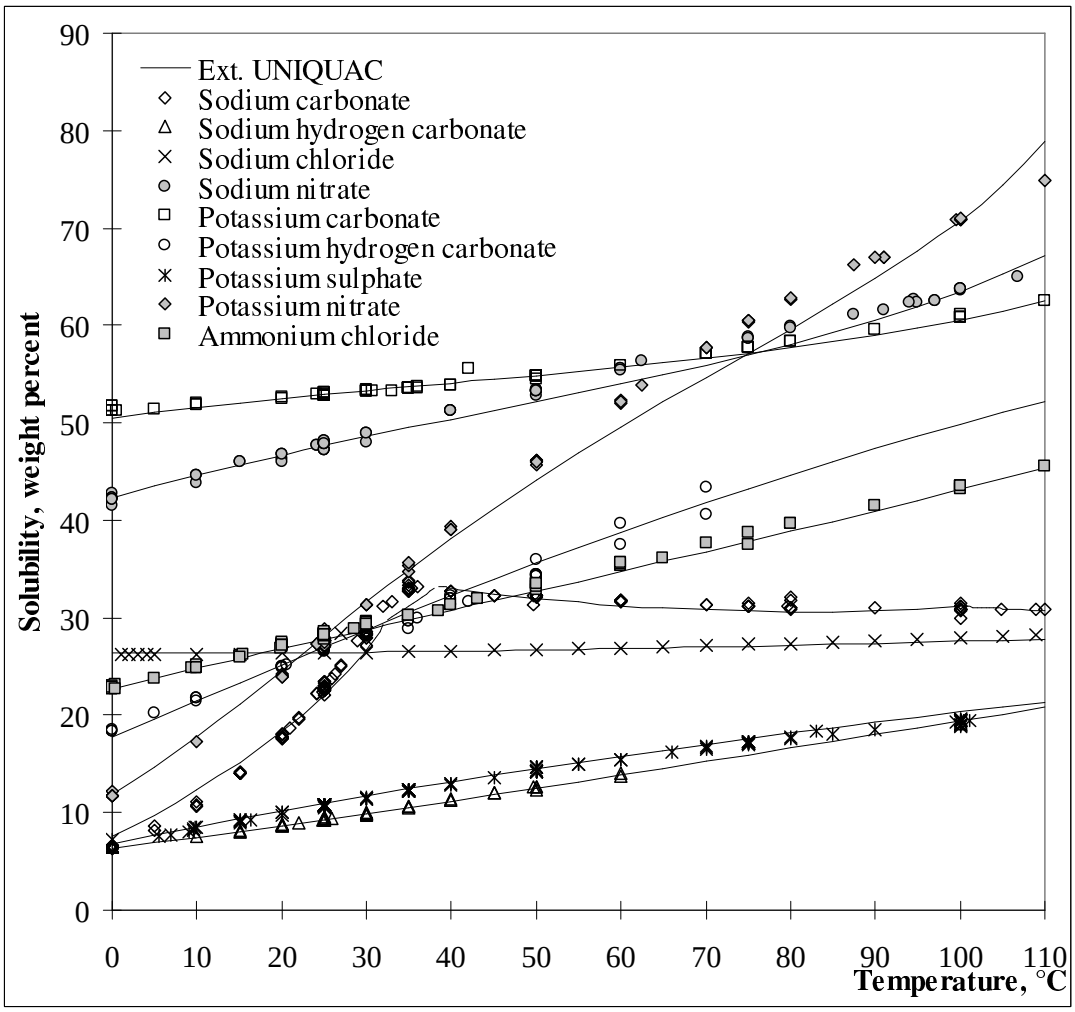

Figure 7-1: The solubility of some salts as a function of temperature. Experimental data from a large number of sources are plotted together with the calculated curves..

culated and experimental values is less than one weight percent.

The particular shape of the solubility curve for sodium carbonate indicates the four different degrees of hydration for sodium carbonate in the temperature range considered. The decahydrate of sodium carbonate is formed at temperatures below 32°C. Between 32 and 35.4°C the heptahydrate is formed. The monohydrate is formed between 35.4 and 109°C, and at temperatures above 109°C, the anhydrate is formed.

7.2 Ternary solubility diagrams

In figure 7-2, the calculated phase diagram for the ternary system H_2O, Na_2SO_4, K_2SO_4 at 35°C is shown together with experimental data. In figure 7-3, the phase diagram for the system H_2O, Na_2CO_3, K_2CO_3 at 25°C is shown. The solid phase $NaKCO_3•6H_2O$ in figure 7-3 is the salt representing the solid solution formed in this system. The experimental data for these systems come from several different sources.

Instead of displaying all the ternary systems at every temperature, temperature/two-salt saturation point diagrams can be used to show the phase behaviour of ternary systems over a temperature range.

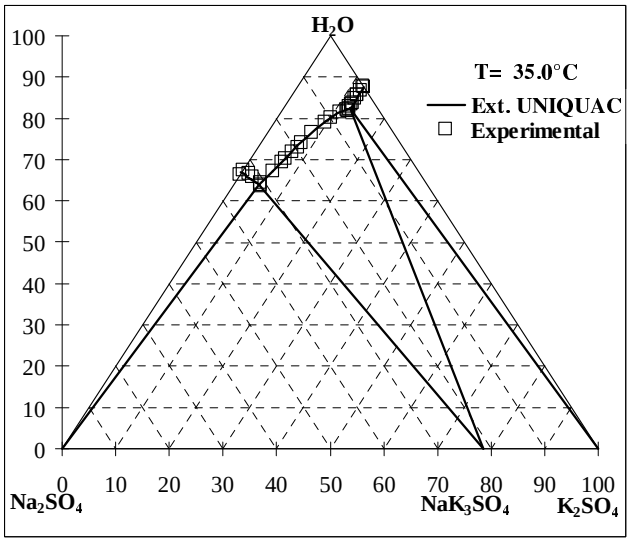

Figure 7-2: Phase diagram for the ternary system H_2O, Na_2SO_4, K_2SO_4 at 35°C.

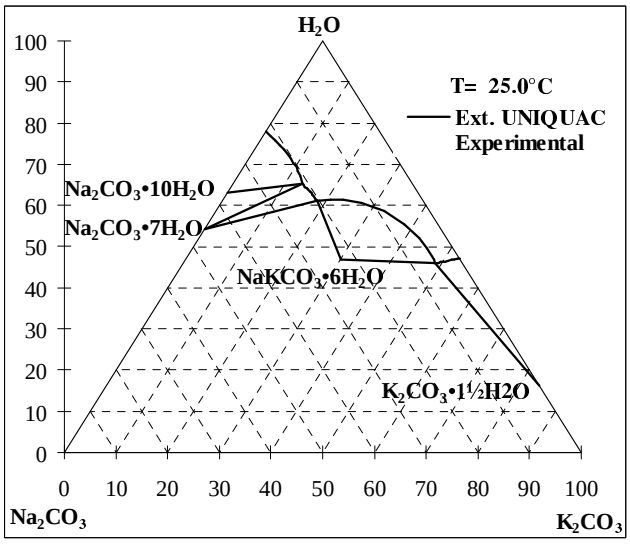

Figure 7-3: Phase diagram for the ternary system H_2O, Na_2CO_3, K_2CO_3 at 25°C

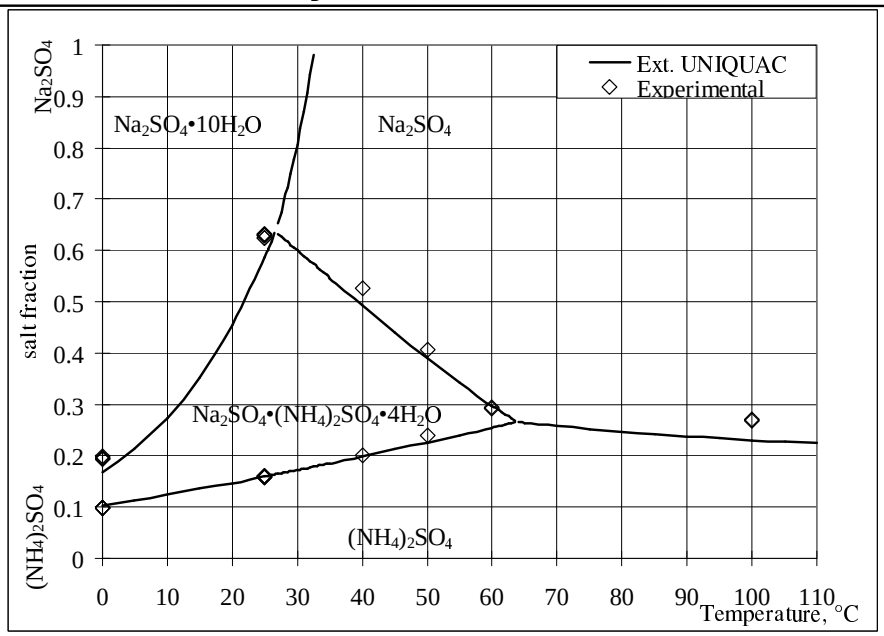

Figure 7-4: Temperature/two-salt saturation point diagram for the sodium/ammonium sulphate system.

In chapter 6, the temperature/two salt saturation point diagram for the sodium nitrate/sulphate system was shown (figure 6-7). Figure 7-4 shows the corresponding diagram for the ammonium/sodium sulphate system and figure 7-5 shows the diagram for

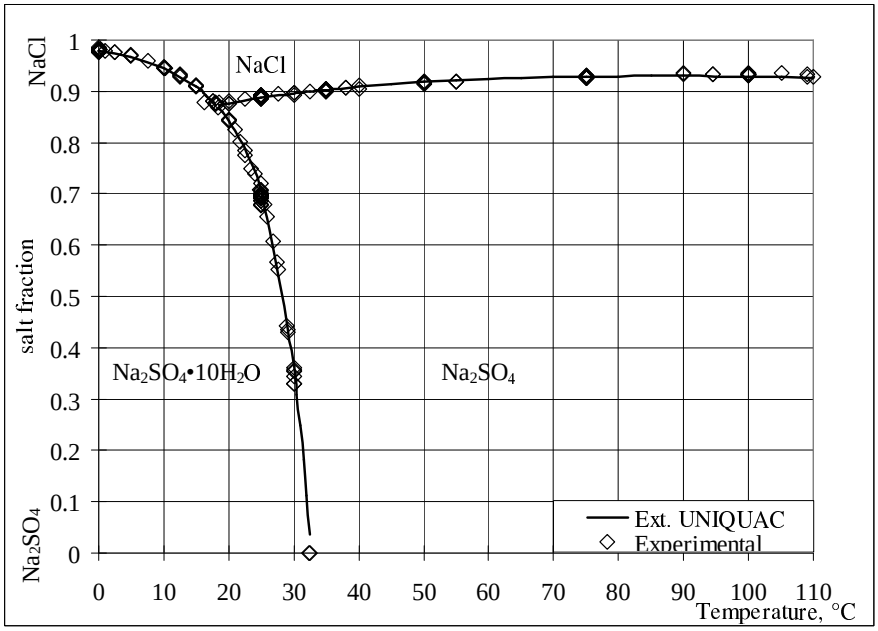

Figure 7-5: Temperature/two salt saturation point diagram for the sodium chloride/sulphate system.

the sodium chloride/sulphate system.

A good agreement between experimental and calculated phase diagrams, and a prediction of the correct phases is generally achieved for all the systems for which parameters were estimated.

The experience with the FMC Corporation showed, that the accuracy of SLE calculations, required for industrial applications, is plus minus one weight percent. This accuracy is not achieved for all of the systems considered here.

Industrial processes with electrolytes might involve large numbers of ions, but not all of the ions appear in such quantities that they influence solid-liquid equilibria for the system. In the case with the FMC Corporation, the main interest was in the phase behaviour of the sodium carbonate/hydrogen carbonate/chloride/sulphate system, although phosphate, calcium and magnesium ions were present in small quantities too. For this sub-system of ions, the required accuracy of SLE and thermal property calculations could be achieved in the temperature range of interest. It is therefore assumed that for any subsystem of industrial interest, it is possible to perform a separate parameter estimation to achieve the required accuracy.

7.3 Prediction of the phase behaviour of multi-component systems

Only binary and ternary experimental data were used for estimating the model parameters for the Extended UNIQUAC model. With the exception of the tetragene salt in the sodium/potassium/carbonate/hydrogen carbonate system, the thermodynamic properties of salts were also estimated from binary and ternary experimental data only. The parameters for the peroxodisulphate ion to be used by the FMC Corporation also included some quaternary experimental data points.

When model parameters are based on binary and ternary data alone, the model calculations for systems with more than three ions are predictions, based on the phase behaviour of binary and ternary systems. In the case of the sodium/ammonium sulphate/peroxodisulphate system, the predictions for the quaternary system were not accurate enough for industrial use. By including quaternary experimental data points in the

parameter estimation, a satisfactory representation of the experimental data was obtained.

The extended UNIQUAC model has only binary interaction parameters. Thus, binary and ternary experimental data should be sufficient for the estimation of the model parameters. When standard state thermodynamic properties of salts are estimated at the same time as the model parameters, a degree of freedom for the numerical values of the activity coefficients is introduced. More experimental data points are then required for the estimation. Quaternary experimental data can be used if the ternary data are insufficient.

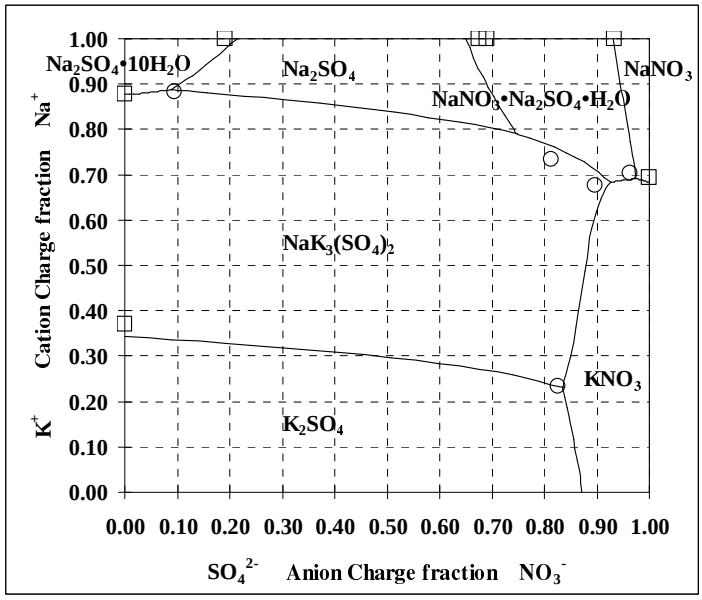

Figure 7-6: Prediction of the phase behaviour of the quaternary system sodium/potassium - sulphate/nitrate at 30°C

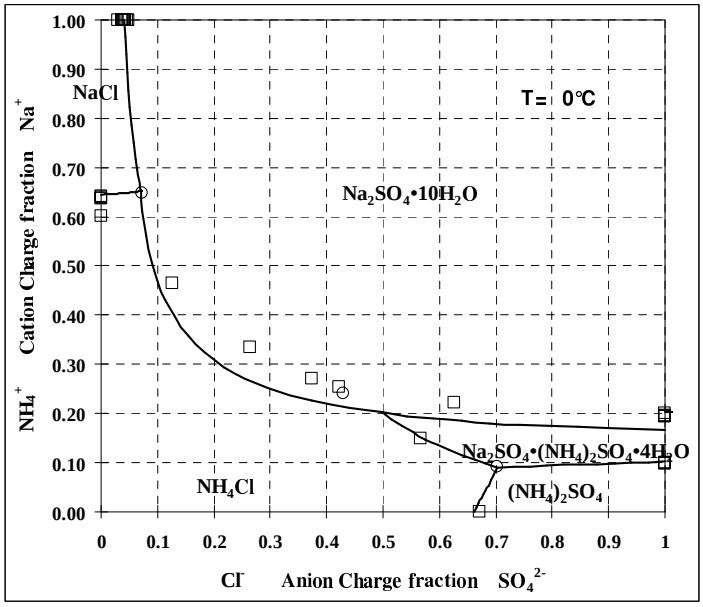

Figure 7-7: Prediction of the phase behaviour of the quaternary system sodium/ammonium - chloride/sulphate at 0°C

The ability of the model to predict the phase behaviour of quaternary systems is illustrated in figures 7-6 to 7-10.

Figure 7-6 is a Jänecke projection of the phase diagram for the aqueous Na^+, K^+, NO_3^-, SO_4^{2-} system at 30°C. Experimental values of three salt saturation points are marked

with circles. These experimental data are from Cornec *et al.*, 1929. Experimental two-salt saturation points are marked with squares (four different sources).

In figures 7-7 to 7-10, Jänecke projections of phase diagrams for the aqueous Na^+, NH_4^+, Cl^-, SO_4^{2-} system are shown at 0, 25, 40, and 80°C. The experimental values of three salt saturation points marked with circles and two salt saturation points internally in these diagrams are all from Rivett, 1923. The experimental points on the edges of the diagrams come from a number of different sources.

Obviously, the model does not predict the phase behaviour of these systems perfectly, but considering the complexity of the systems and the strong temperature dependence, the accuracy must be considered good.

It is also worth noting again, that only the experimental data points on the edges of the diagrams were used for the parameter estimation. If the quaternary data, marked in the internal of the diagrams, were included in the parameter estimation, an even better agreement between experimental and calculated data would be obtained.

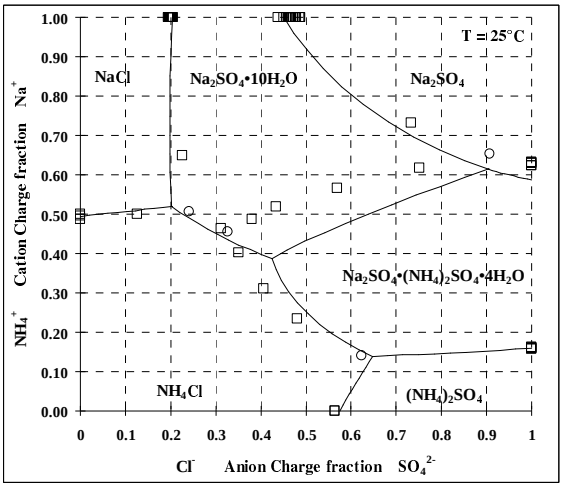

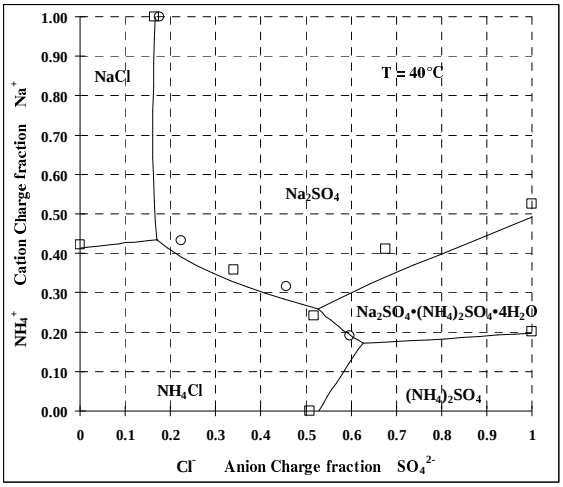

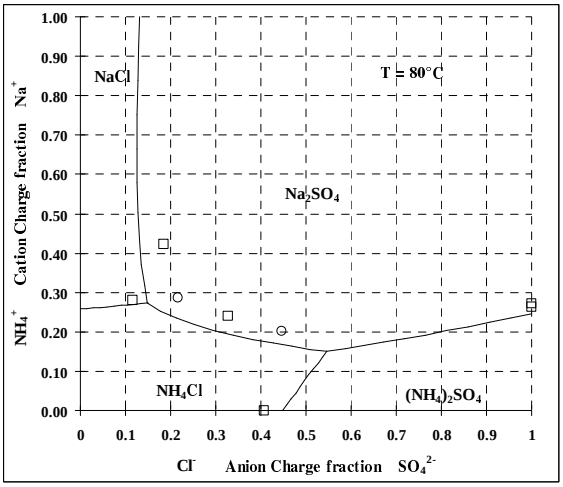

Figure 7-8, 7-9, 7-10: Prediction of the phase behaviour of the quaternary system sodium-ammonium - chloride/sulphate at 25, 40, and 80°C

7.4 Extrapolation

The extended UNIQUAC model parameters and the thermodynamic properties and parameters presented in this work are all based on experimental data in the temperature range from 0 to 110°C.

If the model is employed outside of this temperature range, it constitutes an extrapolation. Figure 7-11 shows the phase diagram for the ternary system sodium sulphate/chloride at 150°C. The solid line represents the phase diagram calculated with the parameters presented in this work. Experimental data from two different sources are marked with squares.

The shapes of the curves are correct, but the extrapolated solubility of sodium sulphate is too high, of sodium chloride too low. By changing the applied value of the standard state heat capacity of Na_2SO_4, from 128.2 to 158.6 J mol^{-1} and the standard state heat

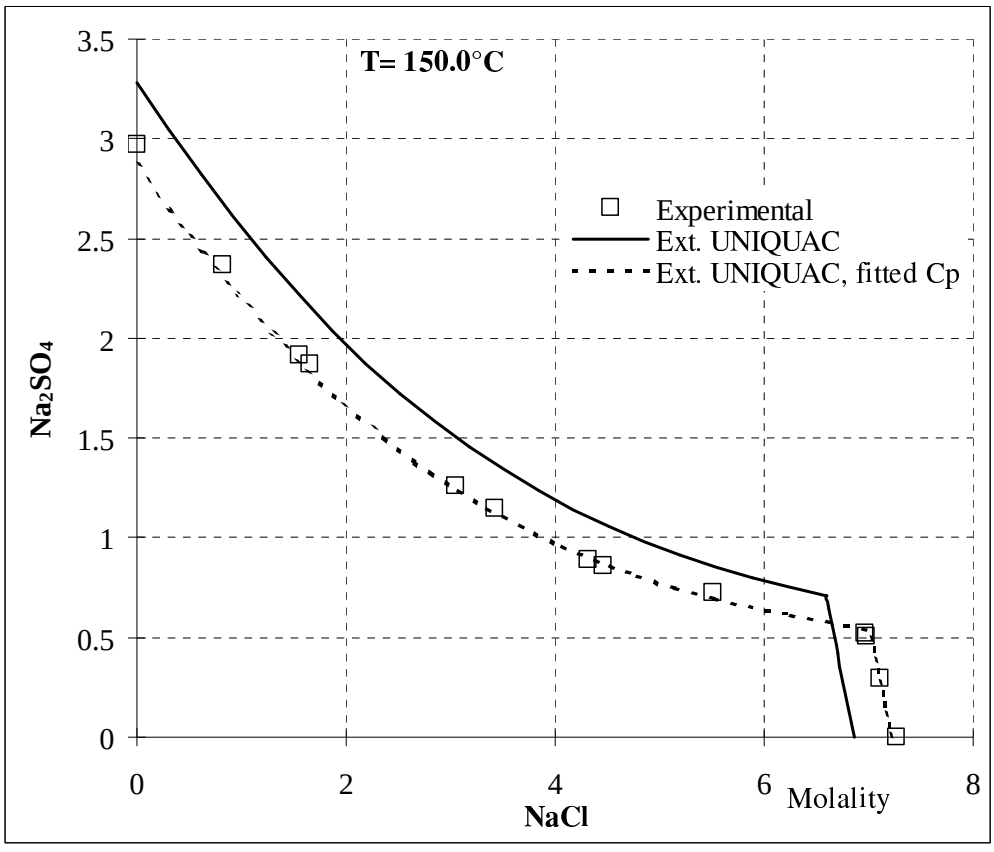

Figure 7-11: Extrapolation to 150°C.

capacity of NaCl from 50.5 to 29.8 J mol^{-1}, but maintaining the values of the model parameters and the other standard state properties of the two salts, the dashed line was obtained.

The model parameters, at least for this ternary system, obviously can be used in a temperature range much larger than that of the experimental data they are based on. All what is needed is to extend the heat capacity correlation for ions or salts to higher temperatures.

Extrapolation beyond the concentrations, the model parameters are based on, also yield promising results. In figure 7-12, the calculated osmotic coefficient of sodium hydroxide is displayed, at molalities up to 29. Experimental data from three different sources are plotted in the diagram. Experimental osmotic coefficients at concentrations up to only 6 molal sodium hydroxide were used for the parameter estimation

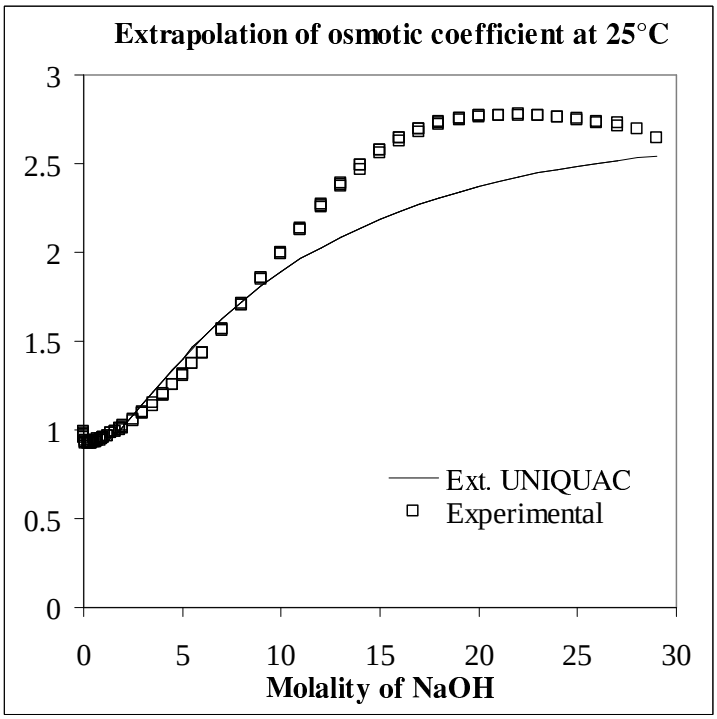

Figure 7-12: Extrapolation of the osmotic coefficient of sodium hydroxide up to 29 molal. The model parameters were fitted to osmotic coefficients for sodium hydroxide up to 6 molal.

8. Simulation and optimization

This chapter is a rewriting of the second part of the article "Simulation and optimization of fractional crystallization processes" by Kaj Thomsen, Peter Rasmussen and Rafiqul Gani, submitted for publication to Chemical Engineering Science in the spring of 1997. A large part of this chapter also appeared in the confidential report: "Soda ash liquors: Phase diagrams and process simulation", (Thomsen, 1996).

8.1 Introduction

A computer program for the calculation and display of phase diagrams and the simulation of processes related to the production of natural soda ash was developed during my six months stay at the FMC Chemical Research and Development Center, NJ, USA. The program applied extended UNIQUAC parameters estimated from experimental data proprietary to the FMC Corporation besides experimental data from the open literature. Specific routines for simulating a solution mine, a causticizer unit, and a carbonator/decarbonator unit were included in the program. The program also contained a correlation for the density of soda ash liquors as well as a correlation for the co-precipitation of sodium sulphate together with sodium carbonate decahydrate.

The carbonator/decarbonator unit gave the option of specifying a certain amount of carbon dioxide added or removed from a stream. This amount was calculated stoichiometrically rather than based on equilibrium calculations. The causticizer unit was also based on stoichiometric calculations rather than equilibrium calculations. The correlations for the density of soda ash liquors and for the co-precipitation of sodium sulphate are proprietary to the FMC Corporation.

The program was later modified to make it a general program for the calculation and display of phase diagrams and excess properties of electrolytes and for simulating and analyzing processes with electrolytes. All the parts of the program, which were specific to processes with soda ash liquors or contained data proprietary to the FMC Corporation, were removed. Under this form, the program is referred to as "IVC-ELEC". An

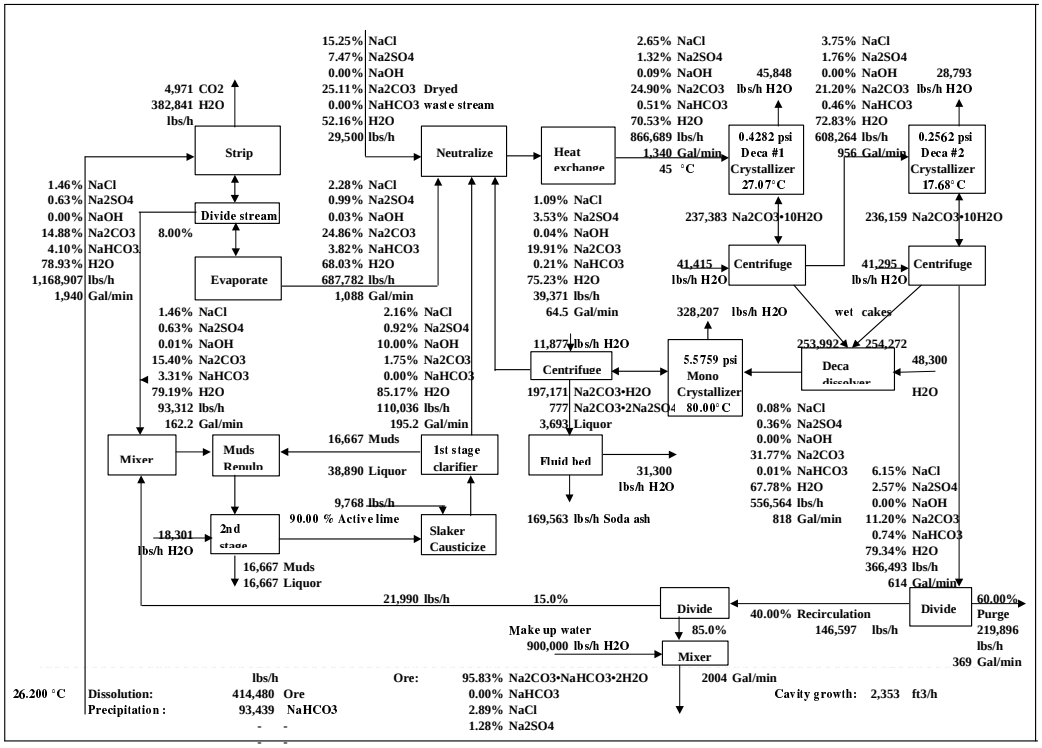

Figure 8-1: An example of the type of process flowsheets that can be calculated with the original version of the steady state simulator.

example of the type of process flowsheets that can be simulated with the original version of the simulator is shown in figure 8-1.

A stream consisting of make up water and a part of the recirculation stream is poured into the solution mine, where it dissolves ore of a certain composition. Some precipitation of sodium hydrogen carbonate from the liquid stream takes place in the mine. At the surface the stream is stripped of some carbon dioxide, whereby hydrogen carbonate is converted to carbonate. Remaining hydrogen carbonate is converted to carbonate by adding sodium hydroxide from the causticizer unit. Sodium carbonate decahydrate is first precipitated by an evaporative cooling process, then dissolved again and precipitated as sodium carbonate monohydrate. Finally, it is converted to anhydrous sodium carbonate in a fluid bed.

8.2 Modelling aspects

8.2.1 The crystallizer/centrifuge unit

The calculation of the equilibrium concentrations in supersaturated electrolyte mixtures follows a pattern similar to the method described in section 2-4 'Equilibrium reactions' for calculating saturation points in phase diagrams. Given the temperature, the pressure and the gross concentrations in a supersaturated mixture, the task is to find a combination of *s* salts that upon precipitation from the mixture in suitable quantities will make the solution saturated with the *s* salts, i.e. satisfy the conditions 2-40 and 2-41. According to Gibbs phase rule, *s* is less than or equal to the number of ions.

The calculated equilibrium concentration together with a mass balance and an enthalpy balance for the system defines the equilibrium precipitation process. The mole balance for component *i* is:

$$n_i(Feed) = n_i(Mother\ liquor) + n_i(Vapor) + \sum_{k=1}^{s} n_i(Solid\ \ phase\ k) \qquad \textbf{(8-1)}$$

The enthalpy balance for the process is:

$$H(Feed) + H(Transfer) = H(Mother\ liquor) + H(Vapor) + \sum_{k=1}^{s} H(Solid\ \ phase\ k) \qquad \textbf{(8-2)}$$

H(Feed) is the enthalpy of the feed mixture; *H(Transfer)* is the amount of heat transferred to the process from the surroundings.

The formation of a vapour phase, indicated in equations 8-1 and 8-2, takes place if the vapour pressure of the aqueous solution, P_w, is larger than or equal to the process pressure:

$$P_w = a_w P_w^{sat.} \geq P_{process} \qquad \textbf{(8-3)}$$

$P^{sat}{}_w$ is the saturation pressure of water at the process temperature, a_w is the activity of water in the solution.

Additional modelling details for the equilibrium precipitation process or the multi-phase flash problem, defined by equations 2-40, 2-41, 8-1, 8-2, and 8-3, can be found in Thomsen, 1993.

The separation process in industrial crystallizers deviates from the equilibrium precipitation process in a number of ways. When simulating a precipitation process and the subsequent separation process, a number of operational parameters therefore can be set:

- Entrainment of mother liquor. A complete separation between crystals and mother liquor is never achieved. The entrainment of mother liquor is defined in terms of the number of moles of mother liquor per number of moles of ions in the crystals.
- Displacements of entrained mother liquor. The addition of wash water is specified in amounts relative to the amount of entrained mother liquor.
- Wash efficiency. This option allows the user to specify the percentage of ions in the entrained mother liquor that is removed by the wash water.
- Entrainment of fines. With this parameter, the percentage of crystals entrained with the mother liquor and wash water is specified.
- Saturation of exit liquor. The addition of wash water may cause some crystals to dissolve. A degree of saturation of the combined mother liquor and wash water is specified.

Co-precipitation is the phenomenon of an unsaturated salt precipitating along with the desired product, forming a solid solution. Empirical correlations for co-precipitation can be specified if necessary.

8.2.2 Process flowsheet

The simulation of a crystallizer/centrifuge unit can be performed either as a separate unit calculation or as part of a process flowsheet. In both cases, the unit can be operated in different modes:

- Fixed temperature and pressure. The simulation is performed at a specified temperature and pressure. The required heat transfer to the unit is calculated.
- Fixed temperature and evaporation percentage. The simulation is performed at a specified temperature, and a specified percentage of the solvent is evaporated. The required heat transfer to the unit and the equilibrium vapor pressure of water is calculated.

- Evaporative cooling I. The simulation is performed adiabatically, and a specified percentage of the solvent is evaporated. The working temperature of the unit and the equilibrium vapor pressure of water are calculated.
- Evaporative cooling II. The simulation is performed adiabatically at a specified working temperature lower than the feed temperature. The percentage of solvent to be evaporated, and the equilibrium vapor pressure of water is calculated.

In order to be able to simulate industrial fractional crystallization processes, a steady state simulator for fractional crystallization processes was constructed. The simulator consists of the crystallizer/centrifuge unit (described above) employed for solid-liquid and solid-liquid-vapour separations, a mixer for the adiabatic mixing of streams, a heater for changing the temperature of streams, a stream divider for dividing/purging streams, and a dryer unit for solid-vapour separation.

8.2.3 Problem formulation

In a simulation/design/optimization problem, the following parameters can be used as design variables:

- The size of feed streams
- Crystallizer temperatures
- The fraction of solvent to be evaporated in a crystallizer
- The temperature to be reached in a heater
- The amount of energy to be added in a heater
- The relative sizes of the two streams from a stream divider.

Design constraints can be specified as:

- The amount of salt in a stream
- The amount of impurity in a stream
- The primary solubility index for a stream
- The secondary solubility index for a stream

The solubility index SI_k of salt k is defined as the activity product of salt k divided by its solubility product (equation 2-42):

$$SI_k = \frac{\prod_i a_i^{\nu_{k,i}}}{K_k} \qquad \textbf{(8-4)}$$

The solubility index thus is an expression for the degree of saturation. The primary solubility index for a stream is the highest solubility index found for any salt in a stream, the secondary solubility index is the next highest. A constraint on the primary solubility index can be used to specify that saturation/supersaturation is wanted/undesired. A constraint on the secondary solubility index for a stream can be used to avoid/achieve the simultaneous precipitation of two salts.

The object function to be minimized can be defined through:

- The amount of a component (product)
- The size of a stream
- The enthalpy of a stream
- The energy consumption of a unit

8.3 Numerical aspects

8.3.1 Method of solution

Convergence of flowsheets containing recirculation streams can optionally be achieved using successive substitution, Wegstein acceleration or the Newton-Raphson method. For the design and optimization of flowsheets, a modified version of the SQP method implemented by Bossen, 1995, is used. The method applied is the infeasible path approach. The convergence of the flowsheet, the fulfillment of the design specifications and the optimization is achieved simultaneously.

8.3.2 Definition of stream variables

The amount of water and the amounts of each ion can describe the composition of an aqueous electrolyte mixture. Under some circumstances however, it is not practical to use water and ions as stream variables. This is for example the case if the convergence of flowsheets for electrolyte systems is being achieved with a gradient method. Pertur-

bation of the stream variables will result in a loss of electroneutrality. To avoid this, a suitable number of neutral compounds with linearly independent stoichiometric coefficients can be chosen as stream variables. As the composition of the tear stream changes during the iterations, one of the chosen stream variables may turn negative, and must be allowed to attain negative values. This can best be explained by an example:

The composition of a stream containing n_{Na}, n_K, n_{Cl}, and n_{SO4} moles of the four ions with $n_{Na} + n_K = n_{Cl} + 2n_{SO4}$, can be described as:

- n_{SO4} moles of Na_2SO_4
- n_K moles of KCl
- $n_{Na} - 2n_{SO4} = n_{Cl} - n_K$ moles of NaCl

If $n_K > n_{Cl}$ the 'moles of NaCl' will be negative. Thus for systems containing more than one anion and more than one cation, one of the stream variables describing the composition of the stream must be allowed to attain negative values.

8.3.3 The IVC-ELEC program

The output from IVC-ELEC can be imported directly into a spreadsheet for further analysis and/or for graphical display. A task such as drawing the operating line for a crystallizer unit in a triangular phase diagram can therefore be performed very rapidly. All the simulation results and process flowsheets highlighted in this chapter were constructed by the use of spreadsheet templates and macros for Microsoft EXCEL.

8.4 Application examples

8.4.1 Example 1: Simulation of precipitation of NaCl and KCl

In this example, the option of performing a crystallizer/centrifuge unit calculation not part of a flowsheet is highlighted through a simple example. Sanders, 1985, presented a case study dealing with the solubility of NaCl and KCl in aqueous HCl. Figure 8-2 shows the result of the same calculation performed with the IVC-ELEC program. A complete separation of the phases is assumed to be attained and the operational parameters for the separation are set to zero. The simulation results then can be compared

with those of Sanders. A small difference in the amounts of solid products is observed, but with the absence of experimental data it can not be determined which result is most correct.

8.4.2 Example 2: Simulation and optimization of potassium nitrate production

Ullmann, 1991, mentions a process employed in Chile for the production of potassium nitrate from potassium chloride and sodium nitrate. The potassium chloride is produced from the Atacama Salar brines by evaporation in solar ponds and subsequent separation from sodium chloride by a grinding and flotation process. Sodium nitrate is produced by leaching crushed caliche ore and cooling the solution. Two alternative flowsheet designs of this fractional crystallization process were made with a process synthesis program (Thomsen *et al.*, 1995).

Both flowsheet designs were then simulated and optimized with the IVC-ELEC program. The objective of the optimization was to maximize the yield of KNO_3. The design variables were the amount of water added to the system, the percentage of water evapo-

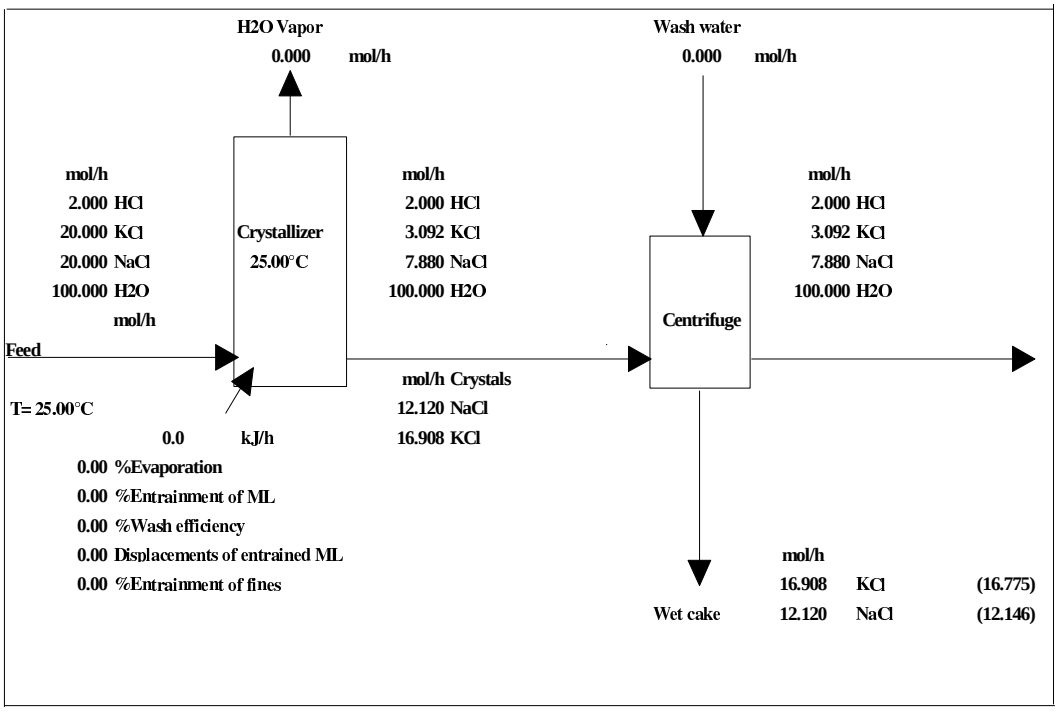

Figure 8-2: Results of crystallizer calculation, example 1. The results obtained by Sanders (1985) are given in parenthesis.

rated in the NaCl crystallizer, and the percentage of recirculation stream purged.

Two constraints were added to ensure a yield of pure KNO_3 and pure NaCl. These constraints were formulated as a maximum value (0.9) of the secondary solubility indices in the mother liquor from the two crystallizers.

The results of the optimizations are displayed in figures 8-3 and 8-4. The yield of potassium nitrate is approximately the same in the two designs (figures 8-3 and 8-4). The energy consumption for heating and cooling, however, is significantly different. Compared to design two, design one requires more than twice as much heating (11867 kJ h^{-1} as opposed to 5201 kJ h^{-1}) but only a little more than half the cooling (1392 kJ h^{-1} as opposed to 3066 kJ h^{-1}). Also the size of the recirculation stream in design one is less than half of the recirculation stream in design two. If the evaporation is performed in solar evaporation ponds as indicated, the heat consumption may be of minor importance and design one can be regarded as the most efficient.

In both optimized designs, the adiabatic flash performed in order to calculate the temperature of the mixed stream from the mixing tank indicates that precipitation begins in

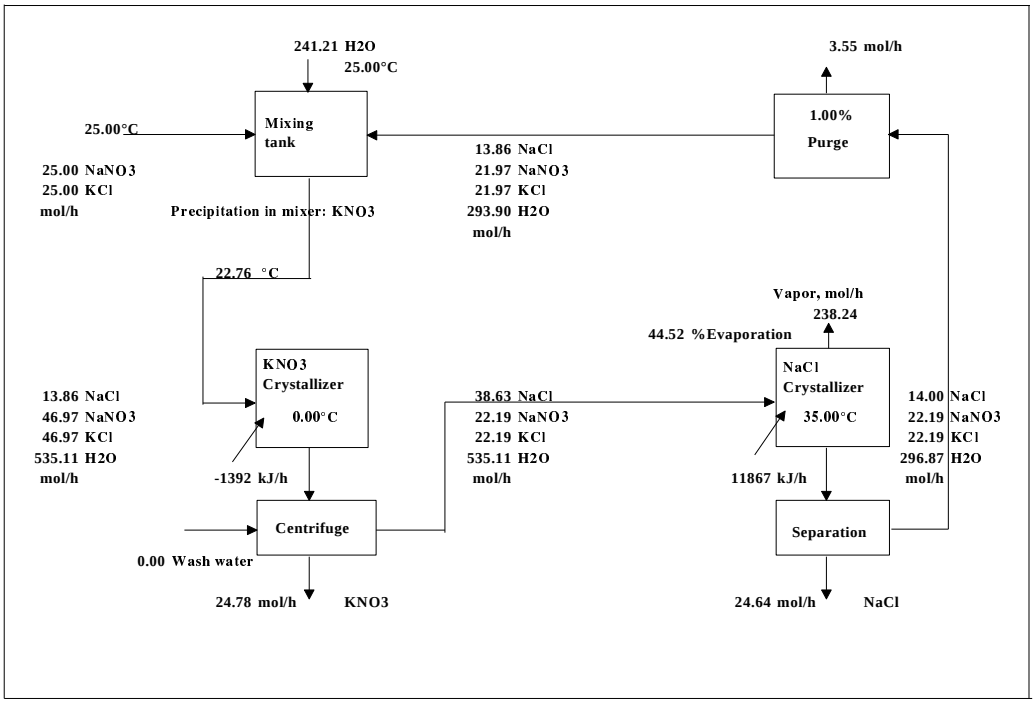

Figure 8-3: Production of KNO_3 from $NaNO_3$ and KCl, design one

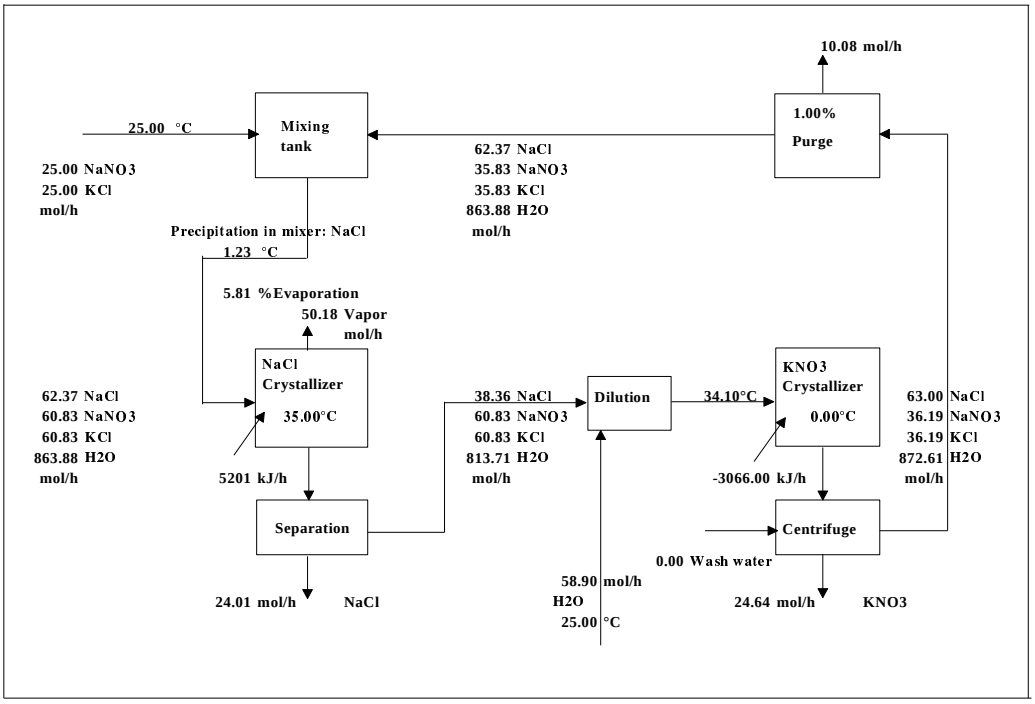

Figure 8-4: Production of KNO_3 from $NaNO_3$ and KCl, design two

the mixing tank. It is therefore necessary to either heat the mixing tank or to perform the mixing in the crystallizer.

The lower boundary for the percentage of recirculation stream purged was set to 1.00%. As it appears from figures 8-3 and 8-4, this lower boundary was reached in the optimal solutions to both designs.

Caliche ore contains sodium sulphate. The raw material for the KNO_3 production may therefore also contain some sodium sulphate. Figure 8-5 shows what effect a small content of sodium sulphate will have on design one. Also here the maximum allowable secondary solubility index in the mother liquor from the KNO_3 crystallizer was set to 0.90 while no constraints were put on the mother liquor from the chloride/sulphate precipitation. The flowsheet was optimized for the maximum yield of KNO_3.

As it appears from figure 8-5, the same yield of KNO_3 can be obtained as in the system without Na_2SO_4 even with a lower cooling capacity. KNO_3 however is the only pure product obtained from the process. A complete separation of the feed into three pure products would require an additional crystallization process.

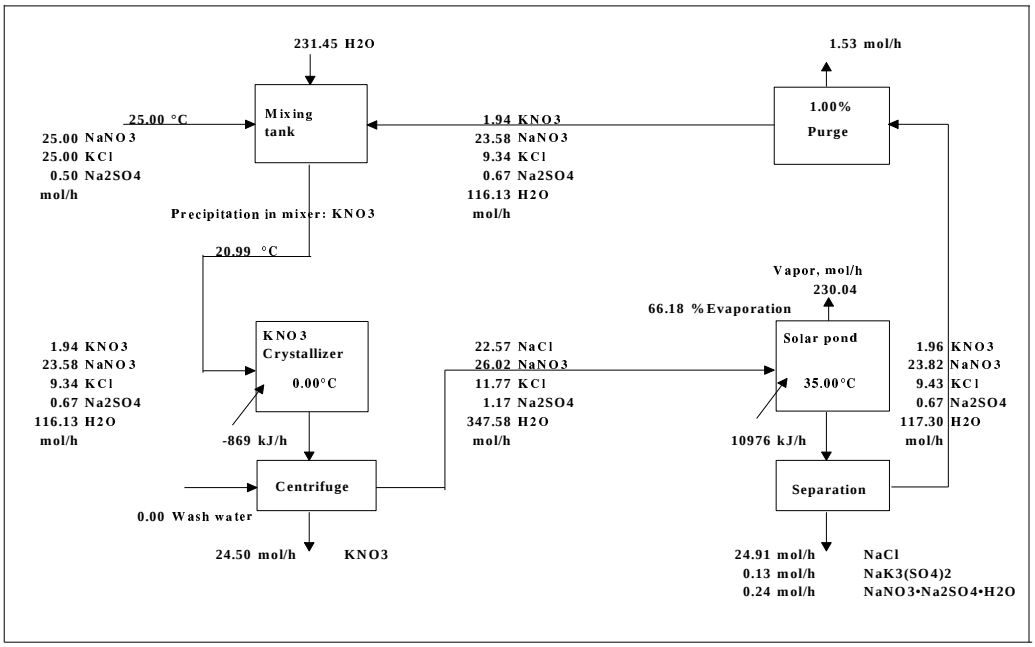

Figure 8-5: Production of KNO_3 from $NaNO_3$ and KCl containing Na_2SO_4, design one

If a feed containing Na_2SO_4 was used in connection with design two, the amount of water added between the two crystallizers would be about ten times as large as the amount used in figure 8-5, the recirculation stream would become larger and the amount of heat required for evaporating water would grow considerably. Thus, design one is clearly the most advantageous if the feed contains Na_2SO_4.

8.4.3 Example 3: Simulation/Optimization of K_2SO_4 production process

A patented process (Sogolov et al., 1982; Neitzel, 1986) for the production of K_2SO_4 and NaCl from Na_2SO_4 and KCl was simulated and improved through optimization. The mass balance given in the patent description (Sogolov et al., 1982) is incomplete, and the temperature of the sodium chloride crystallizer is not given.

An open loop simulation (i.e. the stream supposed to be recycled is purged) of the process was performed with the IVC-ELEC program (figure 8-6). The four solid product streams from the four crystallizers were fitted to less than one per cent deviation by weight compared to the data given in the patent description. The temperature of the sodium chloride crystallizer and the stream variables of the recirculation stream were used as design variables.

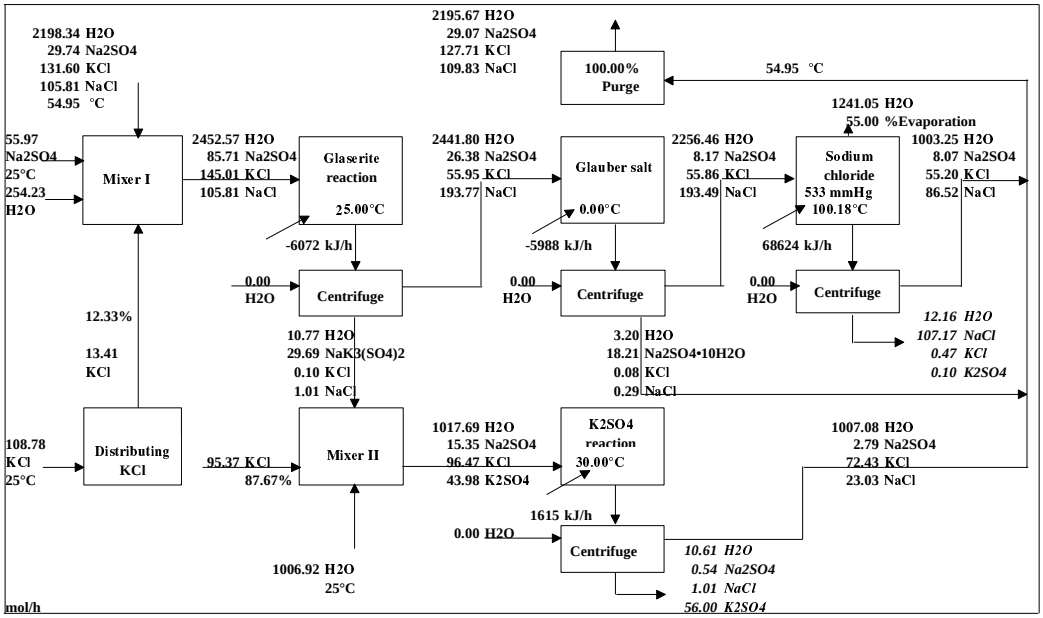

Figure 8-6: Open loop simulation of process for the production of K_2SO_4 and NaCl from Na_2SO_4 and KCl. The boxes marked 'Glaserite reaction', 'Glauber salt', 'Sodium chloride', and 'K2SO4 reaction' are crystallizers.

In all crystallizers the entrainment of mother liquor with the crystals was set to 7.5% . As described above, this percentage means moles of mother liquor per mole of ions in the crystals. A 7.5% entrainment of mother liquor will typically mean 2-5% by weight, depending on the salt. The resulting recirculation stream falls within the boundaries given in the patent description.

The main disadvantage of this process is the large amount of heat needed to evaporate water in the sodium chloride crystallizer. According to the patent description, more than 2.23 kg water are evaporated for each kg of K_2SO_4 produced.

The process was optimized with the IVC-ELEC program. The objective of the optimization was to find the process parameters yielding products of the same purity as described in the patent but with the lowest possible amount of heat exchanged between or added to the four crystallizers. The optimized process is shown in figure 8-7. In the optimized process, only 1.88 kg water needs to be evaporated for each kg of K_2SO_4 produced. Thus, approximately 84% of the amount evaporated in the patented process is needed in the optimal solution.

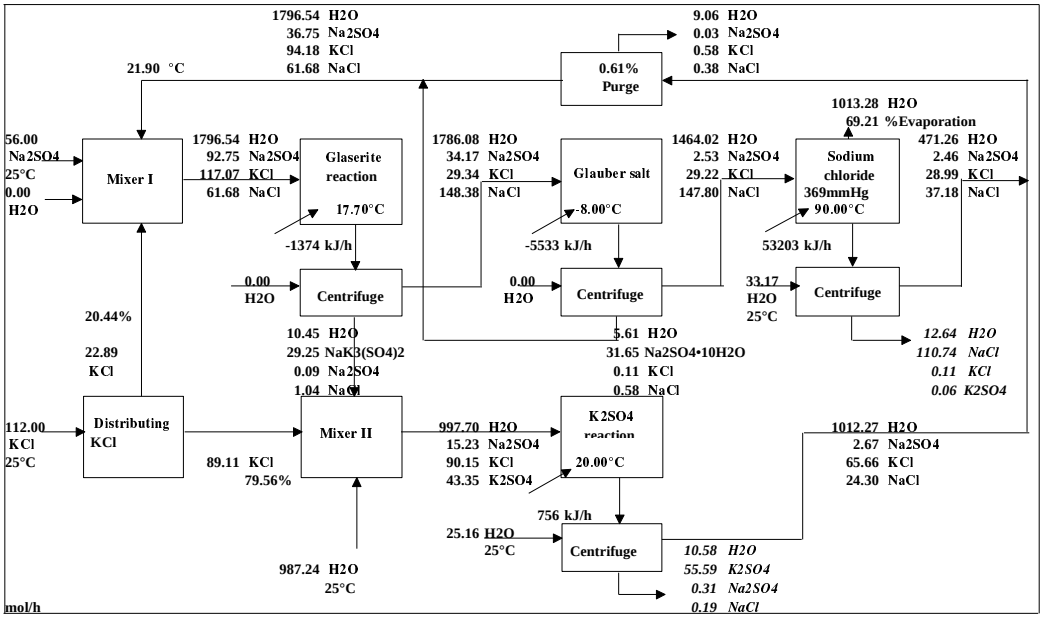

Figure 8-7: Optimized process for the production of K_2SO_4 and NaCl from Na_2SO_4 and KCl.

Nine process parameters were used as design variables in the optimization study (see figure 8-7):

- The amounts of water added in 'Mixer I' and 'Mixer II'
- The distribution of the KCl feed between the 'Glaserite reaction' and the 'K_2SO_4 reaction'
- The temperatures of the four crystallizers
- The fraction of water to be evaporated in the sodium chloride crystallizer
- The fraction of the recirculation stream to be purged

Four design specifications (constraints) were used:

- The amounts of K_2SO_4 and NaCl produced
- The amounts of impurities in the two products

The flowsheet in figure 8-7 requires only one tear stream, the combined recirculation stream to 'Mixer I'. The stream contains 5 components but only 4 of them are independent. The stream composition thus can be described by the amount of water and of three salts. In the optimization of the flowsheet in figure 8-7, the amounts of water, Na_2SO_4, KCl, and NaCl were used to describe the composition of the tear stream.

At the optimal solution, four of the nine design variables used in the optimization ended up on either their lower or upper limit. These four design variables are:

- The amount of water added to 'Mixer I': The final value was 0.00
- The temperature of the 'Sodium chloride' crystallizer: The final value was 90°C equal to the lower boundary for this variable. This boundary value was set arbitrarily. Depending on the equipment, it might be more efficient to operate this crystallizer at the boiling point ≈111°C.
- The temperature of the 'K_2SO_4 reaction' crystallizer: The final value was 20°C equal to the lower boundary for this variable. In the patent description, the temperature range for this crystallizer was given as 25 - 30°C. During the optimization of the process the allowed temperature range was set to 20-35°C.
- The temperature of the 'Glauber salt' crystallizer: The final value was -8°C equal to the lower boundary for this variable. In the patent description, the temperature range for this crystallizer was given as -8 - 3°C.

The most significant result of the optimization is that no water needs to be added to 'Mixer I', which reduces the amount of water to be evaporated by about 16%. The amount of heat exchanged between or added to the crystallizers is reduced by more than 25%. Also the size of the recirculation stream is reduced by about 20%. The temperatures of the 'Sodium chloride' and the 'K_2SO_4 reaction' crystallizers can be increased to for example 111°C and 30°C respectively without altering these facts.

8.4.4 Output multiplicity

The process simulated in example 3 was found to have multiple steady states. The multiple steady states can be explained physically: it is due to the glauber salt trapped in the recycle loop consisting of the 'Glauber salt' crystallizer, 'Mixer I', and 'Glaserite reaction' crystallizer (names referring to figure 8-7). The different steady states can thus be illustrated by the amounts of glauber salt precipitating in the 'Glauber salt' crystallizer.

In the optimized process (figure 8-7), 69.21% of the water in the feed stream to the 'Sodium chloride' crystallizer is evaporated. Figure 8-8 shows the amount of glauber salt

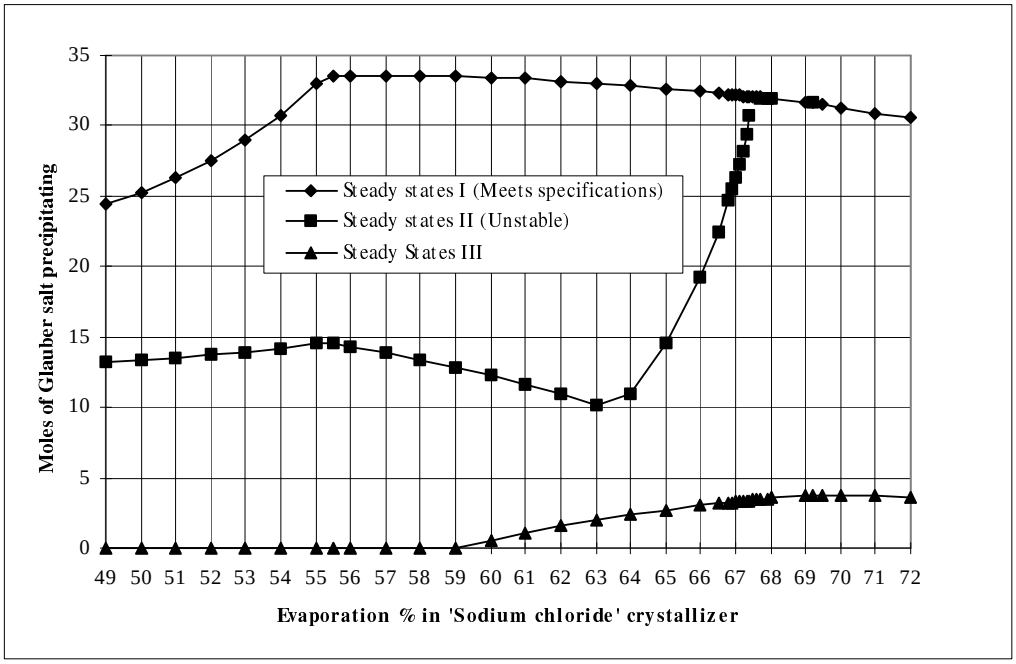

Figure 8-8: Multiple steady states for the K_2SO_4 production process illustrated as the amount of Glauber salt precipitating in the 'Glauber salt' crystallizer as a function of the percentage of water evaporated in the 'Sodium chloride' crystallizer.

precipitating in the 'Glauber salt' crystallizer as a function of the percentage of water evaporated in the 'Sodium chloride' crystallizer.

The graph in figure 8-8 was constructed by solving the optimization problem for different specified values of the percentage of evaporation in the 'Sodium chloride' crystallizer. Each solution to the optimization problem is a set of nine design variables, counting also the fixed value of the percentage of evaporation in the 'Sodium chloride' crystallizer. The points in figure 8-8 indicate the steady state simulation results at the optimal solutions.

In all the optimizations and steady state simulations performed, the mass balance was converged to a deviation less than one nanomole per hour and the energy balance to less than one mJ per hour. The optimized flowsheet in figure 8-7 corresponds to the point on the 'Steady state I' curve (in figure 8-8), with 69.21% evaporation.

The series of steady states denoted as 'Steady states I' in figure 8-8, is characterized by Jacobian matrices becoming increasingly ill-conditioned and close to singular for evaporation percentages higher than 67. The condition number for the Jacobian matrix,

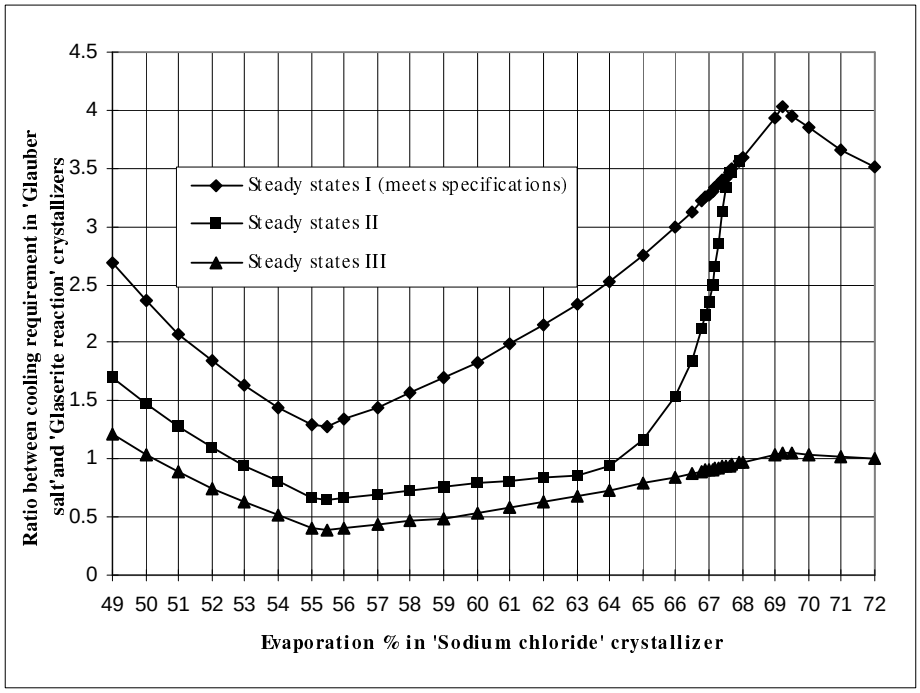

Figure 8-9: Ratio between cooling requirement in the 'Glauber salt' and 'Glaserite reaction' crystallizers

defined as the largest eigenvalue divided by the smallest, increases from 10^3 at 60% evaporation to 10^6 at 67.5% and then decreases to 10^4 at 69.2%. The steady states belonging to 'Steady states 1' are actual solutions to the optimization problem and satisfies all the constraints.

The steady state series denoted as 'Steady states II' in figure 8-8 is characterized by Jacobian matrices having a positive eigenvalue which decreases toward zero with increasing evaporation percentages. For evaporation percentages higher than 67.5% it is difficult to distinguish steady state series I and steady state series II. The steady states series denoted 'Steady states III' in figure 8-8 has well-conditioned Jacobian matrices, the conditon numbers for the Jacobian matrices are all between one and two. The steady states belonging to 'Steady states III' however do not satisfy the specified constraints (defining the optimization problem), neither do 'Steady states II' at evaporation percentages lower than 67.5%. These steady states are solutions to the simulation problem, but not to the optimization problem.

The optimized flowsheet (figure 8-7), with 69.21% evaporation is thus located in the region (see figure 8-8) where 'Steady state I' and 'Steady state II' are coincident. In or-

der to stabilize this optimal solution another constraint has to be added. An analysis of the cooling required by the crystallizers shows that the relative amounts of cooling required in the 'Glauber salt' crystallizer and the 'Glaserite reaction' crystallizer' is significantly different in the different steady states. A plot (figure 8-9) of the ratio between the cooling requirements for the two crystallizers as a function of the percentage of water being evaporated in the 'Sodium chloride' crystallizer, confirms the analysis.

In the steady state that satisfies the specified constraints the cooling requirement for the 'Glaserite reaction' is 1374 kJ h^{-1} and the cooling requirement for the 'Glauber salt' crystallizer is 5533 kJ h^{-1} (figure 8-7). In the other possible steady state for the optimized flowsheet the corresponding numbers are 3342 kJ h^{-1} and 3536 kJ h^{-1}. By simulation it was found that the unwanted steady state could be avoided by specifying the cooling required by one of these crystallizers rather than its temperature.

9. Conclusion

Parameters for the Extended UNIQUAC model have been estimated for eleven ions in aqueous solution. The parameters for a twelfth ion, the hydrogen ion, were given fixed values. The excess properties of the eleven other ions were defined relative to the properties of the hydrogen ion.

The parameters were estimated from a large amount of experimental data collected in a databank. Ten different types of data were used for the parameter estimation. In the parameter estimation, all experimental data of a given type were weighted equally, based on absolute differences between experimental and calculated data.

The estimated parameters make it possible to calculate vapour-liquid, solid-liquid, and speciation equilibria as well as thermal properties such as heat of dilution and heat capacity of aqueous electrolyte mixtures. These calculations can be performed with an accuracy that, at least for two subsystems of the ions, is satisfactory for the simulation of electrolyte processes in large industrial plants.

A computer program for the simulation and optimization of fractional crystallization process flowsheets has been developed. The program employs the extended UNIQUAC thermodynamic model for the thermodynamic description of aqueous electrolyte mixtures. The worlds largest producer of natural soda ash currently uses this program for simulating fractional crystallization processes.

The simulation of industrial crystallizers has been accomplished by combining a thermodynamic equilibrium precipitation process with process parameters that account for the incomplete separation of the solid and the liquid phase in such crystallizers.

Fractional crystallization processes have been simulated and optimized with the developed computer program. The existence of multiple steady states in the flowsheet for a fractional crystallization process has been detected and analyzed. They appear to be caused by compounds trapped in a recycle stream.

Finally, it has been shown through optimization, that significant improvements in the design of a fractional crystallization process are theoretically possible.

References

Abrams D.S. and Prausnitz J.M., 1975, "Statistical Thermodynamics of Liquid Mixtures: a new expression for the Gibbs energy of partly or completely miscible systems", A.I.Ch.E. Journal, volume 21, No. 1. pp. 116-128.

Bach R.-W, 1976, "Druck-Volumen-Temperatur-Messungen am System HCl/H_2O bis 500°C und 1500 bar", Dissertation, Rheinisch-Westfälischen Technischen Hochschule, Aachen, Germany.

Berry D.A. and Ng K.M., 1996, "Separation of Quaternary Conjugate Salt Systems by Fractional Crystallization", AIChE Journal, volume 42, 8, 2162-2174

Bossen B.S., 1995, "Simulation and optimization of ammonia plants", Ph.D. Thesis, Department of Chemical Engineering, Technical University of Denmark, DK-2800 Lyngby, Denmark.

Busey R.H., Holmes H.F., and Mesmer R.E., 1984, "The enthalpy of dilution of aqueous sodium chloride to 673 K using a new heat-flow and liquid-flow microcalorimeter. Excess Thermodynamic properties and their pressure coefficients", J. Chem. Thermodynamics, volume 16, pp. 343-372.

Cabani S., and Gianni P., 1972, "Comments on simultaneous determination of K and ΔH. Analysis of some calorimetric data concerning the formation of bisulfate ion in aqueous solution", Analytical Chemistry, volume 44, pp. 253-259.

Chen H., and Irish D.E., 1971, "A Raman spectral study of Bisulfate-Sulfate Systems", The Journal of Physical Chemistry, volume 75, pp. 2672-2681

Cisternas L.A. and Rudd D.F., 1993, "Process Designs for Fractional Crystallization from Solution", Ind. Eng. Chem. Res., volume 32, pp. 1993-2005

Clarke E.C.W., and Glew D.N., 1985, "Evaluation of the Thermodynamic Functions for Aqueous Sodium Chloride from Equilibrium and Calorimetric Measurements below 154°C", J. Phys. Chem. Ref. Data, volume 14, No. 2. pp. 489-610.

Clegg S.L., and Brimblecombe P., 1990, "Equilibrium Partial Pressures and Mean Activity and Osmotic Coefficients of 0-100% Nitric Acid as a Function of Temperature", J. Phys. Chem., volume 94, pp. 5369-5380.

Cornec, E., Krombach, H. and Spack, A., 1929, Caliche, volume 11, p. 224.

Dawson B.S.W., Irish D.E., and Toogood G.E., 1986, "Vibrational spectral studies of solutions at elevated temperatures and pressures. 8. A Raman spectral study of ammonium hydrogen sulphate solutions and the HSO_4^- - SO_4^{2-} equilibrium", J. Phys. Chem., volume 90, pp 334-341.

Debye P., and Hückel E., 1923, "Zur Theorie der Elektrolyte I/II", Phys. Z., volume 24, pp. 185-206, 305-325

DIPPR, Danner R.P., and Daubert T.E., 1983, Project 801, Design Institute for Physical Property Research, Pensylvania State University.

Fitch B., 1970, "How to Design Fractional Crystallization Processes", Ind. Eng. Chem., volume 62, 6-33

Fletcher R., 1971, "A modified Marquardt subroutine for non-linear least squares", Harwell report, AERE R.6799

Fowler R.H. and Guggenheim A.E., 1949, "Statistical Thermodynamics", Cambridge University Press.

Fredenslund Aa., Gmehling J., and Rasmussen P., 1977, "Vapour-liquid equilibrium using UNIFAC", Elsevier, Amsterdam.

Giauque W.F., Hornung E.W., Kunzler J.E., and Rubin T.R., 1960, "The thermodynamic properties of Aqueous sulfuric acid solutions and hydrates from 15 to 300°K" [sic], J. Am. Chem. Soc., volume 82, pp.62-70.

Gorshtein, G.I. and Silant'eva, N.I., 1954, Zh. Obshch. Khim., volume 24, p.29

Haase R., Dücker K.H, and Küppers H.A., 1965, "Aktivitätskoeffizienten und Dissoziationskonstanten wässriger Salpetersäure und Überchlorsäure", Berichte der Bunsengesellschaft für Physikalische Chemie, Band 69, Nr. 2, pp. 97-109.

Hamer, W.J, and Wu Y.-C., 1972, “Osmotic coefficients and Mean Activity Coefficients of Uni-Univalent Electrolytes in Water at 25°C”, J. Phys. Chem. Ref. Data, volume 1, pp. 1047-1099.

Harned S.H. and Owen B.B., 1964, “The Physical Chemistry of Electrolytic Solutions”, Third edition, Reinhold Publishing Corporation, New York.

Harvie C.E., Møller N., and Weare J.H., 1984, “The prediction of mineral solubilities in natural waters: The Na-K-Mg-Ca-H-Cl-SO_4-OH-HCO_3-CO_3-CO_2-H_2O system to high ionic strengths at 25°C”, Geochimica et Cosmochimica Acta, volume 48, pp. 723-751.

Helgeson H.C., Kirkham D.H., and Flowers G.C.,1981,”Theoretical Prediction of the Thermodynamic Behaviour of Aqueous Electrolytes at High Pressures and Temperatures: IV”, American Journal of Science, volume 281, pp. 1249-1516.

Hill A.E., 1930a, “Double salt formation among the carbonates and bicarbonates of sodium and potassium”, J. Am. Chem. Soc., volume 52, pp. 3813-3817.

Hill A.E., 1930b, “Hydrated potassium sesquicarbonate, K2CO3•2KHCO3•1½H2O”, J. Am. Chem. Soc., volume 52, pp. 3817-3825.

Hill A.E., and Miller F.W.Jr., 1927, “Ternary systems IV: Potassium carbonate, sodium carbonate, and water”, J. Am. Chem. Soc., volume 49, pp 669-686.

Hill A.E., and Smith S.B., 1929, “Equilibrium between the carbonates and bicarbonates of sodium and potassium in aqueous solution at 25°C”, J. Am. Chem. Soc., volume 51, pp. 1626-1636.

Hovey J.K., and Hepler L.G., 1989, “Apparent and partial molar heat capacities and volumes of aqueous $HClO_4$ and HNO_3 from 10 to 55°C”, Can. J. Chem., volume 67, pp. 1489-95.

IVC-SEP Electrolyte Databank, 1997. Unpublished. IVC-SEP Engineering Research Center for Phase Equilibria and Separation Processes, Technical University of Denmark, DK-2800 Lyngby, Denmark

Jänecke E., 1906, "Über eine neue Darstellungsform der wässerigen Lösungen zweier und dreier gleichioniger Salze, reziproker Salzpaare und der van't Hoffschen

Untersuchungen über ozeanische Salzablagerungen", Z. anorg. Chemie, **51**, 132-157.

Kofstad P., 1987, "Uorganisk kjemi", Tano A/S, Oslo, p. 254

Kremann R., and Zitek A., 1909, "Die Bildung von Konversionssalpeter aus Natronsalpeter und Pottasche vom Standpunkt der Phasenlehre", Monatshefte für Chemie, volume 30, pp. 311-340.

Lange E, and Monheim J., 1930, "Verdünnungswärmen bzw. Lösungswärmen von KNO3, KCl, RbF und CaSO4 in grosser Verdünnung", Z. Phys. Chem., volume 150, p. 349-369

Leung W.H., and Millero F.J., 1975, "The enthalpy of dilution of some 1-1 and 2-1 electrolytes in aqueous solution", J. Chem. Thermodynamics, volume 7, pp. 1067-1078.

Lindstrom R.E., and Wirth H.E., 1969, "Estimation of the bisulfate ion dissociation in solutions of sulfuric acid and sodium bisulfate", The Journal of Physical Chemistry, volume 73(1), pp. 218-223.

Loehe J.R. and Donohue M.D., 1997, "Recent Advances in Modeling Thermodynamic Properties of Aqueous Strong Electrolyte Systems", AIChE Journal, volume 43, No. 1, pp. 180-195.

Masson D.O., 1929, "Solute Molecular Volumes in Relation to Solvation and Ionization", Phil. Mag., volume 8, pp. 218-235.

Maurer G., and Prausnitz J.M., 1978, "On the Derivation and Extension of the UNIQUAC Equation", Fluid Phase Equilibria volume 2, pp. 91-99.

Meyerhoffer, 1903, "Über tetragene Doppelsalze mit besonderer Berücksichtigung des Kainits", Z. anorg. Chem., volume 34, pp. 145-173.

Moore J.T., Humphries W.T., and Patterson C.S., 1972, "Isopiestic Studies of Some Aqueous Electrolyte Solutions at 80°C", Journal of Chemical and Engineering Data, volume 17, pp. 180-182.

NBS, 1977, "A bibliography of sources of experimental data leading to activity or osmotic coefficients for polyvalent electrolytes in aqueous solution", NBS special publication 485, U.S. Department of Commerce/National Bureau of Standards.

NBS, 1979, "A bibliography of sources of experimental data leading to thermal properties of binary aqueous electrolyte solutions", NBS special publication 537, U.S. Department of Commerce/National Bureau of Standards.

NBS, 1986, "Bibliographies of Industrial interest: Thermodynamic measurements on the systems CO_2-H_2O, $CuCl_2$-H_2O, H_2SO_4-H_2O, NH_3-H_2O, H_2S-H_2O, $ZnCl_2$-H_2O, and H_3PO_4-H_2O", NBS special publication 718, U.S. Department of Commerce/National Bureau of Standards.

Neitzel U., 1986, "Neue Verfahren und Projekte zur Herstellung von K_2SO_4", Kali und Steinsalz , volume 9, 8, pp. 257-261

Nicolaisen H., Rasmussen P., and Sørensen J.M. 1993, "Correlation and Prediction of Mineral Solubilities in the Reciprocal Salt System (Na^+, K^+) (Cl^-, SO_4^{2-}) - H_2O at 0-100°C". Chemical Engineering Science, volume 48, No. 18, pp 3149-3158

Nicolaisen H., 1994, "Phase equilibria in aqueous electrolyte solutions", Ph.D. Thesis, Technical University of Denmark.

NIST Chemical Thermodynamics Database Version 1.1, 1990, U.S. Department of Commerce, National Institute of Standards and Technology, Gaithesburg Maryland 20899.

Olofsson I.V., Spitzer J.J., and Hepler L.G., 1978, "Apparent molar heat capacities and volumes of aqueous electrolytes at 25°C: Na_2SO_4, K_2SO_4, $Na_2S_2O_3$, $Na_2S_2O_8$, $K_2S_2O_8$, K_2CrO_4, Na_2MoO_4, and Na_2WO_4", Can. J. Chem., volume 56, pp. 1871-1873.

Osaka J., 1911, "On Sodium Potassium Carbonates", Mem. Coll. Sci. Eng. Kyoto, volume 3, pp. 55-61.

Perron G., Desnoyers J.E., and Millero F.J., 1974, "Apparent molal volumes and heat capacities of alkaline earth chlorides in water at 25°C", Can. J. Chem., volume 52, pp. 3738-3741.

Platford R.F., 1973, "Osmotic Coefficients of Aqueous Solutions of Seven Compounds at 0°C", Journal of Chemical and Engineering Data, volume 18, pp. 215-217.

Rard J.A., Habenschuss A., Spedding, F.H., J., 1976, "A review of the Osmotic Coefficients of Aqueous H_2SO_4 at 25°C", Journal of Chemical and Engineering Data, volume 21, pp. 374-379.

Rard J.A., and Platford R.F., 1991, "Experimental methods: isopiestic", in "Activity Coefficients in electrolyte solutions", 2nd edition, editor K.S. Pitzer, CRC Press.

Rivett A.C., 1922, "The Quaternary System Ammonium Chloride - Sodium Sulphate - Ammonium Sulphate - Sodium Chloride - Water", J. Chem. Soc., volume 121-22, p. 379-393.

Robinson R.A., and Stokes R.H., 1965, "Electrolyte solutions", Revised Edition, Butterworths, London.

Sander B., 1984, "Extended UNIFAC/UNIQUAC Models for (1) Gas Solubilities and (2) Electrolyte Solutions". Ph.D. Thesis, Department of Chemical Engineering, Technical University of Denmark, DK-2800 Lyngby Denmark.

Sander B., Fredenslund Aa., and Rasmussen P., 1986a, "Calculation of Vapour-Liquid Equilibria in Mixed Solvent/Salt Systems using an Extended UNIQUAC Equation", Chemical Engineering Science, volume 41, No. 5, pp. 1171-1183

Sander B., Fredenslund Aa., and Rasmussen P., 1986b, "Calculation of Solid-Liquid Equilibria in Aqueous Solutions of Nitrate Salts Systems using an Extended UNIQUAC Equation", Chemical Engineering Science, volume 41, No. 5, pp. 1197-1202

Sanders S.J., 1985, "Case Studies in Modeling Aqueous Electrolyte Solutions", Computers & Chemical Engineering, volume 9, 3, pp. 223-244

Sedel'nikov G.S., and Trofimovich A.A., 1959, Z. Neorg. Khim., volume 4, p. 1443.

Snipes H.P., Manly C., and Ensor D.D., 1975, "Heats of Dilution of Aqueous Electrolytes: Temperature Dependence", Journal of Chemical and Engineering Data, volume 20, pp. 287-291.

Sogolov I.D., Ostanina V.A., Safrygin J.S., Rutkovskaja T.I., Antonova N.V., Naginskaja R.E., 1982, "Verfahren zur Herstellung von Kaliumsulfat", Bundesrepublik Deutschland, Patentschrift DE 2820445C3.

Swallow J.C., and Alty S., 1931, "The Heat of Solution of Sodium Carbonate and the Specific Heats of its Solutions", J. Chem. Soc., 1931, pp. 3062-3079.

Thomsen K., 1996, "Soda ash liquors: Phase diagrams and process simulation", Confidential report, FMC Chemical Research and Development Center, Princeton, NJ.

Thomsen K., 1993 "Simulation and Design of Processes with Electrolyte Mixtures", Preparatory M.Sc. project, Department of Chemical Engineering, Technical University of Denmark, DK-2800 Lyngby, Denmark

Thomsen K., 1994 "Simulation and Design of Processes with Electrolyte Mixtures", M.Sc. project, Department of Chemical Engineering, Technical University of Denmark, DK-2800 Lyngby, Denmark

Thomsen K., Gani R., and Rasmussen P., 1995, "Synthesis and Analysis of Processes with Electrolyte Mixtures", Computers chem. Engng. volume 19, Suppl., pp. S27-S32

Tremaine P.R., Sway K., and Barbero J.A., 1986, "The Apparent Molar Heat Capacity of Aqueous Hydrochloric Acid from 10 to 140°C", Journal of Solution Chemistry, volume 15, No. 1, pp. 1-22

Ullmann's Encyclopedia of Industrial Chemistry, 1991, 5th edition, volume A17.

Vanderzee C.E., Waugh D.H., and Haas N.C., 1980, "Enthalpies of dilution and relative apparent molar enthalpies of aqueous ammonium nitrate. The case of a weakly hydrolysed (dissociated) salt", J. Chem. Thermodynamics, volume 12, pp. 21-25.

Notation

A	Debye-Hückel parameter	N_A	Avogadros number
a	parameter in equation (2-37)	n	mole number
a	activity	P	pressure
aq	aqueous state	q	surface area parameter
b	Debye-Hückel parameter	R	gas constant
b	parameter in equation (2-37)	r	volume parameter
C_p	heat capacity	SI	solubility index
c	parameter in equation (2-37)	s	solid state
d	density	s	number of solid phases
F	Faradays constant	T	temperature
f	rational activity coefficient	u	interaction energy parameter
f	fugacity	V	volume
G	Gibbs energy	w	weighting factor
g	function name	x	mole fraction
H	enthalpy	y	value of data point
H	Henrys constant	y	mole fraction
I	ionic strength	z	coordination number
J	relative heat capacity	z	ionic charge
K	solubility product	**Subscripts**	
L	relative enthalpy	i	component i
M	molar mass	s	salt
m	molality	w	water

x	constant composition
x	rational
1	initial condition
2	final condition
θ	Helgeson parameter

Superscripts

C	combinatorial part
calc	calculated
D-H	Debye-Hückel
E	excess
exp	experimental
∇	Standard state
k	salt identifier
R	residual part
sat	saturation
t	temperature derivative
0	constant part
0	standard state
•	standard state
∞	standard state

Greek letters

A	anion
α	degree of dissociation
α	stoichiometric coefficient for anion
Δ	increment
ε	reaction coordinate
ε_0	vacuum permittivity
ε_r	relative permittivity
θ	surface area fraction
φ	apparent
K	cation
κ	stoichiometric coefficient for cation
μ	chemical potential
ν	stoichiometric coefficient
ρ	density
σ	volume specific heat vapacity
ϕ	volume fraction
Φ	Osmotic coefficient
Ψ	UNIQUAC parameter

Index